Performance of GFRP Reinforcement as Friction Shear Connectors in Concrete Composite Elements

By

Basel Hazem Aljada

A Thesis submitted to the Faculty of Graduate Studies of

The University of Manitoba

in partial fulfilment of the requirements of the degree of

MASTER OF SCIENCE

Department of Civil Engineering

University of Manitoba

Winnipeg, MB, Canada

ABSTRACT

Composite reinforced concrete (RC) beams composed of cast-in-situ slabs and pre-cast beams have been commonly used due to their economic advantage over ordinary beams. Maintaining integrity between the beam and slab components is essential to ensure monolithic behaviour. This integrity can be maintained only if the friction shear along the joint interface resulted from the gravity load is resisted. The characteristics of the reinforcement crossing the joint interface (shear plane), concrete strength, and shear plane condition are some of the main factors controlling the integrity of composite elements. Given their lighter structures, composite beams are widely utilized in structures that require long spans, such as bridges and parking structures. However, these RC structures are usually susceptible to severe environmental conditions, especially in cold regions, that will accelerate the steel corrosion process. Substituting the conventional steel with a non-corrodible material such as glass fibre-reinforced polymer (GFRP) has proven to be a viable alternative.

In this study, a pioneer investigation was conducted to assess the feasibility of using GFRP as shear connectors in concrete composite elements. The study involved constructing and testing 26 large-scale push-off specimens under monotonic axial load. Twenty-one out of these specimens were reinforced with GFRP connectors, whereas the remaining were reinforced with steel connectors serving as control specimens. Each specimen consisted of two L-shaped blocks that were cast either monolithically or at different times to simulate the cold-joint condition. The specimens were 1,050 mm long × 600 mm wide × and 300 mm deep. The main tested parameters were reinforcement type (GFRP or steel), ratio (0.17, 0.24, 0.33, 0.36, 0.42, and 0.48%), and shape (closed stirrups and Z-shaped bars), concrete strength (35 and 70 MPa) and shear plane condition (cold-jointed not roughened, cold-joint roughened, and monolithic). The test results demonstrated

that GFRP can be used as shear connectors and the overall, behaviour is dependant on the reinforcement ratio and concrete strength. Increasing the reinforcement ratio and concrete strength increased the load carrying capacity significantly. Moreover, the results showed that closed stirrups provided better clamping stresses than the Z-shaped bars. Furthermore, monolithic shear plane condition resulted in having much higher capacities over the cold-jointed counterpart specimens.

ACKNOWLEDGEMENTS

I am sincerely grateful to Dr. Ehab El-Salakawy, Ph.D., PEng, FACI, FCSCE, FEIC, FIIFC, Professor of Structural Engineering in the Department of Civil Engineering, Associate Dean of Faculty of Graduate Studies at the University of Manitoba for giving me the opportunity to pursue graduate studies, his tremendous guidance and support, and priceless shared knowledge and advice.

The endless assistance provided by the technical staff of the W. R. McQuade structures laboratory, Dr. Chad Klowak, Samuel Abraha, and Daniel Szara, for all working stages, is acknowledged. Also, I would like to express my gratefulness to the journey's brothers Ibrahim Abdelwahed, Yazan Hatamleh, and Yasser Selmy for their support. In addition, the financial support from the Natural Science and Engineering Research Council of Canada (NSERC) is appreciated.

I am profoundly grateful to my dear cousin Dr. Ibrahim Aljada for the invaluable support and assistance he provided throughout this journey of mine. Beyond being just a relative, he has been a pillar of strength and a source of comfort, making me feel at home in times of uncertainty. Also, the role of my dearest friend Dr. Ahmed Assad during this journey in the ups and downs was significant. All the appreciation goes to my friends Osama Ghassan, Osama Azzam, Belal, Ahmed, Zidan, Zaid, and Ashraf for their persistent support.

Last but not least, I would like to express my heartfelt gratitude to my parents (Hazem Aljada and Wafa Qunebi), brothers (Waleed and Wael), and sister (Bodoor) for their unwavering support and encouragement throughout the journey of completing this project. Their constant belief in my abilities, love, and understanding has been a pillar of strength during the highs and lows of this academic endeavor. I am truly fortunate to have such loving and supportive family by my side, and this thesis would not have been possible without them.

TABLE OF CONTENT

LIST OF TABLES

LIST OF FIGURES

LIST OF NOTATIONS

A_{cv}	=	area of the concrete section resisting shear transfer
A_g	=	Gross area of interface
A_{vf}	=	area of the reinforcement crossing the shear plane
A_s	=	Total cross-sectional area of reinforcing bars crossing the shear plane
A_x	=	the projected contact area due to crack slip
A_y	=	the projected contact area due to crack width
b	=	width of the cross section at the level under consideration
b_w	=	Beam's web thickness
C	=	cohesion stress at the interface
E_f	=	modulus of elasticity of FRP
f_{fu}	=	tensile strength of GFRP bars
f_y	=	specified yield strength of steel reinforcement
f'c	=	specified concrete compressive strength
I		moment of inertia of the entire uncracked cross section
k	=	constant in Loov's equation (Loov, 1978)
k	=	constant in Anderson's equation (Anderson, 1960)
N	=	unfactored permanent load normal to the shear plane. Positive for compression and negative for tension
P	=	clamping stress.
Q	=	first moment of the area above or below the level of the cross section under consideration with respect to the natural axis of the section

s	=	Spacing between shear reinforcement
T	=	tension force induced at the shear connectors
v	=	shear resistance of the plane
V_u	=	Ultimate friction shear force
w	=	crack width
Δ	=	crack slipping
α	=	angle between the shear plane and the shear friction reinforcement
ε_f	=	strain in the FRP reinforcement at ultimate shear transfer load
λ	=	factor to account for low-density concrete
μ	=	friction coefficient at the interface
ρ_v	=	shear reinforcement ratio crossing the shear plane
σ	=	total compressive stress to the shear plane
σ_n	=	externally applied normal stress (N/Acv)
$\tau\ (\Delta, w)$	=	shear stress along the interface
$\theta_1, \theta_2, \theta_3, \Upsilon^{\theta_3}, \mu'^{\theta_2}$	=	Connor's and Kim's (2016) model parameters
Φ	=	relative incremental path of the crack
ϕ_c	=	resistance factor for concrete

CHAPTER 1. INTRODUCTION

1.1. Background

Reinforced concrete (RC) elements usually comprise concrete and steel reinforcement. These components are preferred due to the proper bonding characteristics between concrete and steel. Such bonding facilitates composite behaviour, which compensates for concrete weak tensile strength. Moreover, steel reinforcement is protected from corrosion by the alkalinity of concrete. Yet, steel is susceptible to corrosion in severe environmental conditions, especially when de-icing salt is used. Steel reinforcement coated with epoxy was used in structures subjected to severe environmental conditions, such as bridges, parking garages, and marine structures, to prevent the reinforcement from corroding. It was proven that such type of bars requires continuous maintenance programs incurring significant money spending. In addition, this way is insufficient to prevent corrosion (Pianca et al. 2005). Moreover, in efforts to alleviate the corrosion-related issues, galvanized and stainless steel were utilized for this purpose. Yet, these materials have proven to delaying rather than eliminating corrosion [ACI 222R-19, (ACI 2019b)]

The deficit in damaged infrastructure is estimated at CAD $388 billion. A cost of CAD $415 billion is estimated for upgrading about 33% of the damaged infrastructure to an acceptable level of performance (Mirza and Ali, 2017)

Therefore, an alternative to the traditional combination shall be adopted. As a non-corrosive material, fibre-reinforced polymer (FRP) has been established as an effective substitute to steel. FRP is not only considered to overcome the corrosion problem, but also used where magnetic transparency is required. Another significant merit of FRP is its lightweight, which is approximately 20-25% of that of conventional steel. Through the last few decades, glass fibre -

reinforced polymers (GFRP) has proven its efficiency under flexural and shear stresses (El-Sayed et al., 2005). FRP has multiple internal, external, and prestressing reinforcement applications in concrete and masonry structures. Nonetheless, GFRP reinforcements are anisotropic, which means that their properties depend on the reinforcing orientation. Also, the same GFRP reinforcement may have different properties depending on the way of manufacturing. In addition, the high tensile strength of FRP reinforcement is only exhibited along the direction of the reinforcing fibres. This anisotropic behaviour affects the shear strength and dowel action of FRP bars. GFRP composite bars are relatively weak in interlaminar shear, where layers of unreinforced resin lie between the fibre layers because there is usually no reinforcement across the layers. Unlike steel, GFRP composites exhibit linear-elastic behaviour up to failure, i.e., they do not undergo any ductile phase in terms of a yielding plateau prior to the brittle rupture, as shown in Figure 1.1.

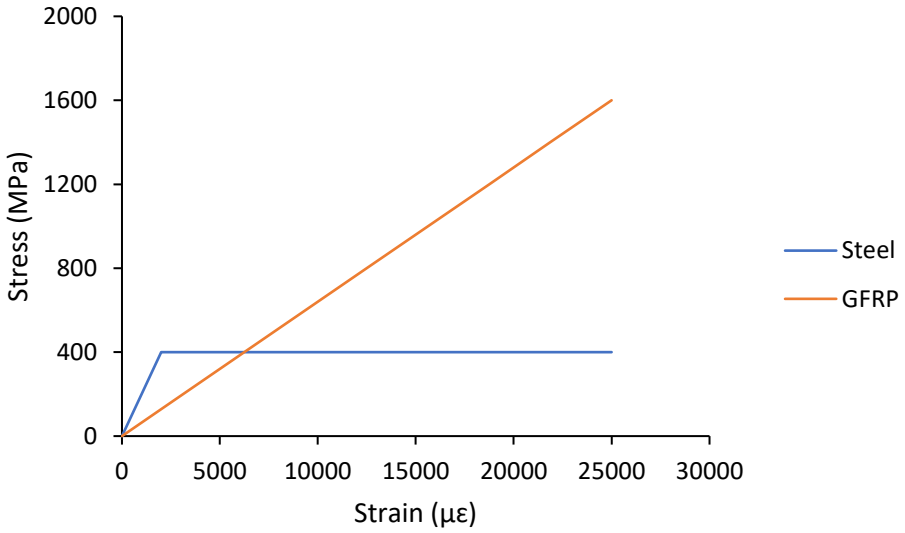

Figure 1.1: Stress-strain diagram for steel and GFRP

Glass FRP (GFRP) is widely used in civil engineering due to its lower cost and higher tensile strain at failure than other types of fibres. However, it has lower shear and compressive strengths than

conventional steel, resulted from the lower transverse strength. Additionally, these composites have a lower modulus of elasticity, affecting the bond between concrete and reinforcement at the ultimate stages. This compromises the shear strength following the occurrence of wider cracks that affect the aggregate interlock and, ultimately, the un-cracked concrete contribution. Furthermore, the dowel action of the longitudinal FRP reinforcement is considerably lower than that of steel reinforcement due to the low transverse shear strength of FRP reinforcement. Accordingly, the shear capacity of FRP-RC members is expected to be considerably lower than that of their steel-RC counterparts with the same flexural reinforcement ratio. In the last two decades, extensive research has been conducted to examine the applicability of replacing steel with GFRP as concrete reinforcement. Nevertheless, the applicability of using FRP as shear connectors at concrete-to-concrete interfaces still needs to be thoroughly investigated.

1.2. Problem Definition

Composite members have been utilized as an economical way to produce smaller, shallower, and lighter structures (Loov and Patnaik 1994) Also, the use of composite members has proved its efficacy in accelerating the construction process. This results in overall cost savings. An RC composite member could be a combination of a precast girder and a concrete slab. A composite beam requires the flange or cast-in-place slab and the girder to act as a single unit.

Composite members' merits can only be achieved if shear induced by the external loads along the joint interface can be transferred without causing a separation between the two different elements, as shown in Figure 1.2. Such separation could be prevented or controlled by several means but mainly by the reinforcement across the shear interface. This reinforcement is responsible for resisting the shear along the interface to satisfy the composite action requirements and act as monolithic members. However, this reinforcement, especially in cold regions where de-icing salt

is used, is subjected to corrosion. As stated earlier, the use of FRP reinforcement as an alternative to the conventional steel would overcome the corrosion problem.

Previous studies such as Birkeland and Birkeland (1966), Badoux and Hulsbos (1967), Mast (1968), Hofbeck et al. (1969), Loov and Patnaik (1994), and design codes such as ACI 318-19 (ACI 2019) and CSA A23.3-19 (CSA 2019a) assumed that shear reinforcement yields at failure. Such an assumption conflicts with FRP characteristics, which fails by brittle rapture (Connor and Kim 2016). Based on FRP characteristics, the available design guidelines of steel-RC are unapplicable to FRP-RC.

Composite concrete members with conventional steel at the interface were extensively studied and proved their efficacy. Moreover, design guidelines are provided in building codes such as ACI 318-19 (ACI 2019) and CSA A23.3-19 (CSA 2019a). However, the friction shear mechanism for FRP is not yet fully investigated. Despite that CSA S6-19 (CSA 2019b) allows the use of GFRP as friction shear reinforcement. Yet, ACI 440.11-22 (ACI 2022) and CSA S806-12 (CSA 2021) have no design provisions for this GFRP application.

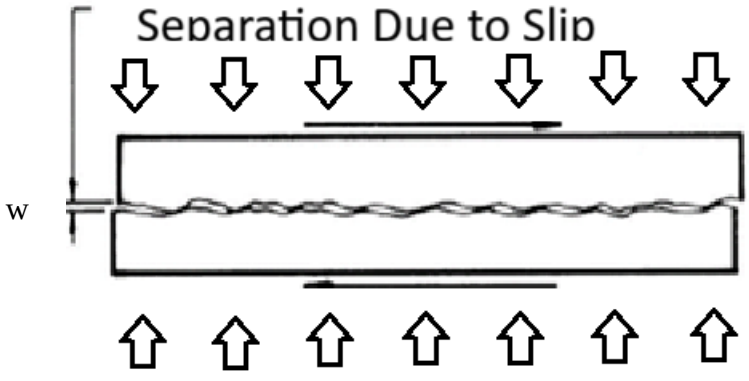

Figure 1.2: Shear along crack (reproduced from Mast 1968)

1.3. Research Significance

Despite that the Canadian Highway Bridge Design Code, CSA S6-19 (CSA 2019b), permits the use of GFRP as friction shear reinforcement, the other North American codes are silent on the use of GFRP reinforcement in such application due to lack of experimental data. This study aims to experimentally investigate the feasibility of using GFRP bent bars as friction shear reinforcement. The results are depicted in terms of cracking pattern, load-carrying capacity, reinforcement strain and slipping. In addition, a comparison between the experimental results and the predicted capacities, using the available design provisions, is presented.

1.4. Scope of Work

To investigate the capacity and performance of the proposed GFRP shear friction reinforcement and to quantify the effect of different design parameters, large-scale double L-shaped push-off tests were conducted. The test specimens included normal-strength (NSC of 35 MPa) and high-strength concrete (HSC of 70 MPa). Closed stirrups and Z-shaped bars were used as shear connectors. The test data included the ultimate load, the relative slippage between the interconnected members, the strain of the reinforcement crossing the shear plane, and the friction shear capacity. The friction shear mechanism for different concrete interfaces with GFRP connectors was also described.

1.5. Objectives:

The main objectives of this research are to:

1. Investigate the feasibility of using GFRP as friction shear reinforcement in concrete composite elements.

2. Comparing the behaviour between GFRP and conventional steel shear connectors under same conditions.
3. Evaluate the available design models for this application against the experimental results.

To achieve these objectives, the effect of the following parameters was investigated:

1. Shear connectors type (steel or GFRP) shape (closed stirrups or Z-shaped) and ratio (0.17, 0.24, 0.33, 0.36, 0.42, and 0.48%).
2. Shear plane condition (cold-joint not roughened, cold-joint roughened, and monolithic).
3. Concrete compressive strength (35 MPa for NSC and 70 MPa for HSC).

1.6. Methodology

The research program included an extensive experimental study conducted in the Heavy Structures Laboratory at the University of Manitoba. This study tested 26 large-scale specimens consisting of 2-L shaped blocks measuring 1,050 × 600 × 300 mm under monotonic axial load. The experimental program included specimens that were cast monolithically as well as where the concrete L-blocks were placed in two stages to simulate the cold-joint conditions. The L-block was poured in a horizontal position in the first stage and cured for seven days before the second pouring of concrete, which was also placed horizontally. The concrete interface was cleaned and treated to achieve two different interfaces, rough and smooth. The rough surface was reached by scraping the concrete surface transversely with a steel trowel to create a rough surface with a 6-mm minimum depression, ACI 318-19 (ACI 2019). Also, the surface was chiseled to remove all the laitance before the second cast. The smooth surface was achieved by leaving the cast surface as is. These two surface finishes were obtained to investigate the effect of interface conditions on the selected design parameters. Twenty out of the 26 specimens had a cold-jointed including 5 and 15 with and without roughened interface, respectively. Four out of the 15 were reinforced with Z-

shaped bars, four were cast with HSC, and seven specimens with NSC. Lastly, seven specimens were placed monolithically.

1.7. Thesis Organization

The thesis consists of five chapters described below:

- Chapter 1 presents a general background for the research topic, problem definition, research significance, scope of work, objectives, and methodology.
- Chapter 2 includes the essential properties of FRP composites, the established fundamentals for steel-RC composite elements, and the effect of different parameters such as interface roughness, pre-cracking, concrete strength, reinforcement ratio, concrete strength, dowel action, and shear-span-to-depth ratio. Additionally, the available design models adopted in North American codes for steel-RC and GFRP-RC members are presented.

The following chapters (3 and 4) are presented in journal article format. The articles have been submitted to the respective journals and are currently under review.

- Chapter 3 (Article 1) Investigates the feasibility of experimentally using GFRP as friction shear reinforcement in concrete composite elements at cold-joint not roughened interface. This paper includes 15 specimens with different reinforcement ratios, concrete strength, and connectors shape to explore their effects on the overall behaviour. Moreover, an evaluation of the available models against experimental results was presented. Article 1 incorporates the results of Series I, II, and V (Appendix A) which are 15 out of 26 specimens tested in this research program.

Aljada, B.H., El-Ragaby, A., and El-Salakawy, E.F. "GFRP Bars as Friction Shear Reinforcement for Concrete Cold Joints," ACI Structural Journal, under review.

- Chapter 4 (Article 2) examines the impact of different shear plane conditions on the overall friction shear behaviour. The article includes 18 specimens with different reinforcement ratios and three different shear plane conditions to explore their combined behaviour. Article 2 incorporates the results of Series II, III, and IV (Appendix A) which are 18 out of 26 specimens tested in this research program.

  Aljada, B.H., El-Ragaby, A., and El-Salakawy, E.F. "GFRP Stirrups as Friction Shear Reinforcement for Different Concrete Interfaces," ASCE, Journal of Composites for Construction, under review.

- Chapter 5 provides an overview of the major findings and conclusions of the study and recommended work for the future.

CHAPTER 2: LITERATURE REVIEW

2.1. Overview

Reinforced concrete elements are designed to resist different types of stresses. In some cases, the transfer of shear stresses along a definite plane needs attention. Such cases include joints in RC elements where concrete is placed at different times and monolithically. Examples for these joints are footing-column joint, beam-column joint, pre-cast beam and cast-in-situ slab as shown in Figure 2.1. In general, it may be divided to shear along cracked and uncracked planes. Such joints are part of any structure that should be safely constructed.

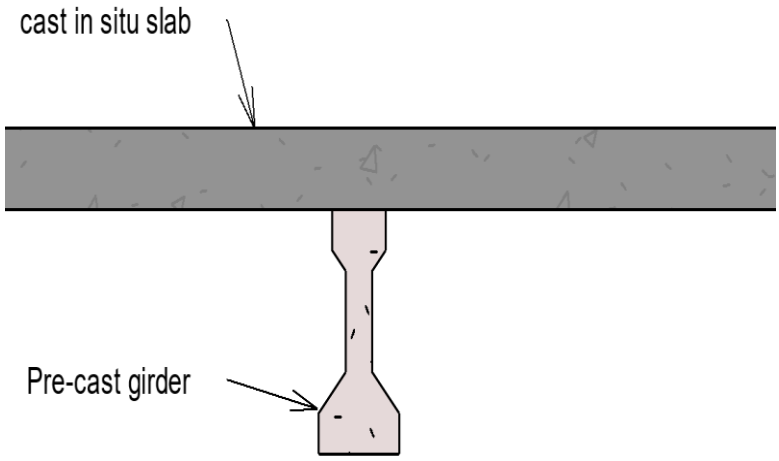

Figure 2.1: Typical composite concrete beam

Hunter (1953) suggested casting the beam and the slab in two different placements. The reason is that cracks may occur at the junction between the slab and the beam, especially in deep beams, if the placement happens monolithically due to vertical shrinkage. Accordingly, the ACI 318-19 (ACI 2019) code permitted this placement method, considering a sufficient reinforcement is provided at the junction to resist the horizontal shear that may lead to slipping. Moreover, one of

the critical connections that can be seen in bridges and garages is the connection between the steel or pre-cast girders and the cast in-situ deck slab. This connection significantly influences depth, width, weight, and, ultimately, the material and workmanship costs. In addition to the reinforcement required at the connection, the interface bond plays a vital role in horizontal shear transfer. Weak bond interface may lead to the beam and slab separation. Subsequently, each element will resist the load separately rather than acting as a composite element, as shown in Figure 2.2.

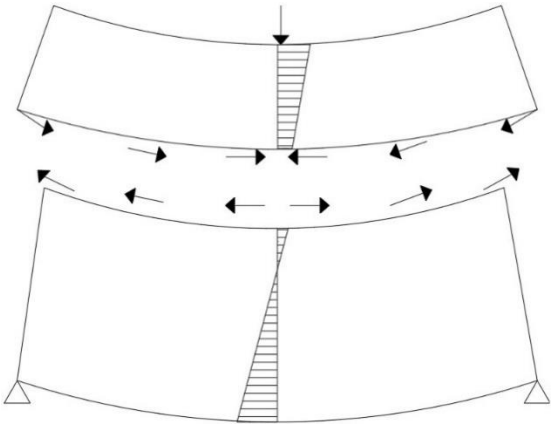

(a)

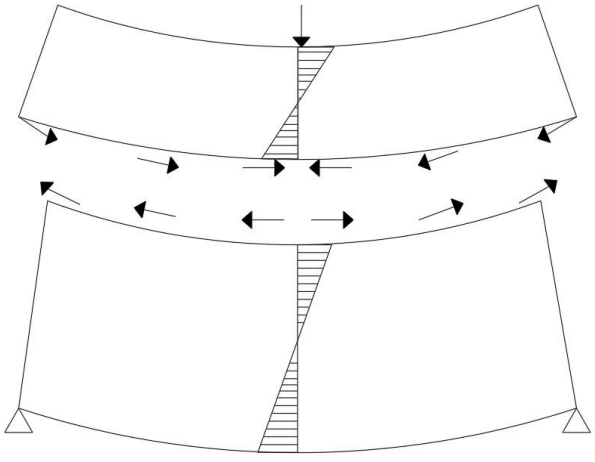

(b)

Figure 2.2: Horizontal shear transfer in concrete composite elements: (a) composite element and (b) non composite element

A shear connector is used in various types of structures. It is a steel projection at the top of the flange of the steel or concrete beam to connect with the cast-in-situ or pre-cast slab to ensure composite action, as shown in Figure 2.3. It is used to transfer the shear from the slab to the beam. This type of connector can be found mainly in bridges. In cold regions such as Canada, de-icing salt is used regularly on roads to clear the driveways. Such agents may expedite the occurrence of corrosion. Usually, a tremendous amount of money is spent on maintenance to prolong the life span of steel-RC structures due to corrosion-related problems. Nevertheless, maintenance will never eliminate corrosion; it just delays it.

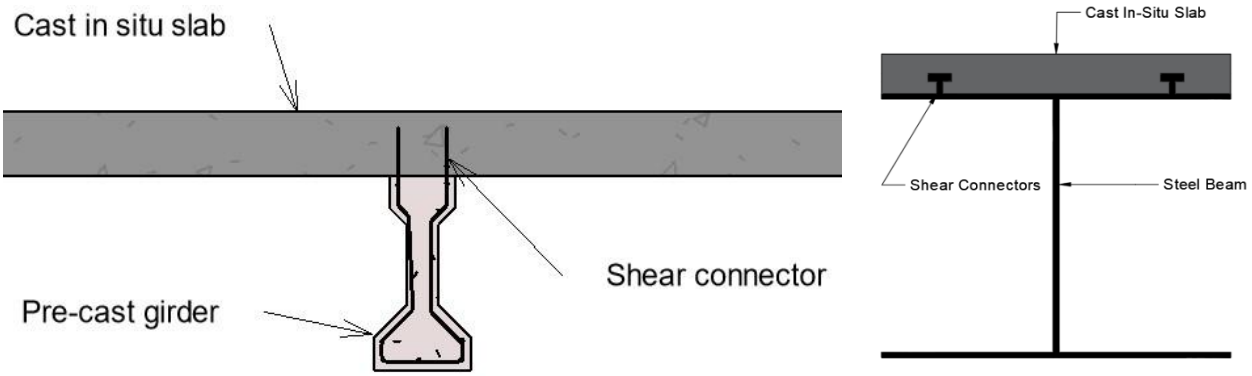

(a) (b)

Figure 2.3:(a) Concrete composite member, and (b) steel composite member

This chapter presents a discussion of the previous research available on both steel-RC and FRP-RC composite elements. A summary of the friction shear provisions in the current codes and guidelines in North America is also presented. In addition, the main physical and mechanical properties of FRP material are briefly presented.

2.2. FRP Properties

2.2.1. Physical properties

Density and coefficient of thermal expansion are physical properties that are described in ACI 440.1R-15 (ACI 2015).

2.2.1.1 Density

FRP bars have lower density estimated by one-fourth to one-sixth that of conventional steel. Lower density reduces transportations and handling fees of these materials. Table 2.1 shows the densities of different FRP materials as given by ACI 440.1R-15 (ACI 2015).

Table 2.1:Typical densities of reinforcing bars

Material	Steel	GFRP	CFRP	AFRP
Density (gm/cm^3)	7.9	1.25-1.4	1.5-1.6	1.25-1.4

2.2.1.2 Coefficient of thermal expansion

FRP bars have different thermal expansion coefficients in the longitudinal and transverse directions depending on the fibre types, resins, and fiber volume fraction. The properties of fibres control the longitudinal coefficient, while the properties of resins control the transverse coefficient. The coefficients of thermal expansion of different types of reinforcing bars, as given by the ACI 440.1R-15, are listed in Table 2.2. The negative sign means that material shrinks with the temperature increase and vice versa. The difference in thermal expansion coefficient between concrete and FRP materials is challenging when combined as composite members. This leads to splitting cracks when temperature changes.

Table 2.2: Typical coefficients of thermal expansion for reinforcing bars

Direction	Coefficient ($\times 10^6/^oC$)				
	Steel	GFRP	CFRP	AFRP	Concrete
Longitudinal	11.7	6.0 to10.0	-9.0 to 0	-6 to -2	7.2 to 10.8
Transverse	11.7	21.0 to 23.0	74.0 to 104.0	60.0 to 80.0	7.2 to 10.8

2.2.2 Mechanical properties

2.2.2.1 Tensile behaviour

FRP bars exhibit linear behaviour till failure when subjected to tension. FRP tensile strength is mainly controlled by fibre-volume fraction. FRP consists of fibers that are bounded by resins. The volume of fibres in the bar to the overall volume affects its tensile strength. Moreover, the manufacturing process has a significant effect on the tensile strength. Therefore, the tensile strength shall be provided by the manufacturer.

FRP bars can not be bent once manufactured since it is made from thermoplastic resins that cannot be reshaped. Nevertheless, they can be fabricated with bends. These bends lead to a 40%- 50% reduction in the strength of the bent portions.

2.2.2.2 Compressive behaviour.

The compressive strength of FRP bars is less than its tensile strength and is recommended to be neglected in design consideration as indicated by current FRP design codes; CSA S806-12 (CSA ,2021) and ACI 440.1R-15 (ACI 2015). The reason behind that is the end brooming and internal fiber micro-buckling under compressive loading, where the compressive strength of FRP reinforcement is limited to a corresponding 0.002 compressive strain as permitted by CSA S6-19 (CSA 2019b).

FRP bars can reach up to 0.7% strain when subjected to a compressive axial load (Mohamed et al., 2014). Also, it was found that HSC columns reinforced with longitudinal GFRP bars show similar concrete and reinforcement strains compared with steel-RC columns (Almomani et al., 2022).

2.2.2.3 Shear behaviour

FRP materials are weak in interlaminar shear where layers of unreinforced resin lie between layers of fibers. The orientation of fibers in the off-axis direction increases the shear strength. This can be achieved by placing transverse fibers to the main fibers.

2.2.2.4 Bond behaviour

Bond performance depends on surface preparation of the bar the mechanical properties of the bar, manufacturing properties, and the environmental conditions. The bond force between a GFRP bar and the concrete may be transferred by adhesion (chemical bond), friction, and mechanical interlock.

2.3 Horizontal Shear Mechanism

Many studies were carried out to understand the requirements of concrete joints to ensure the proper integrity of the structure. One of the most critical joints is the concrete-to-concrete joint subjected to horizontal shear. Horizontal shear was initially studied by Anderson (1960) and Hanson (1960) and Birkeland and Birkeland (1966), then developed through the subsequent years. Different researchers investigated shear hypotheses depending on multiple factors. The shear hypothesis was first introduced by Birkeland and Birkeland (1966). The hypothesis focused on the effect of slipping after crack occurrence resulting from external shear load rather than tension crack. It was assumed that if external shear was applied horizontally, it would lead to slippage at the interface accompanied by separation between the two concrete blocks. However, such slippage would be resisted by the friction factor of μP resulting from the clamping force P. It was also assumed that reinforcement provided through the interface is subjected to tension stresses resulting

from the separation that causes steel yielding. This tension (T) induces an equal magnitude external clamping compression force at the interface. The roughness was assumed as a series of sawtooth ramps with a slope of tan ϕ. The hypothesis is illustrated in Figure 2.4.

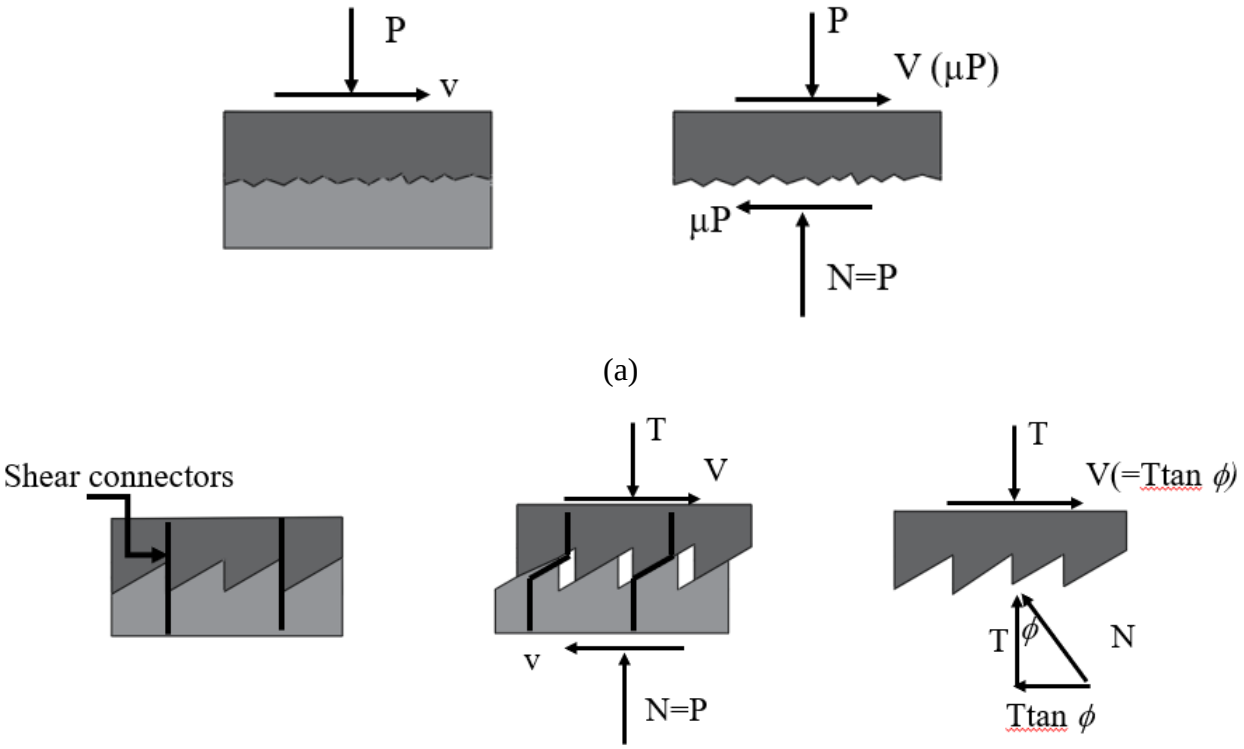

Figure 2.4: Friction shear hypothesis (reproduced from Birkeland and Birkeland 1966)

It was concluded that the ultimate shear capacity at the interface assuming steel yielding could be calculated by:

$$V_u = T_u \tan \emptyset = A_s f_y \tan \emptyset \qquad \text{Equation 2-1}$$

$$v_u = V_u / A_g = \rho f_y \tan \emptyset \qquad \text{Equation 2-2}$$

Where:

$tan\emptyset$ =1.7 for monolothic concrete.

$tan\emptyset$ = 1.4 for artificially roughened construction joints

$tan\emptyset$ = 0.8 to 1.0 for ordinary construction joints and for concrete to steel interface.

V_u= total ultimate shear force

A_s= total cross sectional area of reinforcing across interface.

f_y = yield strength of reinforcing (< 60 ksi, 414 MPa).

A_g = gross area of interface.

v_u = ultimate shear stress on gross area (< 800 psi, 5.5 MPa).

ρ = steel ratio, A_s/A_g (useful limit = 0.015).

Concrete strength, $fc^{'}$ > 4000 psi, 28 MPa.

Maximum reinforcing size = #6 rebar, or ½ in., diameter headed studs.

2.4 Research on Steel-Reinforced Concrete Members

This section presents a summary of some main parameters that affect the behaviour of cold jointed concrete reinforced with steel bars.

2.4.1 Interface roughness

Concrete elements may be placed monolithically with the support or may be placed at different times. Interface surface condition plays a crucial role in horizontal shear capacity. Hanson (1960) investigated horizontal shear, through 62 push-off specimens and 10 T-shaped girders as illustrated in Figure 2.5.

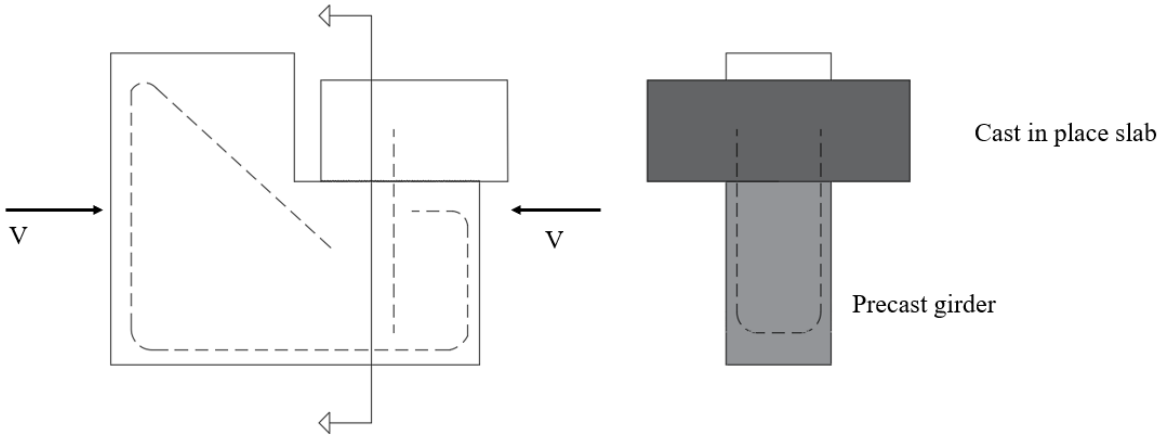

Figure 2.5: Push off specimen (reproduced from Hanson, 1960)

The author concluded that the composite action is assured if the joint integrity between the pre-cast girder and cast-in-situ slab is maintained. The finished surface was intentionally roughened to achieve a 9.5-mm depth. The results have shown the significant effect of rough bonded connection over the smooth bonded connection on shear capacity. Maximum shear strengths of 2.07 and 3.45 MPa were attained for smooth-bonded and rough-bonded connections, respectively.

Saemann and Washa (1964) tested 42 T-beams with three different roughness levels: smooth, intermediate, and rough. Intermediate roughness was 1/8 in. (3.2 mm), and high roughness was 3/8 in. (9.5 mm). The authors concluded that the shear strength increases with the increase of interface roughness.

Birkeland and Birkeland (1966) and Badoux and Hulsbos (1967) also studied the effect of interface roughness. These studies showed a significant effect of interface roughness on shear capacity, evidenced by higher shear capacity for rough interfaces. Badoux and Hulsbos (1967) reported a 75% increase in shear capacity when using a rough interface. This matches the results of Birkeland and Birkeland (1966), which showed that intentionally roughened surfaces can provide 40% -75%

more shear capacity than ordinary construction joints. Whereas monolithic casting may provide a higher shear capacity ranging between 70% and 112% than the ordinary construction joint. The results of the studies by Mattock (2001) and Kahn and Mitchell (2002) coincided with the above studies.

2.4.2 Crack effect

Mast (1968) claimed that an unexpected crack may occur at the interface of the precast and cast-in-situ concrete. Therefore, he examined the effect of adding steel reinforcement to resist the horizontal shear at the cracked interface, considering the effect of internal friction resulting from crack roughness. The concept of his study was based on considering a simply supported composite beam in which, at failure, the compressive strength acts on the flange C_u that is in equilibrium with the tension force from the yielded steel, as shown in Figure 2.6. The total required steel will be:

$$\frac{T_u}{f_y \tan(\emptyset)}$$ Equation 2-3

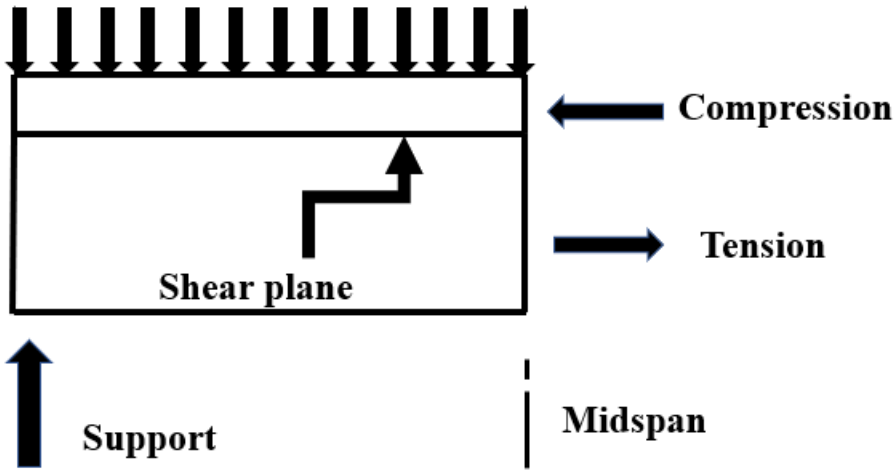

Figure 2.6: Equilibrium for concrete composite beam under gravity load (reproduced from Mast1968)

If the compression force at failure acts on the beam web, the equilibrium will be as shown in Figure 2.7.

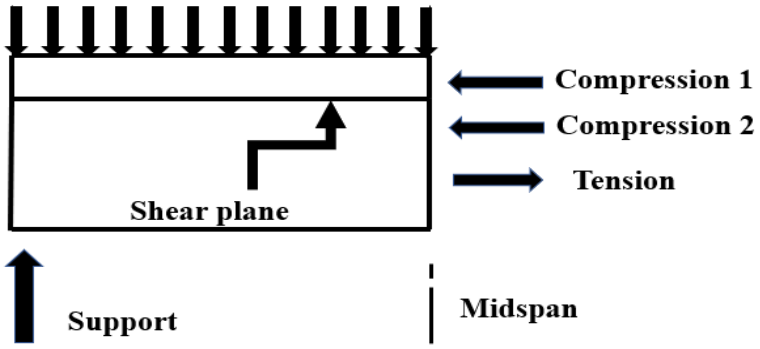

Figure 2.7: Equilibrium for concrete composite beam under compression load at web (reproduced from Mast 1968)

Moreover, this theorem was implemented on corbels as well. The author suggested adding horizontal steel bars in the corbels to prevent the failure along the shear plane in case of $a/d > 0.7$, as shown in Figure 2.8. The required reinforcement is:

$$\frac{P_u}{f_y \tan(\emptyset)}$$ Equation 2-4

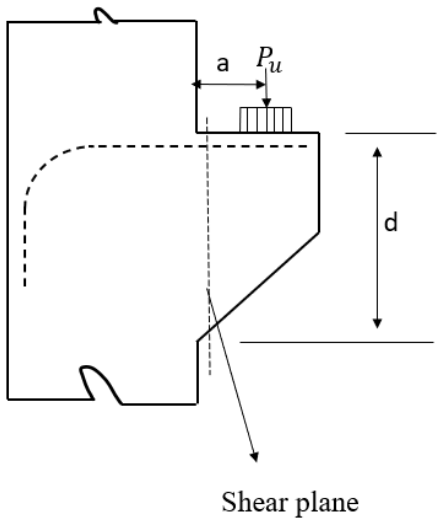

Figure 2.8: Shear friction in corbels (reproduced from Mast 1968)

Hofbeck et al. (1969) showed that the slipping is higher for cracked specimens during all load stages. This leads to reduce the shear strength at the interface as illustrated in Figure 2.9.

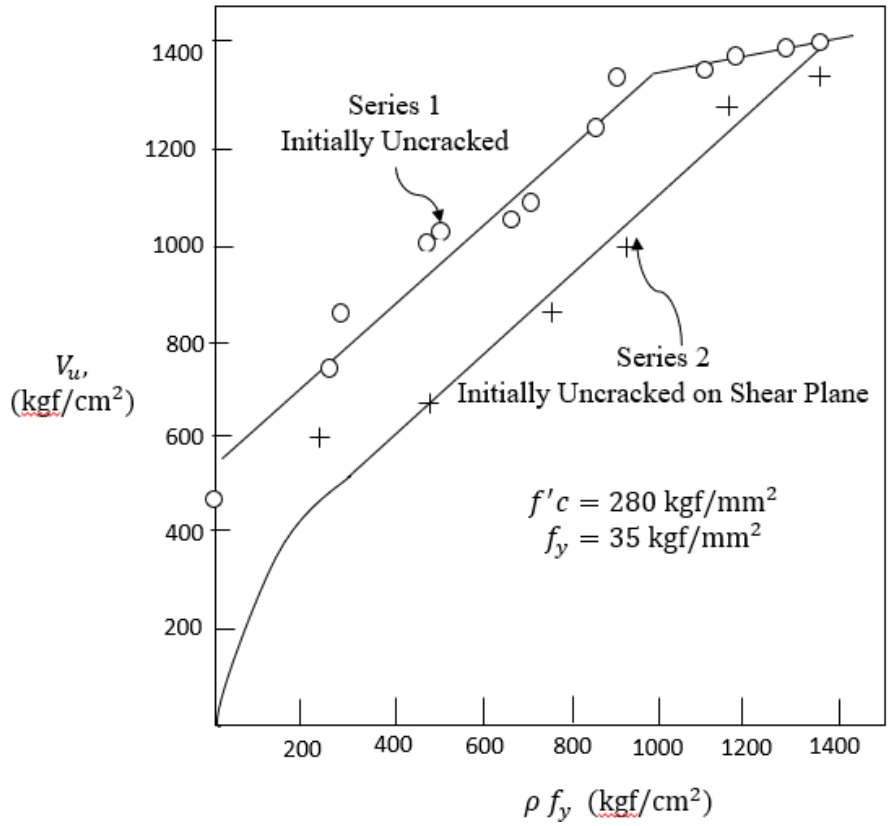

Figure 2.9: Effect of crack with different pf_y, (reproduced from Hofbeck et. al. 1969)

Mattock and Hawkins (1972), Mattock (1974), Walraven and Stroband (1994), Kahn and Mitchell (2002), and Harries et al. (2012) examined the effect of pre-existing cracks on shear capacity. It was agreed that shear strength is noticeably decreased when cracks exist.

2.4.3 Concrete strength

Many studies were applied to investigate the influence of concrete compressive strength on the horizontal shear capacity. However, there was no common conclusion from these studies. Anderson (1960) applied push-off tests on composite beams with two different compressive

strengths, 20.7 and 51.7 MPa, to predict the horizontal shear capacity at the interface. Based on the results, the following expression is introduced to calculate the horizontal shear strength:

$$v_u = v_o + k\rho_v \qquad \text{Equation 2-5}$$

where k and v_o are experimental parameters that depend on concrete compressive strength such that v_o = 4.41, 5.52 and k = 229, 276 for f_c' = 20.7 and 51.7 MPa, respectively.

Loov (1978) proposed the first equation to calculate the horizontal shear stress through a concrete-concrete interface that included concrete compressive strength as shown below:

$$\frac{v_u}{fc'} = k\sqrt{\frac{\rho f_y + \sigma_n}{fc'}} \qquad \text{Equation 2-6}$$

Where k = 0.5 for initially uncracked interface.

The previous two studies, along with Mansur et al. (2008) and Loov and Patnaik (1994) studies, showed that the increase in concrete strength results in an increase in shear capacity. Conversely, Hofbeck et al. (1969) and Mattock and Hawkins (1972) concluded that the concrete compressive strength effect depends on the reinforcement density crossing the shear plane. This means concrete strength has no effect on shear capacity below a certain limit of the reinforcement while it increases above this limit, as shown in Figure 2.10.

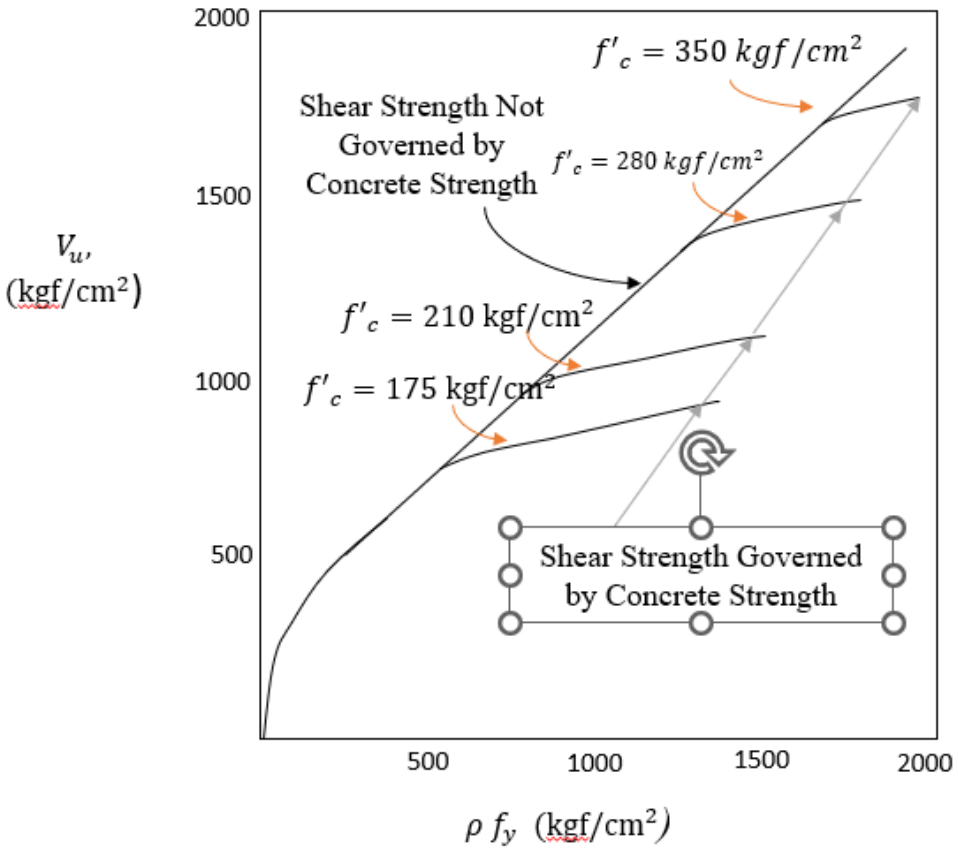

Figure 2.10: Relationship between pf_y and v_u for different concrete strength (reproduced from Hofbeck et al. 1969)

Saemann and Washa (1964) found that the increase of concrete strength has no considerable effect on shear strength. Patnaik (2001) plotted a Figure 2.11. to predict the relation between concrete compressive strength and shear strength based on the testing results of 15 copmiste beams. It was found that effect of concrete strength on shear strength is not following any trend.

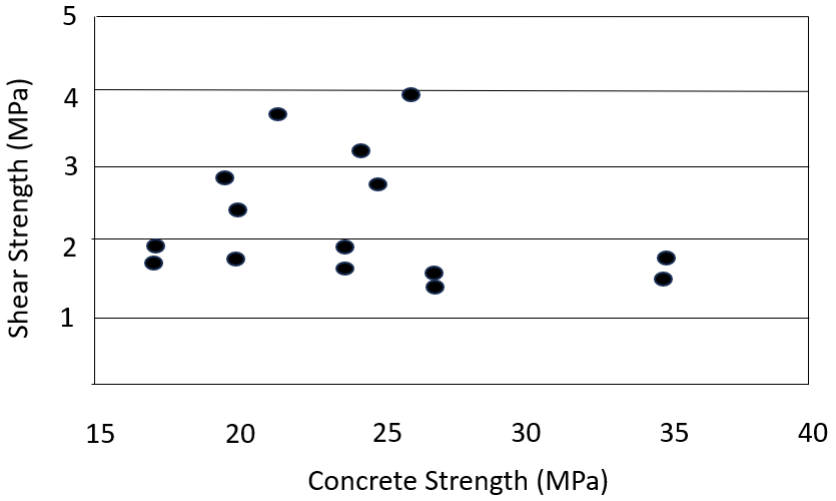

Figure 2.11: Effect of concrete strength on horizontal shear strength (reproduced from Patnaik 2001)

2.4.4 Stirrup reinforcement

Mattock and Hawkins (1972) studied the effect of reinforcement crossing the shear plane. Parameter pf_y was used to investigate this effect on shear capacity as p represents the shear reinforcement ratio crossing the shear plane. The study included the bar diameter and spacing change while yielding strength was constant. Additional steel was added in the 2L-shaped blocks away from the shear plane to ensure that failure occurs at the shear plane. It was concluded that shear capacity remains constant unless there is a change in p or f_y. This study, along with Saemann and Washa (1964), Birkeland and Birkeland (1966), Badoux and Hulsbos (1967), Hofbeck et al. (1969), Mattock and Hawkins (1972), Kahn and Mitchell (2002), and Mansur et al. (2008) noticed that the increase in steel area across the joint increases shear strength.

2.4.5 Dowel action

Dowel action of reinforcement crossing the shear plane was studied by Hofbeck et al. (1969) on pre-cracked and non-cracked specimens. Rubber sleeves covered stirrups for four specimens out of 38 to prevent the dowel action. This was done to compare the effect of the dowel action on shear capacity. Research results indicated that, on the one hand, the dowel action has no considerable

effect on shear strength for uncracked concrete. On the other hand, dowel action considerably affected the shear strength of initially cracked specimens.

2.4.6 Span to depth ratio

Saemann and Washa (1964) tested 42 T-beams and Badoux and Hulsbos, (1967) tested 29 T-beams as well to investigate the effect of shear span to depth ratio ($^{a}/_{d}$) along with other parameters. Shear span (a) is the distance from the reaction to the first applied concentrated load on the beam Authors concluded that the crack is more likely to occur in specimen's joint at a lower load when the ($^{a}/_{d}$) becomes higher. Accordingly, the shear strength is reversely proportional to the span-to-depth ratio.

2.5 Research on Horizontal Shear using GFRP:

Connor and Kim (2016) proposed a shear-friction model for sand coated GFRP reinforcement. Four main parameters were the core of this study: crack parameters, slip, width, and orientation angle of reinforcing bars crossing the crack plane. Nine push-off specimens with different steel orientation (45, 90, and 135 degree) using GFRP and conventional reinforcements as shown in Figure 2.12 to evaluate the strength provided by concrete interlock and reinforcement.

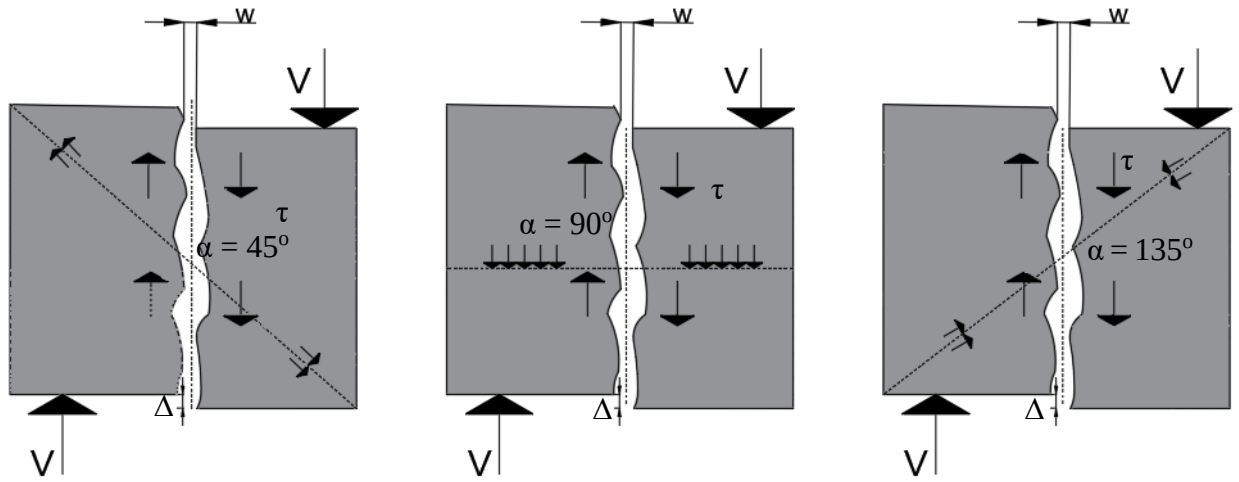

(a) (b) (c)

Figure 2.12: Push off specimens with different reinforcement orientation (reproduced from Conor and Kim 2016)

It was noticed that shear behaviour depends on the crack width. Shear stress can be expressed as a function of crack width *w* crack slip Δ, and orientation angle. Total shear stress is the summation of steel and concrete stresses. The following equation was proposed as a model for shear friction by concrete and reinforcements:

$$\tau\ (\Delta, w) = \ \theta 1\ (0.707\ + cos\alpha)\ pf_{fu}\ \varphi\ + \sigma_{pu}\ (\mu'^{\theta_2}\ A_x + \ \ \Upsilon^{\theta_3}\ A_y) \qquad \text{Equation 2-7}$$

and found that the term $\mu'^{\theta_2}\ A_x$ equals zero. Values of coefficients are shown in Table 2.3.

Table 2.3: Connor and Kim (2016) model coefficients value

Specimens ID	MLE			Coefficients ($\rho f_{fu}\varphi$, A_x, A_y)		
	θ_1	θ_2	θ_3	$\theta_1\ (0.707\ + cos\ \alpha)$	Υ^{θ_3}	μ'^{θ_2}
G45 series	0.84	25	1.66	1.2	0.37	0
G90 series	0.86	25	0.81	0.6	0.62	0
G135 series	0	55	0.36	0	0.82	0

The authors concluded that failure in GFRP was related to the dowel mechanism, which is influenced by crack width and slip. It was also found that GFRP shear strength increases steadily with the gradual increase of crack and slip. On the other hand, steel gained strength rapidly.

2.6 International Friction Shear Code Provisions for Steel-RC Structures:

In this section, Design requirements for friction shear in North America codes will be presented. Current codes and guidelines have no provisions on shear friction for FRP-RC structures.

2.6.1 ACI 318-19 (ACI 2019)

Horizontal shear for concrete in elastic phase (uncracked) can be calculated using the following equation:

$$v = VQ/Ib \qquad \text{Equation 2-8}$$

Minimum reinforcement for horizontal shear transfer shall be the greater of:

- $0.062\sqrt{f_c}\,\frac{b_w\,s}{f_y}$
- $0.35\,\frac{b_w\,s}{f_y}$
- The spacing of the reinforcement shall be the lesser of 600mm and four times the least dimension of the supported element.

The code proposed an equation based on Birkeland and Birkeland (1966) assumptions to calculate the Horizontal shear strength for reinforcement perpendicular to the shear plane as the following:

$$V_n = \mu A_{vf}\, f_y \qquad \text{Equation 2-9}$$

Where:

A_{vf}: Reinforcement area crossing the assumed shear plane to resist shear.

μ: coefficient of friction that depends on contact surface condition as per Table 2.4.

which depends on the parameter λ as shown in Table 2.5.

Table 2.4 Values of coefficient of friction μ as per ACI 318-19 (ACI 2019)

Contact surface condition	Coefficient of friction μ
Concrete placed monolithically	1.4 λ
Concrete placed against hardened concrete that is clean, free of laitance, and intentionally roughened to a full amplitude of approximately 6 mm	1.0 λ
Concrete placed against hardened concrete that is clean, free of laitance, and not intentionally roughened	0.6 λ
Concrete placed against as-rolled structural steel that is clean, free of paint, and with shear transferred across the contact surface by headed studs or by welded deformed bars or wires	0.7 λ

Table 2.5: Values of λ as per ACI-318-19

Concrete	Composition of aggregates	λ
All-lightweight	Fine: ASTM C330M Coarse: ASTM C330M	0.75
Lightweight, fine blend	Fine: Combination of ASTM C330M and C33M Coarse: ASTM C330M	0.75 to 0.85[1]
Sand-lightweight	Fine: ASTM C33M Coarse: ASTM C330M	0.85
Sand-lightweight, coarse blend	Fine: ASTM C33M Coarse: Combination of ASTM C330M and C33M	0.85 to 1[2]

[1] Linear interpolation from 0.75 to 0.85 is permitted based on the absolute volume of normal weight fine aggregate as a fraction of the total absolute volume of fine aggregate.

[2] Linear interpolation from 0.85 to 1 is permitted based on the absolute volume of normal weight coarse aggregate as a fraction of the total absolute volume of aggregate.

For inclined shear plane, Mattock's equation is used to calculate the nominal shear strength:

$$V_n = A_{vf}\, f_y\, (\mu sin\alpha + cos\alpha) \qquad \text{Equation 2-10}$$

Where α**:** angle between shear-friction reinforcement and assumed shear plane.

Table 2.6 depicts the maximum values above which the previous equations become nonconservative.

Table 2.6: Maximum V_n value as per ACI-318-19

Condition	Maximum V_n		
Normal weight concrete placed monolithically or placed against hardened concrete intentionally roughened to a full amplitude of approximately 6 mm.	Least of (a), (b), and(c)	$0.2\, f_{c'} A_c$	(a)
		$(3.3+0.08\, f_{c'})\, A_c$	(b)
		$11 A_c$	(c)
Other cases	Lesser of (d) and (e)	$0.2\, f_{c'} A_c$	(d)
		$5.5\, A_c$	(e)

2.6.2 CSA A23.3-19 (CSA 2019a)

A crack shall be considered a long the shear plane and all of cohesion and friction maintained by the reinforcement crossing the shear plane are responsible to resist the relative displacement. The code proposed the following equation to calculate the factored shear resistance:

$$V_r = \lambda \emptyset_c (c + \mu\sigma) + \emptyset_s\, \rho_v f_y\, cos\alpha_f \qquad \text{Equation 2-11}$$

Where $\lambda \emptyset c(c + \mu\sigma)$ shall not exceed $0.25 \emptyset_c f'_c$ or 6.5 MPa, α_f is the angle between the shear friction reinforcement and the shear plane, and C and μ are the cohesion stress and the friction coefficient at the interface, respectively. Values of C and μ depend on the interface condition and given as shown in Table 2.7.

Table 2.7: Values of *c* and μ as in CSA A.23.3-19 (CSA 2019a)

Surface condition	*c* (MPa)	*μ*
Concrete placed against hardened concrete with the surface clean but not intentionally roughened	0.25	0.60
For concrete placed against hardened concrete with the surface clean and intentionally roughened to a full amplitude of at least 5 mm and a spacing of about 15mm	0.50	1.00
Concrete placed monolithically	1.00	1.40
Concrete placed against as-rolled structural steel with headed studs or reinforcing bars	0.00	0.60

Moreover, CSA A23.3 proposed an alternative equation to find the factored shear resistance for concrete placed monolithically or against hardened concrete with cleaned and intentionally roughened surface with at least of 5.0 mm amplitude as follow:

$$v_f = \lambda \emptyset c k \sqrt{\sigma f_{c'}} + \emptyset s \rho_v f_y \cos\alpha_f \quad \text{Equation 2-12}$$

Where:

k = 0.5 for concrete placed against placed hardened.

k = 0.6 for concrete placed monolithically.

$$\sigma = \rho_v f_y \sin\alpha_f + \frac{N}{A_g} \quad \text{Equation 2-13}$$

N = unfactored permanent load perpendicular on the shear plane. Positive for compression and negative for tension.

$$\rho_v = \frac{A_{vf}}{A_{cv}} \quad \text{Equation 2-14}$$

2.7 Available Design Models for FRP Friction Shear Reinforcement

2.7.1 CSA S6-19 (CSA 2019b)

The model provided by these standards adopts the same formula used for steel replacing the yielding stress (f_y) with $E_f \times \varepsilon_f$, where ε_f = 0.004. the model requires that a crack shall be considered along the shear plane and that cohesion and friction, maintained by the reinforcement crossing the shear plane, are responsible for resisting the relative displacement. The standards proposed the following equations to calculate the factored shear resistance:

$$v = \phi_c(c + \mu\,\sigma) \qquad \text{Equation 2-15}$$

$$\sigma = \rho_v E_f \varepsilon_f + \frac{N}{A_{cv}} \qquad \text{Equation 2-16}$$

$$\rho_v = \frac{A_{vf}}{A_{cv}} \qquad \text{Equation 2-17}$$

where $\phi_c(c + \mu\,\sigma)$ shall not exceed 0.25 $\phi_c\ f'_c$ or 6.5 MPa. Values of c and μ are the same as adopted for steel shown in Table 2.7.

2.7.2 Alkatan (2016)

This model was developed based on cold joint push-off specimens initially uncracked. The model incorparates the term proposed by Birkeland and Birkeland (1966) and Mast (1968) assuming a rough interface with a coeficient of friction of 1.0. In addition, cohesion and bond contributions were represented by a term related to the concrete strength (0.04 f'_c).

$$v_u = 0.04\,f'_c + \varepsilon_{FRP}\,E_{FRP}\,\rho_v\,sin\,\alpha_f + \varepsilon_{FRP}\,E_{FRP}\,\rho_v\,cos\,\alpha_f \qquad \text{Equation 2-18}$$

Where $0.04\,f'_c + \varepsilon_{FRP}\,E_{FRP}\,\rho_v\,sin\,\alpha_f < 0.25\,f'_c$ and where ε_f = 0.005.

2.8 Research Gaps

The demand for FRP reinforcement to overcome the corrosion problem and reduce maintenance costs has increased. Though the use of conventional steel as friction shear reinforcement has been extensively investigated. The behaviour of FRP under friction shear has yet to be clarified. Current FRP design codes and guidelines, such as CSA S806-12 (CSA 2021) and ACI 440.11-22 (ACI 2022), have no design equations to predict the friction shear in concrete composite elements due to the lack of experiments. Based on the precedent literature, the effect of several parameters was not studied for FRP shear connectors, and no design models are developed to predict the interface-shear capacity when FRP connectors are used. Therefore, this pioneering study will investigate the effect of different design parameters on FRP when used as shear connectors to resist friction shear.

CAPTER 3. GFRP BARS AS FRICTION SHEAR REINFORCEMENT FOR CONCRETE COLD JOINTS

Authors and Affiliations

- Basel H. Aljada, M.Sc. Student, Department of Civil Engineering, University of Manitoba.
- Amr El-Ragaby, Associate Professor, Department of Civil Engineering, University of Wisconsin-Platteville.
- Ehab F. El-Salakawy, Professor, Department of Civil Engineering, University of Manitoba.

Journal and Status

ACI Structural Journal, under review.

Reference:
Aljada, B.H., El-Ragaby, A., and El-Salakawy, E.F. "GFRP Bars as Friction Shear reinforcement for Concrete Cold Joints," ACI Structural Journal.

Note:

The manuscript had been slightly edited from the original paper by renumbering the tables and figures to include the chapter number. The abbreviations of the specimen names are explained in the Appendix A under Section A.1. In addition, the reference list and list of notations have been moved to the appropriate sections in the thesis as indicated in the Table of Contents.

3.1 Abstract

Concrete composite elements are susceptible to friction shear stresses at the junction. Therefore, shear connectors are provided at the concrete joint interface to maintain their integrity. Due to its high tensile strength and non-corrodible nature, glass fiber-reinforced polymer (GFRP) reinforcement can be used as a friction shear reinforcement in such elements. Fifteen push-off specimens were constructed and tested to failure. The specimen consisted of two L-shaped blocks cast at two stages to provide the cold joint interface. The main test parameters were the type, shape, and ratio of friction shear reinforcement and concrete strength. It was demonstrated that GFRP-reinforced concrete (RC) specimens with reinforcement ratios of 0.36% or more could resist the friction shear stresses similarly to their steel-RC counterparts. Also, increasing the concrete strength increased the friction shear capacity significantly. Moreover, the design model in the Canadian Highway Bridge Design Code resulted in very conservative predictions.

Keywords: Cold joint, composite elements, friction shear, glass fiber-reinforced polymers (GFRP), push-off, shear connectors.

3.2 Introduction

Composite members have been utilized as an economical way to produce smaller, shallower, and lighter structures (Loov and Patnaik, 1994). In addition, composite members have proven efficiency for accelerating construction, which ultimately results in cost savings. A concrete composite element usually comprises a pre-cast girder and a cast-in-situ slab. These elements are prone to friction shear induced by the gravity loads that cause slipping, which leads to a complete separation between the girder and the slab, and consequently, the member will not behave as a single unit. The strength in a concrete-to-concrete interface is provided by adhesion or cohesion, aggregate interlock, and the clamping stresses by the interface's reinforcement crossing (Zilch and Reinecke, 2000). These factors ensure the composite element requirements and act as the same monolithic members.

Composite concrete members with conventional steel at the interface were extensively studied and proved their efficacy. Moreover, design guidelines are provided in different building codes such as ACI 318-19 (ACI, 2019) and CSA A23.3-19 (CSA 2019a). However, steel reinforcement corrosion is the principal reason for the structural deterioration of reinforced concrete (RC) structures. As a result, the overall capacity decreases, and the requirement for rehabilitation increases, especially for structures subjected to severe environmental conditions. As a non-corrosive material, FRP has been investigated for application in beams, slabs, and columns as flexural and shear reinforcement (El-Sayed et al., 2005). On the other hand, the application of glass fiber-reinforced polymers (GFRP) as a friction shear reinforcement in concrete composite elements still needs to be thoroughly investigated. The shear reinforcement ratio effect has been extensively investigated for steel-RC composite elements, which indicated that the increase in steel area across the joint results in an increase in shear strength (Badoux and Hulsbos, 1967; Birkeland and Birkeland, 1966; Hofbeck et al., 1969; Mansur et al., 2008;

Mattock and Hawkins, 1972; Loov and Patnaik, 1994; Saemann and Washa, 1964; and Rahal et al. 2016).

The effect of concrete strength is a controversial point in the literature. Previous studies by Anderson (1960), Loov and Patnaik (1994), and Mansur et al.(2008) showed that the increase in concrete strength increases the shear capacity. Conversely, Hofbeck et al. (1969) and Mattock and Hawkins (1972) concluded that the concrete compressive strength effect depends on the reinforcement ratio crossing the shear plane. In other words, the shear capacity is not affected by concrete strength below a specific shear-friction reinforcement limit, while it increases above this limit. Saemann and Washa(1964) found that the increase in concrete strength has no considerable effect on shear strength. Patnaik(2001) attempted to predict the relation between concrete compressive strength and shear strength based on the testing results of 15 composite beams. It was found that the effect of concrete strength on shear strength is not following any trend. Gohnert (2003) recommended not to relate the friction-shear capacity with the concrete strength.

The anisotropic properties and lower modulus of elasticity of GFRP weaken the interlaminar shear capacity. Due to the lack of experiments, GFRP as shear connectors is not yet adopted by GFRP building codes such as CSA S806-12(CSA 2021) and ACI 440.11-22 (ACI Committee 440, 2022). In contrast, CSA S6-19 (CSA 2019b) includes design provisions for this phenomenon. Previous studies (Badoux and Hulsbos, 1967; Birkeland and Birkeland, 1966; Hofbeck et al., 1969; Mast (1968), and Loov and Patnaik, 1994) and design codes; ACI 318-19 (ACI 2019) and CSA A23.3-19 (CSA 2019a) assumed that steel shear reinforcement yields at failure. Such an assumption contradicts GFRP characteristics, which fails by rapture without any yielding plateau(Connor and Kim, 2016). As such, available design guidelines for steel-RC are not applicable to GFRP-RC counterparts.

Limited studies were performed using GFRP as friction shear reinforcement. Thus, only the Canadian Highway Bridge Design code (CSA S6-19) permits using FRP in this application. Another model was proposed based on experimental studies. The models are discussed below.

3.2.1 Canadian standards CSA S6-19 (CSA 2019b)

The model provided by these standards adopts the same formula used for steel replacing the yielding stress (f_y) with $E_f \times \varepsilon_f$, where ε_f = 0.004. the model requires that a crack shall be considered along the shear plane and that cohesion and friction, maintained by the reinforcement crossing the shear plane, are responsible for resisting the relative displacement. The standards propose the following equations to calculate the factored shear resistance:

$$v = \phi_c(c + \mu\,\sigma) \qquad \text{Equation 3-1}$$

$$\sigma = \rho_v E_f \varepsilon_f + \frac{N}{A_{cv}} \qquad \text{Equation 3-2}$$

$$\rho_v = \frac{A_{vf}}{A_{cv}} \qquad \text{Equation 3-3}$$

where $\phi_c(c + \mu\,\sigma)$ shall not exceed 0.25 $\phi_c\ f'_c$. Values of c and μ depend on the interface condition, which are given in Table 3.1.

Table 3.1:Values of c and μ as in CSA S6-19 (CSA 2019b)

Surface condition	c (MPa)	μ
Concrete placed against hardened concrete with the surface clean but not intentionally roughened	0.25	0.60
For concrete placed against hardened concrete with the surface clean and intentionally roughened to a full amplitude of at least 5 mm	0.50	1.00
Concrete placed monolithically	1.00	1.40

3.2.2 Model by Alkatan (2016)

This model was developed based on cold joint push-off specimens initially uncracked. The model incorporates the term proposed by Birkelnad and Birkeland (1966) and Mast (1968) assuming a rough interface with a coefficient of friction of 1.0. In addition, cohesion and bond contributions were represented by a term related to the concrete strength (0.04 f'_c).

$$v_u = 0.04\, f'_c + \varepsilon_{FRP}\, E_{FRP}\, \rho_v\, sin\, \alpha_f + \varepsilon_{FRP}\, E_{FRP}\, \rho_v\, cos\, \alpha_f \quad \text{Equation 3-4}$$

where ε_{FRP} = 0.005

$$\text{and } 0.04\, f'_c + \varepsilon_{FRP}\, E_{FRP}\, \rho_v\, sin\, \alpha_f < 0.25\, f'_c \quad \text{Equation 3-5}$$

3.3 Research Significance

Despite that the Canadian Highway Bridge Code, CSA S6-19, permits the use of GFRP as friction shear reinforcement, the other North American codes are silent on the use of GFRP reinforcement in such application due to lack of experimental data. This paper is dedicated to experimentally investigate the feasibility of using GFRP bent bars as friction shear reinforcement. The results are depicted in terms of cracking pattern, load-carrying capacity, reinforcement strain and slipping. In addition, a comparison between the experimental results and the predicted capacities, using the available design provisions, is presented.

3.4 Experimental Investigation

3.4.1 Material properties

All specimens were poured using ready-mixed concrete with a design strength of 35 MPa or 70 MPa for normal and high-strength concrete, respectively, using a maximum aggregate size of 19 mm. On the test day, 100 × 200 mm concrete cylinder samples were tested to determine the actual compressive strength according to ASTM C39-20. No.15 GFRP bars were used for the Z-shaped connectors. Whereas No.10 and No.13 bars were used for the GFRP closed stirrups connectors. Also, No.15M and No.10M steel bars were used for steel Z-shaped and

closed stirrups shear connectors, respectively. No.15M and No.10M were used for steel bars and stirrups away from the shear plane, respectively. The properties of the used bars (GFRP and steel), as provided by the manufacturer or obtained from laboratory tests, are listed in Table 3.2. The mechanical properties of the steel bars were determined in accordance with CSA G30.18-09 (CSA 2019c)

Table 3.2: Mechanical properties of GFRP bent bars.

Bar type	Nominal diameter, (mm)	Bar area, (mm^2)	Modulus of elasticity, (GPa)	Tensile strength, (MPa)	Strain at ultimate, (%)
15M (Steel)	15.9	200	200	460	0.23
10M (Steel)	11.3	100	200	460	0.23
No.15 (GFRP)	15.9	198	54	1,042	1.93%
No.13 (GFRP)	12.7	129	53	1,078	2.03%
No.10 (GFRP)	9.5	72	49	1,125	2.28%

3.4.2 Test specimens

Fifteen large-scale push-off specimens were constructed in the McQuade Heavy Structures Laboratory at the University of Manitoba and tested under monotonic axial load until failure. All specimens were 1,050 mm long, 600 mm wide, and 300 mm thick, resulting in a 400 × 300 mm shear plane of area 120,000 mm^2. Specimens were cast in two stages to simulate the actual condition of the cold joint interface (concrete-concrete). Each specimen comprised two L-shaped concrete blocks, in which the first block was placed with the intended shear connectors projected from the block with no further surface treatment. Seven days later, the second block was placed and connected to the first through the shear connectors. To prevent premature failures other than those along the shear plane, each block was reinforced with No.15

longitudinal bars and No.10 stirrups (steel or GFRP) away from the shear plane. Specimens were classified into three series according to the test parameter. Series I included four specimens reinforced with Z-shaped connectors (steel or GFRP) with two reinforcement ratios, namely, 0.17 or 0.33%. Series II included seven specimens with closed stirrup connectors. Five were reinforced with different GFRP ratios (0.24, 0.36, 0.42, and 0.48%) using different bar diameters and spacings. One was reinforced with No. 10M steel stirrups with 0.33% reinforcement ratio for comparison purposes. and one specimen had no connectors to evaluate the concrete contribution to friction shear resistance. Series III had four specimens with a high-strength concrete (HSC), corresponding to four of the specimens in Series II, to investigate the effect of concrete strength on the overall behaviour. Table 3.3 shows the detailed test matrix where the first character represents connector type (G = GFRP, S = Steel and X = no reinforcement). The second character indicates the number of connectors. The third character represents connector diameter and shape (C = closed stirrups and Z = Z-shaped bar). The last character represents the type of concrete (N = normal-strength concrete, H = high-strength concrete). For example, specimen G4-10C-N has four GFRP connectors produced by two No.10 closed stirrups poured with normal-strength concrete. The details of tested specimens with the different reinforcement configurations, along with the casting stages, are provided in Figures 3.1 and 3.2, respectively.

Table 3.3: Test matrix

Specimen	Series	Target concrete strength, f_c' (MPa)	Connector type	Connector shape	Number of connectors	Reinforcement area (mm^2)	Reinforcement ratio (%)
S1-15Z-N	I	35	15M Steel	Z shape bars	1	200	0.17
S2-15Z-N					2	400	0.33
G1-15Z-N			No.15 GFRP		1	198	0.17
G2-15Z-N					2	396	0.33
X0-000-N	II		N/A	N/A	N/A	N/A	N/A
S4-10C-N			10M Steel	Closed stirrups	4	400	0.33
G4-10C-N			No.10 GFRP		4	288	0.24
G4-10C- N*					4	288	0.24
G6-10C- N					6	432	0.36
G8-10C- N					8	576	0.48
G4-13C-N			No.13 GFRP		4	508	0.42
S4-10C-H	III	70	10M Steel		4	400	0.33
G4-10C-H			No.10 GFRP		4	288	0.24
G6-10C-H					6	432	0.36
G8-10C-H					8	576	0.48

*Replicate specimens using GFRP bars and stirrups in the L-shaped blocks, away from the shear plane.

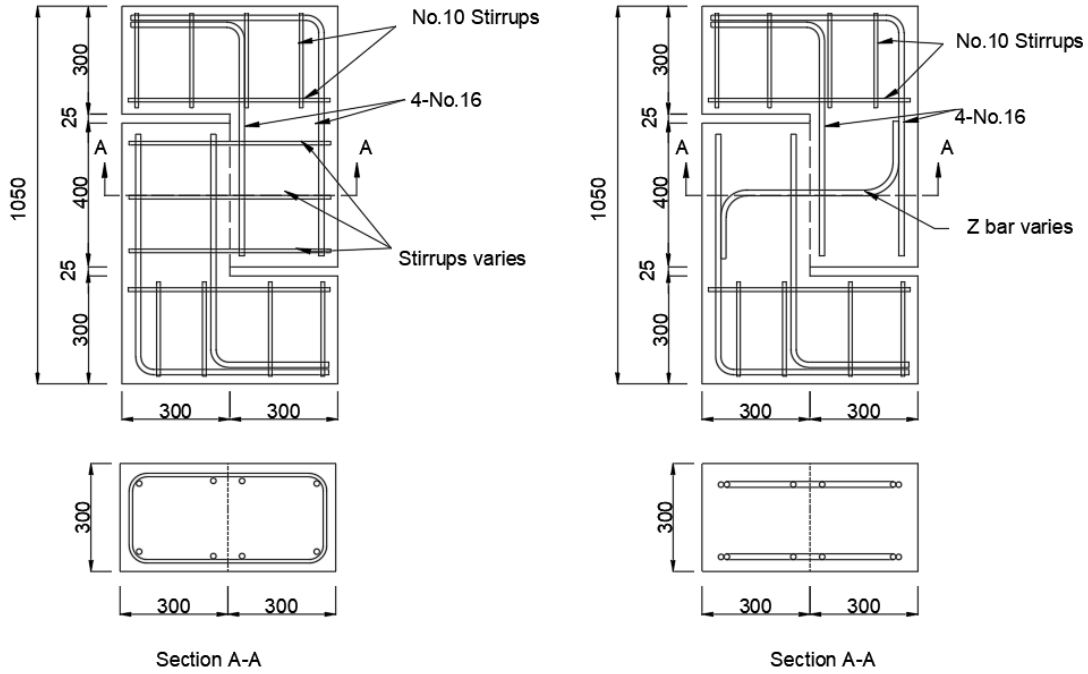

(a) (b)

Figure 3.1:Specimen geometry and reinforcement configurations: (a) Specimens with closed stirrups connectors, and (b) Specimens with Z-shaped connectors

(a) (b)

Figure 3.2: Casting stages, (a) reinforcement for first L-block with the intended connectors, and (b) reinforcement for the second block

3.4.3 Test setup and instrumentation

A 5000-kN capacity hydraulic actuator was used to apply a concentric monotonic load with a displacement-controlled rate of 0.1 mm /minute. A pure shear, without any associated moment,

was induced along the shear plane. Specimens were placed in a vertical position on a concrete block. Two linear variable displacement transducers (LVDTs) were provided on each side of the push-off specimen to measure the slippage of the two L-blocks along the shear plane. One PI-gauge was provided on each side of the specimen at the centre of the shear plane to measure the crack width through the test. Strain gauges were attached to the connectors at the interface to measure strain during testing up to failure. Test setup and instrumentation are shown in Figure 3.3.

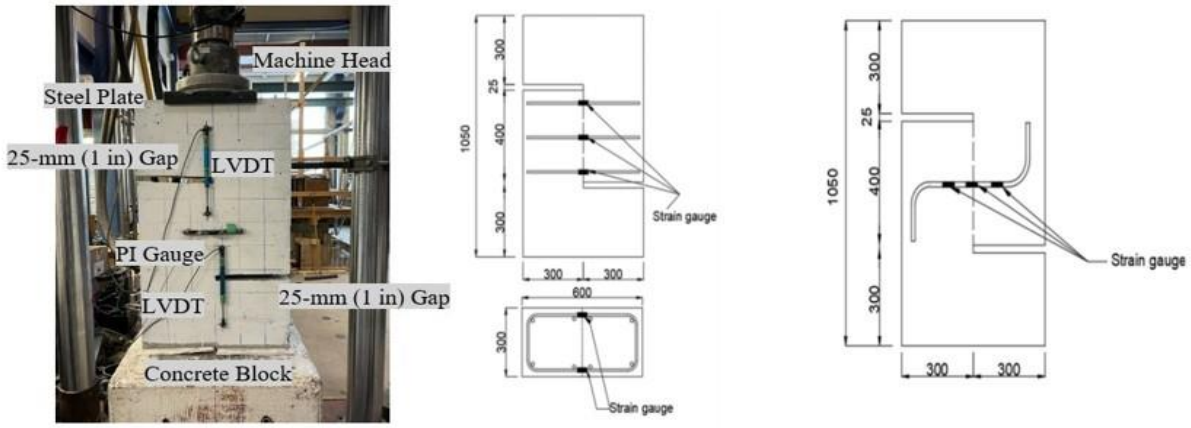

(a) (b) (c)

Figure 3.3:(a) Test set up and instrumentation, (b) strain gauge arrangement for closed stirrups, and (c) strain gauge arrangement for closed stirrups.

3.5 Experimental Results and Discussions

3.5.1 General behaviour, cracking, and mode of failure

Table 3.4 provides the recorded ultimate load capacity, relative slippage, strains in the reinforcement, and residual shear capacity. For all specimens, the development of the main crack corresponding to the peak load was at the shear interface. However, internal cracks (debonding) were initiated before the development of the main interfacial crack as evidenced by the change in the reinforcement strain, which is in good agreement with previous studies (Rahal et al., 2016). The concrete resisted the friction shear stresses up to the interfacial

cracking limit with a negligible reinforcement contribution. This interfacial cracking limit was obtained by testing a specimen with no shear connectors crossing the shear plane (X0-000-N). Between the cracking stage and the peak, shear stresses were resisted by the friction of the surface due to the aggregate interlock, and clamping stresses provided by the connector reinforcement crossing the shear plane. Based on the connector reinforcement ratio, the load-carrying capacity either continued to increase or suddenly dropped when the main crack became visible at the interface. Thus, the general behaviour can be divided into three phases, pre-cracking, post-cracking, and post-peak phase, as shown in Figure 3.4. Concrete strength affected all three phases, whereas reinforcement ratio and shape affected the last two phases.

Table 3.4: Test results

Specimen	Series	Actual concrete strength f_c' (MPa)	Reinforcement ratio (%)	$\boldsymbol{E\rho_v}$ (MPa)	Peak load ($\boldsymbol{V_u}$), (kN)	Residual shear capacity ($\boldsymbol{V_r}$), (kN)	Residual shear capacity as percentage of $\boldsymbol{V_u}$ (%)	Ultimate relative slippage, mm	Strain at peak load ($\mu\boldsymbol{\varepsilon}$)
S1-15Z-N	I	38	0.17	333	304	172	57	0.17	130
S2-15Z-N			0.33	666	322	235	73	0.17	150
G1-15Z-N			0.17	90	298	209	70	0.17	50
G2-15Z-N			0.33	180	308	277	90	0.17	190
X0-000-N	II	36	-	-	293	-	-	0.18	-
S4-10C-N		33	0.33	666	404	254	63	0.33	220
G4-10C-N			0.24	118	399	247	62	0.20	410
G4-10C- N*			0.24	118	387	261	67	0.20	280
G6-10C- N		36	0.36	176	439	342	78	0.21	440
G8-10C- N		33	0.48	235	451	373	83	0.22	500
G4-13C-N		36	0.42	223	419	377	90	0.20	310
S4-10C-H	II	76	0.33	666	1052	392	37	0.82	2600
G4-10C-H			0.24	118	668	303	45	0.49	3900
G6-10C-H			0.36	176	890	389	44	0.66	3600
G8-10C-H			0.48	235	897	427	48	0.74	5000

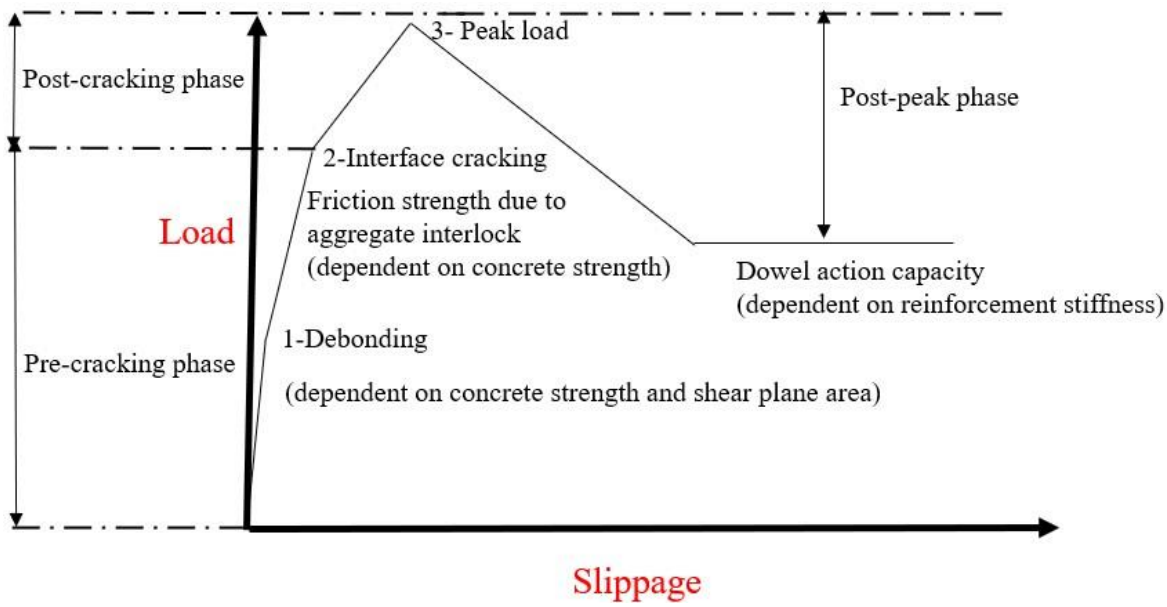

Figure 3.4:Typical load-slip relationship

3.5.2 Pre-cracking phase

A similar pre-cracking behaviour was noticed for all specimens, where the load-slip relationship was bi-linear. In the first part, the load was carried by the adhesion at the interface between the concrete blocks associated with negligible slipping and reinforcement strain. Once the adhesion capacity was reached, debonding of the two concretes (internal cracking) started to occur (point 1 in Figure 3.4), and the shear resistance depended mainly on the friction provided by the aggregate interlock and the cement matrix at the interface with negligible contribution from the reinforcement. The slope of this second portion of the line was less steep than the first part. This phase continued until the main crack was formed (point 2 in Figure 3.4) corresponding to an average stress of 2.9 MPa for the NSC specimens. This phase is mainly dependent on the concrete strength.

3.5.3 Post-cracking phase

This phase started by gradually transferring the load from the concrete to the connector reinforcement, which was evidenced by an increase in reinforcement strain accompanied by increased slipping and interface crack dilatation. The slippage and dilation of the crack induced tensile stresses in the reinforcement, which in turn, activated the clamping force. The connector

reinforcement ratio and shape mainly controlled the post-cracking phase. In other words, the increase in load-carrying capacity after the initiation of the interface crack was contingent on the amount and distribution of connector reinforcement. Furthermore, the effect of dowel action was pronounced and contributed to the overall behaviour for HSC specimens, particularly for the higher reinforcement ratios. This is attributed to the higher slippage values that activated this mechanism. The end of this phase was marked with the full development of a wide visible crack along the interface corresponding to the peak load (point 3 in Figure 3.4).

3.5.4 Post-peak phase

This phase is characterized by sudden load drop accompanied by a noticeable increase in slippage, reinforcement (GFRP or steel) strain, and crack dilation. These deformations were followed by a continuous load drop for the steel-RC specimens due to steel yielding and the degradation of the aggregate interlock. On the other hand, GFRP-RC specimens experienced load regain after the initial drop, which can be attributed to the linear elastic behaviour of GFRP connectors. This phase represents the residual shear load carried merely by the connectors, referred to as dowel action (Liu et al., 2019). This phase ended when the reinforcement rapture occurred, associated with noticeable concrete spalling. The load drop and the residual shear capacity were dependent on reinforcement stiffness rather than concrete strength.

3.5.5 Load-slip behaviour

The load-slip relationship for Series I, II, and III specimens are plotted in Figure 3.5. Series I specimens had similar pre-cracking and post-cracking behaviours with a slip of 0.17 mm at the peak load. This slippage is slightly larger than the 0.13 mm recommended by Hanson (1960) and Saemann and Washa (1964). Afterward, the load dropped suddenly, accompanied by an increase in the slippage rate. Then started to increase till the GFRP rapture. On the other hand, specimens reinforced with steel connectors had different post-peak behaviour due to the different material characteristics. After reaching the peak load, the specimens experienced a

27-43% gradual drop in the load. Then this load was maintained for large slip values more than 10 mm without significant load change which represents the residual shear capacity. Figure 3.6 shows the mode of failure for Series I specimens.

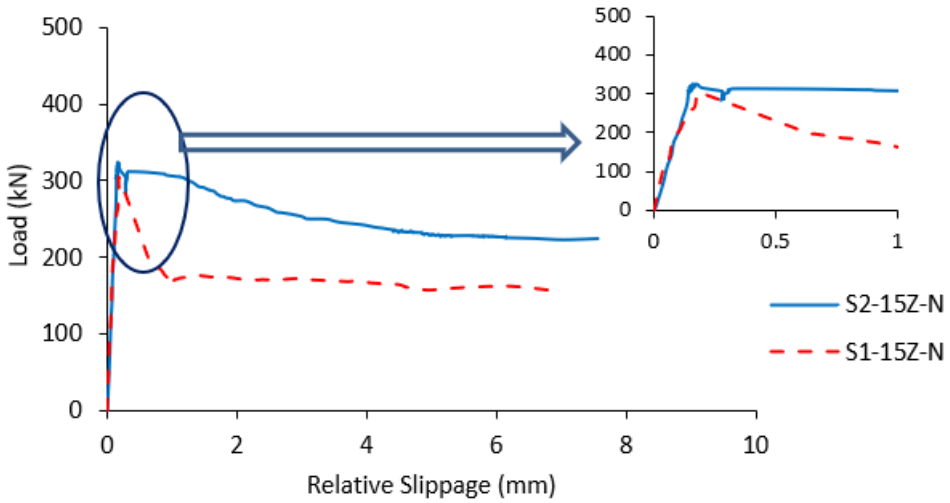

(a)

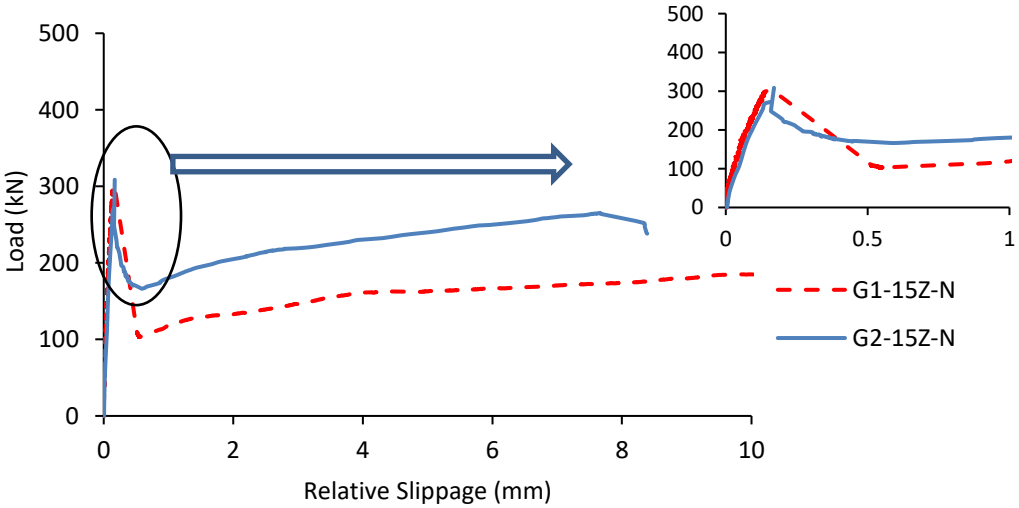

(b)

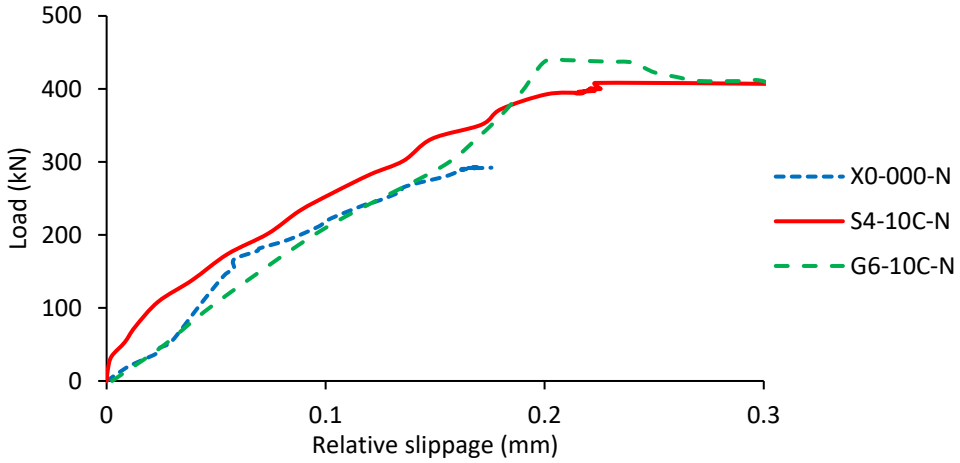
500
400
300
200
100
0
Load (kN)
0
0.1
0.2
0.3
Relative slippage (mm)
X0-000-N
S4-10C-N
G6-10C-N

(c)

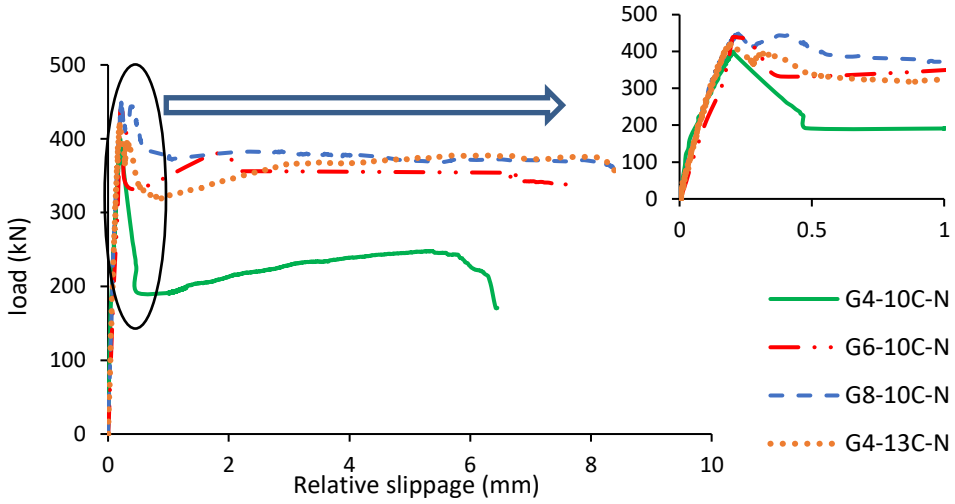
500
400
300
200
100
0
load (kN)
0
2
4
6
8
10
Relative slippage (mm)
0
0.5
1
G4-10C-N
G6-10C-N
G8-10C-N
G4-13C-N

(d)

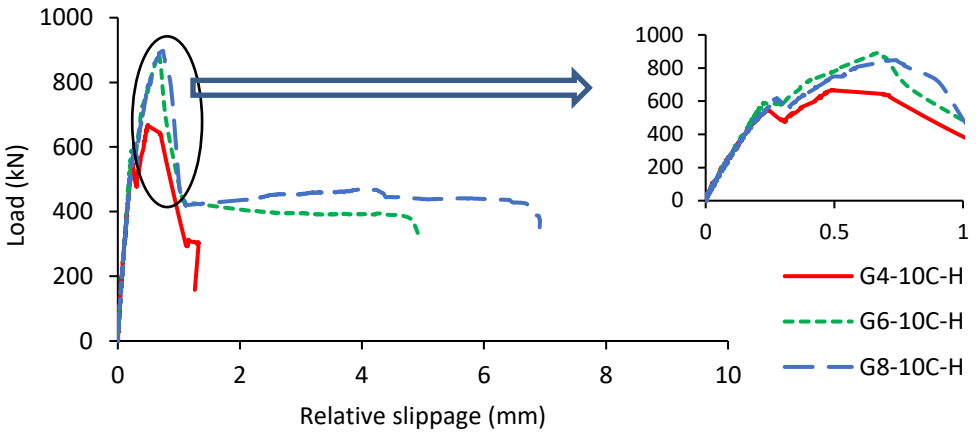

(e)

Figure 3.5: Load-slip relationship: (a) Series I (steel-RC specimens), (b) Series I (GFRP-RC specimens), (c) Series II (GFRP-RC specimens), (d) X0-000-N, G6-10C-N, and S4-10C-N, and (e) Series III (GFRP-RC specimens)

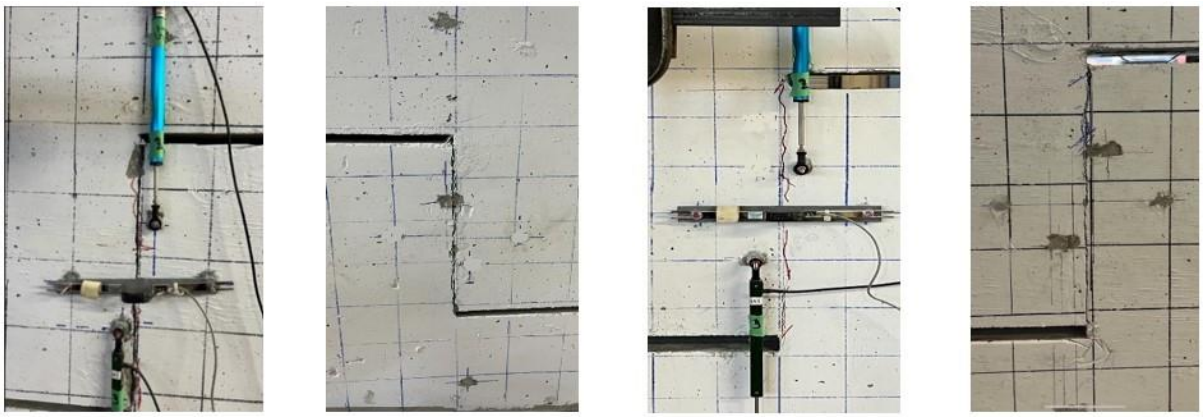

(a) (b) (c) (d)

Figure 3.6: Modes of failure for Series I, (a) G1-15Z-N, (b) G2-15Z-N, (c) S1-15Z-N, and (d) S2-15Z-N

Specimen X0-000-N, without any connectors, failed promptly after the crack formation at a load of 293 kN. All other specimens in Series II showed higher slippages at failure than those in Series I., G4-10C-N, and G4-10C-N* had a relative slippage of 0.20 mm at the peak load. Whereas a slippage of 0.21 and 0.22 mm was observed for G6-10C-N and G8-10C-N, respectively. Specimen G4-13C-N had a reinforcement ratio of 0.42% provided by changing

the stirrups diameter from No. 10 to No. 13. This specimen had a corresponding relative slip of 0.20 mm at the peak load. This value was 0.33 mm for the steel-RC specimen. The post-peak load-carrying capacity for those specimens was similar to those in Series I. Figure 3.7 shows the mode of failure for specimens in Series II.

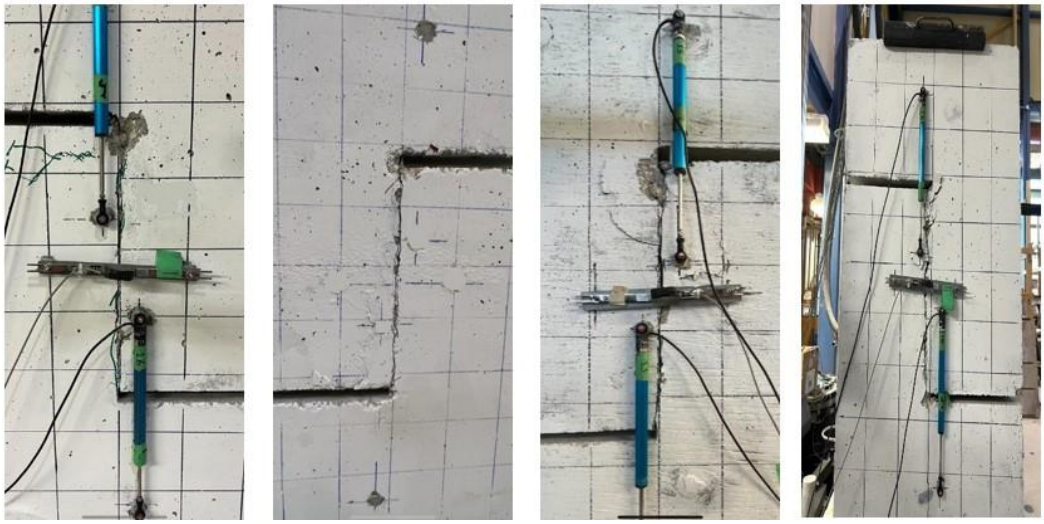

(a) (b) (c) (d)

(e) (f) (g)

Figure 3.7: Modes of failure for Series II: (a) G4-10C-N, (b) G4-10C-N*, (c) G4-13C-N, (d) G6-10C-N, (e) G8-10C-N, (f) X0-000-N, and (g) S4-10C-N.

Series III had a different post-cracking behaviour. All specimens in this series had no change in the slippage rate after the crack formation compared to the previous two series. In addition,

the peak load was reached at larger slippage values after the crack formation. Figure 3.8 shows the mode of failure for the specimens in Series III.

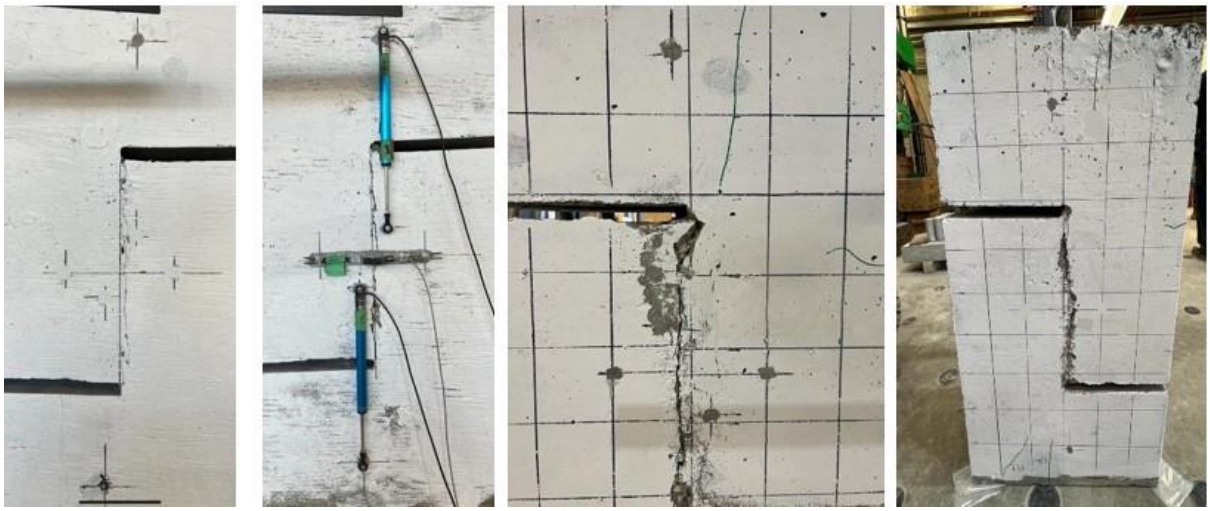

(a) (b) (c) (d)

Figure 3.8: Failure mode for series III: (a) G4-10C-H, (b) G6-10C-H, (c) G8-10C-H, and (d) S4-10C-H

3.5.6 Reinforcement strain

Figure 3.9 shows the load-strain relationship for all test specimens. To further support the above discussion related to the first two phases up to the peak load, Figure 3.9c shows the load-strain relationship for specimen G8-10C-N from Series II as an example. As expected, the reinforcement crossing the shear interface had an insignificant contribution to shear resistance during the pre-cracking phase. Once the main crack initiated, the strain in the connectors increased, which indicated the load transfer to the reinforcement. The measured reinforcement strain at the peak load was 500 με, which is in a good agreement with previous research findings (Harries et al., 2012). For the steel-RC specimen reinforced with one Z-shaped connector in Series I (S1-15Z-N), the reinforcement yielded immediately after reaching the peak load, followed by a continuous load drop. Whereas for the specimen with two steel Z-shaped connectors (S2-15Z-N), the reinforcement did not reach the yielding strain at the peak load and the load drop was less. Once reinforcement reached yielding, the load remained constant until

significant concrete spalling occurred. This may be attributed to the decrease in the crack width with the increased reinforcement ratio, which improved the friction (aggregate interlock) contribution provided by the concrete at the interface. Furthermore, at this phase, the clamping force provided by the reinforcement was not affected by the displacement (Loov and Patnaik,1994 and Kahn and Mitchell, 2002), similar to the observations by Harries et al.27. On the other hand, GFRP connectors exhibited higher strain in the post-peak phase before the rapture of the first GFRP bar. All attached strain gauges were damaged before reinforcement rupture. Yet, reinforcement in both GFRP-RC specimens reached more than 9,000 με.

For Series II, all specimens had higher slippage at the peak load than those of Series I. This indicated that higher strains were induced in reinforcement at cracking leading to higher peak loads than Series I. However, the reinforcement is still believed to have a very small contribution at the pre-cracking phase. All specimens exhibited more than 12,000 με prior the GFRP rapture. Specimen S4-10C-N showed 4,000 με at the dropped constant load.

Series III, with HSC specimens, had a similar pre-cracking behaviour and strain values to those obtained in Series II. However, the load continued to increase after the full development of the interface crack in contrast to what was observed in series I and II. The GFRP-RC specimens in this series exhibited higher strain values of 3,600-5,000 με at the peak load.

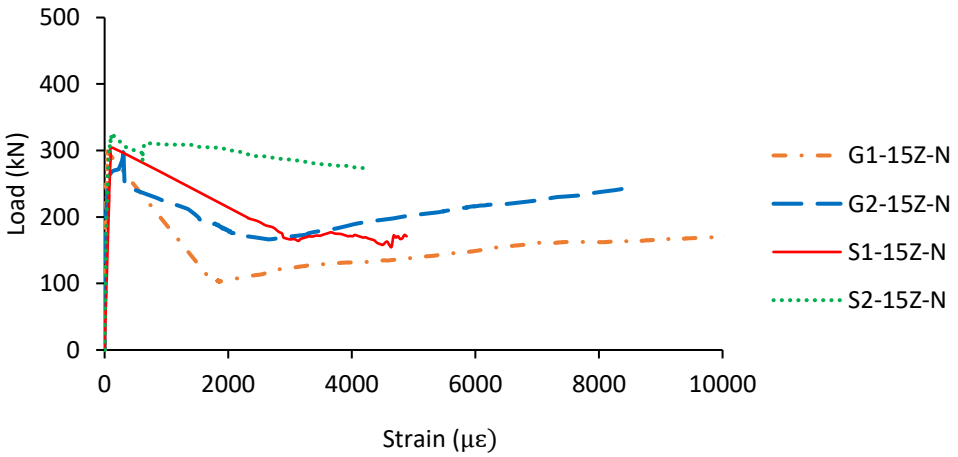

(a)

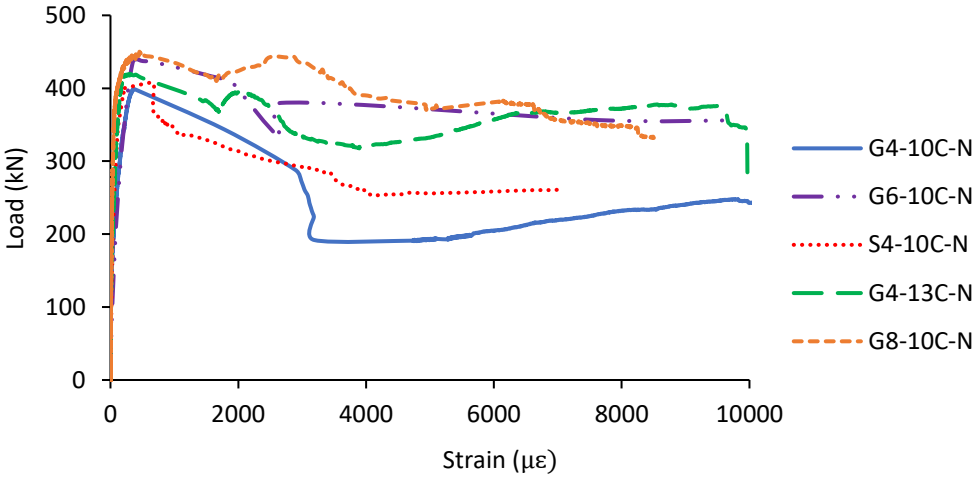

(b)

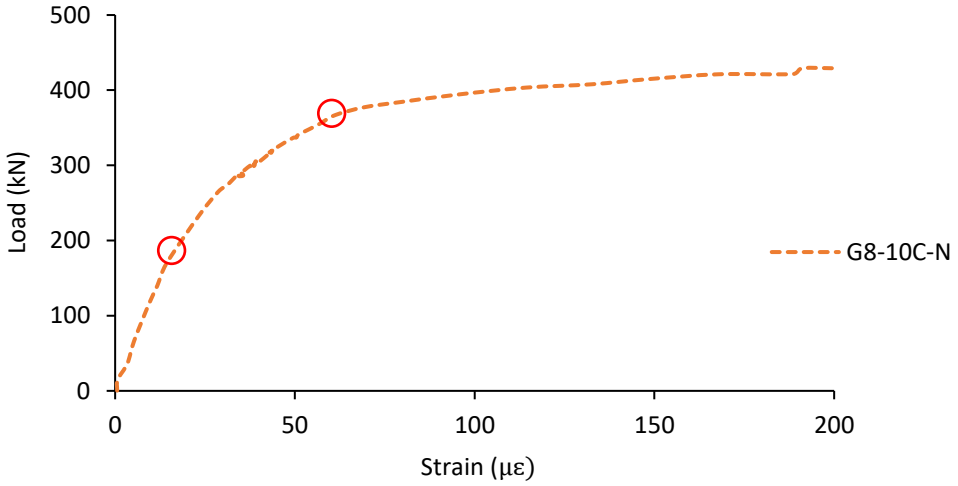

(c)

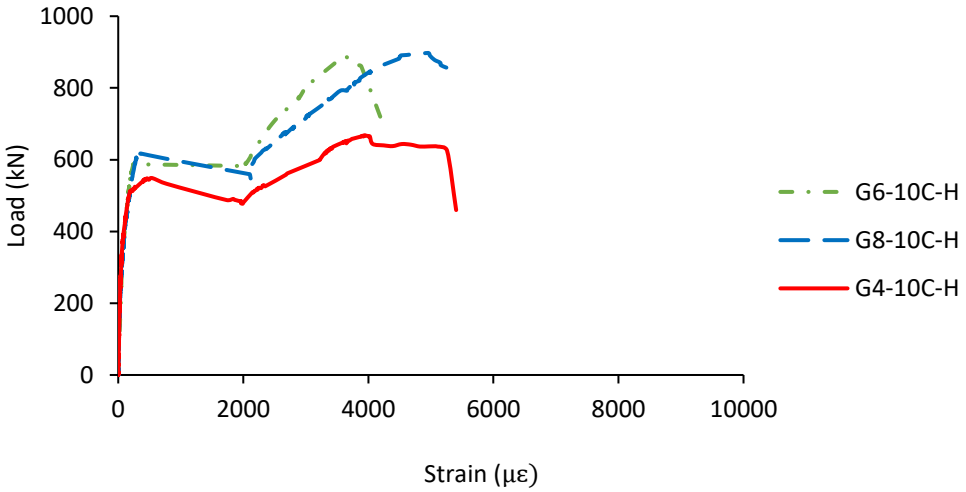

(d)

Figure 3.9: Load-strain relationship: (a) Series I, (b) Series II, (c) zoom in for G8-10C-N, and (d) Series III

3.5.7 Effect of reinforcement stiffness ($E\rho_v$)

Harries et al. (2012) concluded that the reinforcement does not necessarily reach the yielding at the ultimate load, especially for high-strength steel. Thus, it is recommended that the clamping force should be a function of the modulus of elasticity (E), not the yield strength. This phenomenon utilizes the GFRP characteristics of having linear elastic behaviour till failure.

The effect of reinforcement stiffness ($E\rho_v$) will be discussed in terms of the specimens in each group separately. Specimens in Series I had a reinforcement ratio of 0.17 or 0.33 % for both steel and GFRP. The specimens had a similar behaviour of having approximately the same ultimate load that was 2-10% higher than those without interface reinforcement. This demonstrates that the concrete controls the overall friction shear behaviour specifically for such low reinforcement ratios. In other words, the provided reinforcement was not enough to attain additional load capacity after cracking. However, the reinforcement stiffness controlled the amount of load drop and post-peak behaviour. Increasing the reinforcement stiffness from 90 to 180 MPa resulted in a 33% higher residual capacity before the GFRP rapture. Moreover, the higher reinforcement stiffness resulted in a lower load drop after failure and reduced the rate of slippage. Furthermore, even though the reinforcement ratio did not affect the crack width at the crack formation, it significantly reduced the crack width at the maximum post-peak load in G2-15Z-N than G1-15Z-N, which enhanced the concrete contribution due to the aggregate interlock. A similar behaviour was noticed for the steel-RC counterparts.

Specimens in Series II reinforced with closed stirrups with a reinforcement stiffness of 118 MPa had approximately the same average peak of 393 kN, which is 32 – 36% higher than X0-000-N. Compared to G4-10C-N and G4-10C-N*, G6-10C-N, with reinforcement stiffness of 176 MPa, had a 10% higher peak load (439 kN) and a similar post-peak behaviour. In addition, the post-peak load drop was significantly less than the specimens with $E\rho_v$ 176 MPa; from 439

to 322 kN resulting in higher residual shear capacity. Specimens G4-13C-N and G8-10C-N had a higher reinforcement stiffness than G6-10C-N. However, they showed a similar behaviour to the steel-RC specimen in the same series. In other words, those specimens showed a deformable post-peak behaviour with high strain and slippage prior to the GFRP rapture.

To better highlight the effect of replacing steel with GFRP connectors, a comparison was made between three specimens: X0-000-N (unreinforced), S4-10C-N (steel-RC), and G6-10C-N (GFRP-RC with the closest reinforcement ratio to S4-10C-N). Specimen X0-000-N failed immediately after the formation of the main crack at 0.18 mm slippage. The absence of shear connectors at the interface resulted in a sudden and brittle failure where the top block slipped entirely against the bottom one without having any residual capacity. On the other hand, the presence of the shear connectors (steel or GFRP) in S4-10C-N and G6-10C-N provided clamping forces that resulted in increasing the load-carrying capacity by 38 and 49 %, respectively, compared to X0-000-N. In addition, the shear connectors prevented the sudden failure since a gradual load drop accompanied by increased slippage was observed. The difference between steel and GFRP behaviour is discussed later in this paper. Similar behaviour was observed in Series III due to the reinforcement ratio.

3.5.8 Effect of concrete strength

The effect of concrete strength on the friction shear capacity has no consensus in previous studies as discussed in the preceding sections. Thus, the load-slip relationship for specimens with the same reinforcement stiffness (steel or GFRP) in Series II and III was plotted in Figure 3.10. As can be seen in this figure, increasing the concrete strength resulted in a stiffer behaviour but a more brittle failure.

The NSC specimens developed the full interface cracks at peak loads (point 3 in Fig. 3.4) between 387 to 451 kN and slippage between 0.20 to 0.22 mm. Meanwhile, the initiation of the internal cracking (point 2 in Fig. 3.4) started at a significantly lower load (approximately

300 kN) and a low slippage value (0.12 mm). On the other hand, in the HSC specimens, the internal cracks rapidly developed to full interface cracks at loads ranging from 549 to 617 kN, which were 59-82% of the peak loads. This can be attributed to the brittleness of HSC resulting in a sudden transfer of the full load from concrete to reinforcement as shown in Fig. 3.9-d. At this high load level (more than 25% of the peak load of NSC), significant slippage of about 0.3 mm accumulated at the interface. This slippage was about 50% more than the slippage at peak load in NSC specimens. At this large slippage, the exceptional dowel action, in addition to the HSC typical friction of the fully cracked concrete interface maintained by the clamping stress from the shear friction reinforcement, resulted in the load continued to increase reaching significantly higher peak loads than the NSC specimens (Rahal et al., 2016). Specimens G4-10C-H, G6-10C-H and G8-10C-H had a 67, 103, and 99% higher peak load than their counterparts G4-10C-N, G6-10C-N, and G8-10C-N, respectively. The concrete strength effect was more pronounced in the steel-RC specimens as the ultimate load increased by 160%. Also, all HSC specimens showed stiffer behaviour until the cracks became visible. The higher capacity of the steel-RC specimens was due to the higher reinforcement stiffness and dowel action that resisted the load after the crack formation. The reinforcement in this specimen reached the yielding strain before the brittle concrete failure. It can be concluded that the development of the full interface crack represents the capacity of the un-reinforced HSC interface, about 549 to 617 kN. However, despite the significant increase in the shear capacity due to the HSC, it had no noticeable effect on the residual capacity. In other words, the residual capacities for NSC and HSC specimens were close. Similar results were obtained by by Rahal et al. (2016) and Alkatan (2016). The residual capacity was in the range of 250-380 kN depending on the reinforcement ratio, which can be considered as the dowel capacity of the GFRP reinforcements.

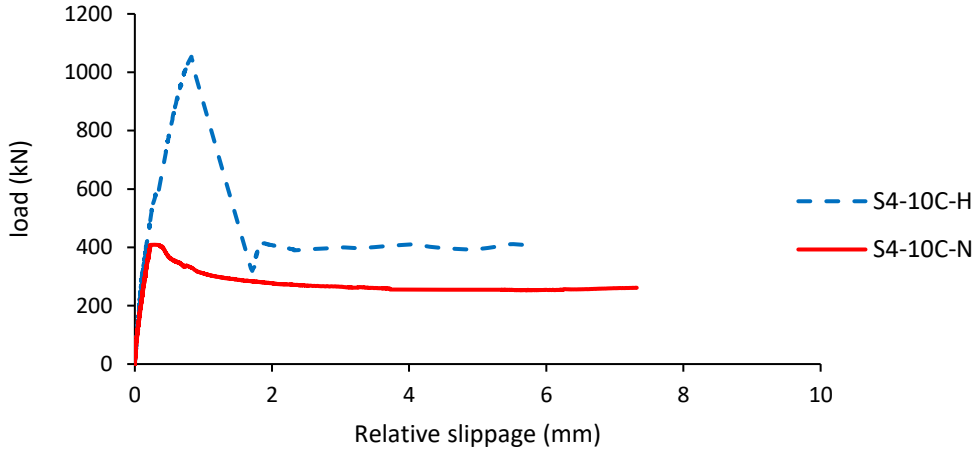
load (kN)
1200
1000
800
600
400
200
0
0
2
4
6
8
10
Relative slippage (mm)
S4-10C-H
S4-10C-N

(a)

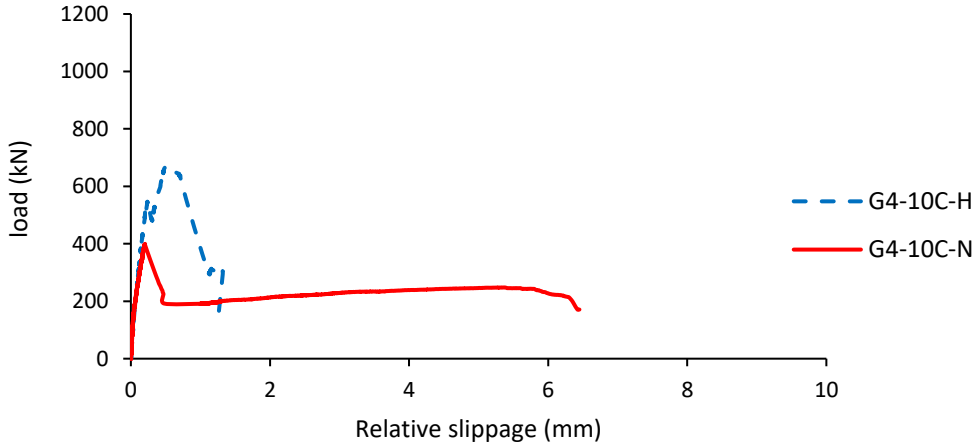
load (kN)
1200
1000
800
600
400
200
0
0
2
4
6
8
10
Relative slippage (mm)
G4-10C-H
G4-10C-N

(b)

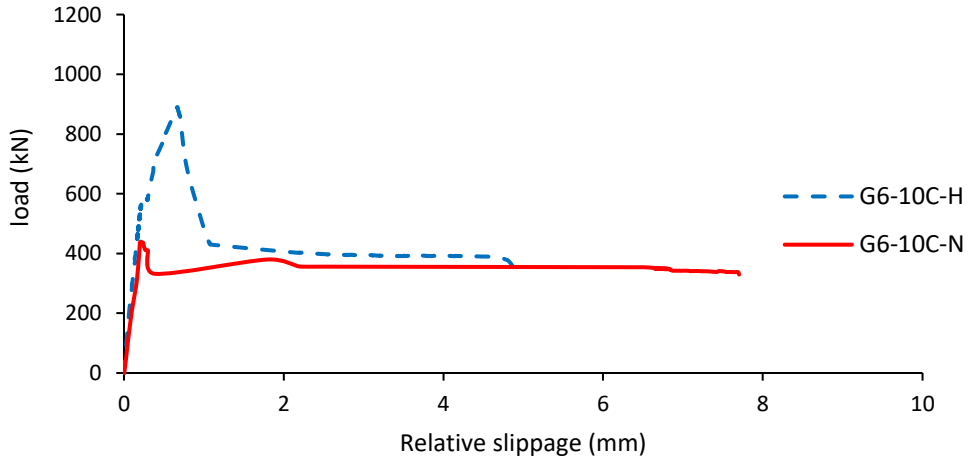
load (kN)
1200
1000
800
600
400
200
0
0
2
4
6
8
10
Relative slippage (mm)
G6-10C-H
G6-10C-N

(c)

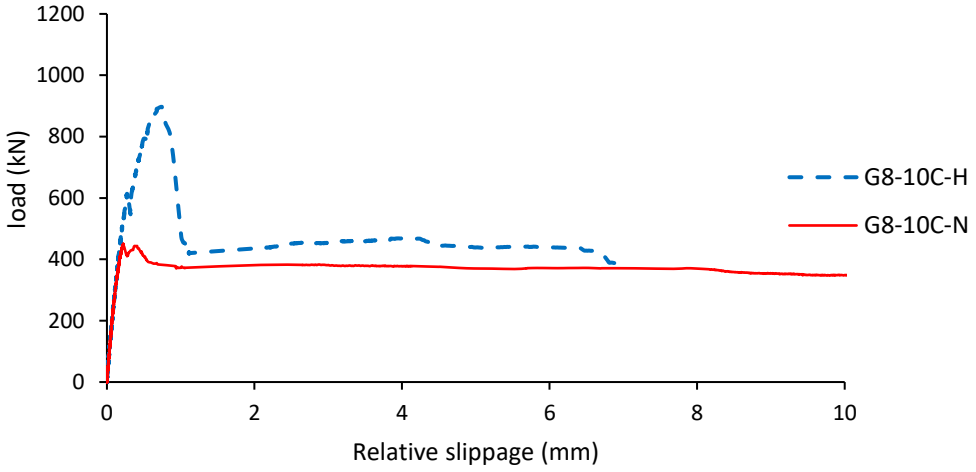

(d)

Figure 3.10: Effect of Concrete strength on the load-slip behaviour: (a) steel (0.33%), (b) GFRP (0.24%), (c) GFRP (0.36%), and (d) GFRP (0.48%)

3.5.9 Effect of reinforcement distribution

Series II steel-RC specimen (S4-10C-N) had a total reinforcement ratio equal to that of Series I (S2-15Z-N). However, produced by more bars with smaller diameters and a different connector shape. On the other hand, GFRP RC specimens had different reinforcement ratios. This configuration seemed to provide better and more uniform clamping force. The load-slip relationship for specimens with Z-shaped and closed stirrups with the closest reinforcement ratio is plotted in Figure 3.11 to explore the effect of the reinforcement shape exclusively. The specimen with three closed stirrups (G6-10C-N) had almost the same reinforcement stiffness as the specimen with two Z-shaped bars (G2-15Z-N). The specimen with closed stirrups had 43 and 23 % higher ultimate load and residual capacity, respectively than the specimen with Z-shaped bars, respectively. The higher load is attributed to the better and uniform distribution of the clamping forces provided by the stirrups. The results showed that the average strain corresponded to the ultimate load in the stirrups was 410 με while it was 190 με for the specimen with the Z-shaped bars. The higher strain was due to the higher slippage exhibited by those specimens that induced higher tension to the shear connectors and higher clamping

stresses accordingly. On the other hand, steel-RC specimens with closed stirrups had approximately 25% higher ultimate load due to the same reason mentioned earlier and the same residual load, which depends primarily on the dowel action.

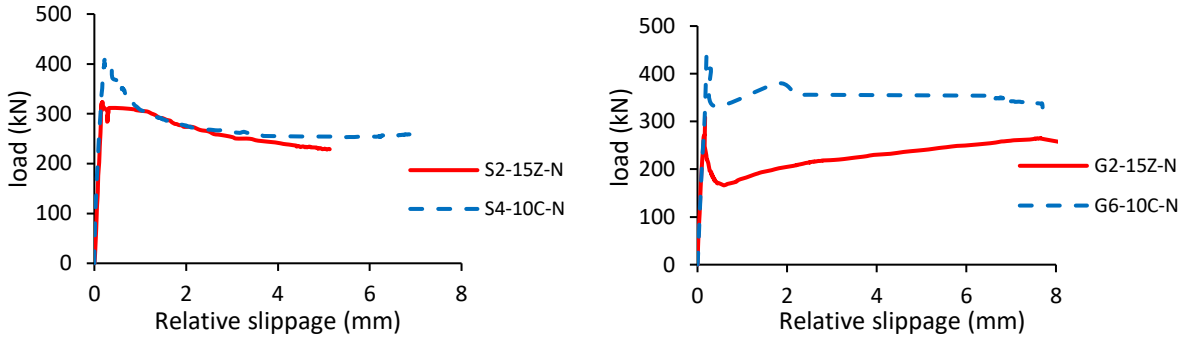

(a) (b)

Figure 3.11: Effect of reinforcement shape and distribution on the load-slip behaviour: (a) steel (0.33%) and (b) GFRP (Z bar, [0.33%] and closed stirrups [0.36%])

3.5.10 Effect of reinforcement type

Series I, II, and III had specimens with similar reinforcement ratios using either steel or GFRP connectors. Figure 3.12 shows the load-slip relationship for those specimens to explore the effect of the reinforcement type solely. An identical pre-cracking behaviour with ultimate loads ranging from 298 to 322 kN were observed in the specimens in these series (steel or GFRP). However, Series I specimens reinforced with steel connectors exhibited a more gradual load drop after cracking. Then, the connectors reached the yielding strain with no significant load change. On the other hand, despite the higher load drop in the GFRP-RC specimens after reaching the ultimate load, yet, due to the linear elastic behaviour of the GFRP, the load started to increase after the drop. It continued to increase, reaching higher loads than the steel-RC counterpart specimens associated with crack widening and increase in the slipping. This trend was more noticeable in higher reinforcement ratios.

In Series II, the GFRP specimen, G6-10C-N, had a lower load drop and a similar post-peak behaviour to the steel-RC with the closest reinforcement ratio, in which the slipping was

increasing without any visible load change. This could be attributed to the reinforcement distribution, as the GFRP RC specimen had more connectors with less bar diameter resulting in a close reinforcement ratio. Furthermore, despite the lower reinforcement stiffness in the GFRP-RC specimen, yet it exhibited 35% higher residual capacity than the steel one. Such a results demonstrates the superior performance for GFRP in this application. Similar behaviour was noticed in Series III specimens at the post-peak phase.

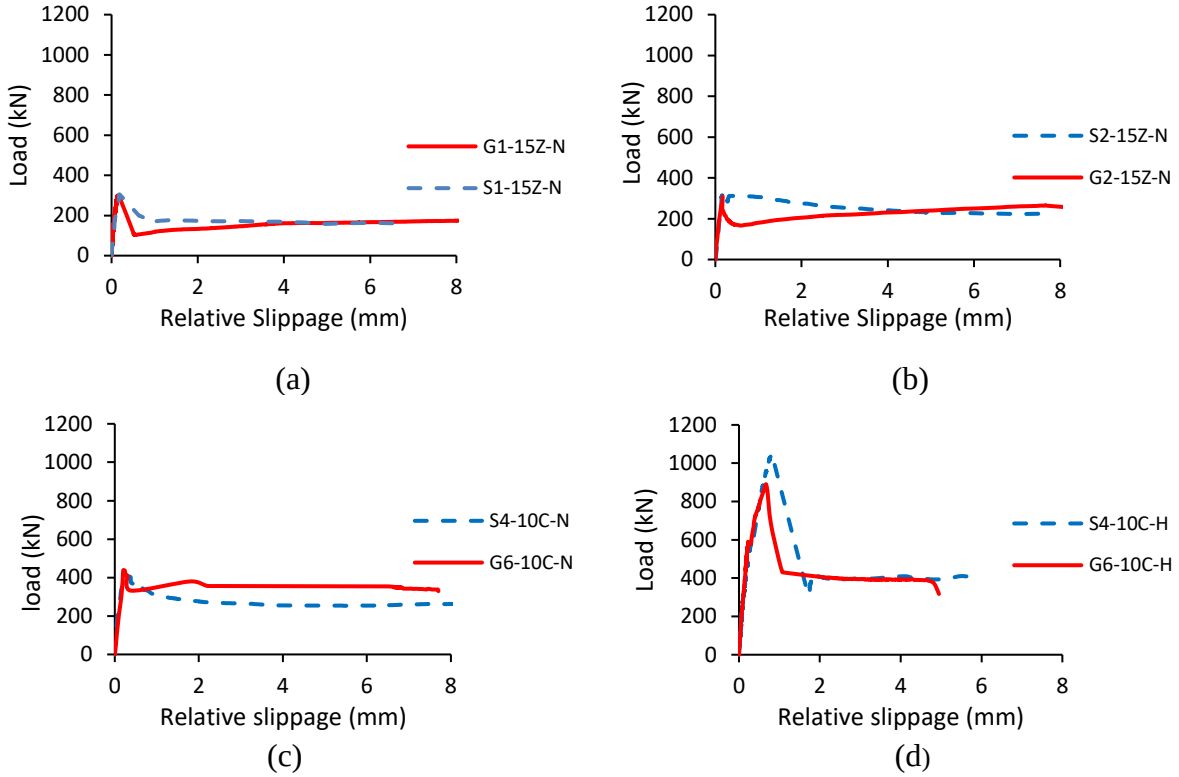

Figure 3.12: Effect of reinforcement type on the load-slip behaviour (a) Z bars (0.17%), (b) Z bars (0.33%), (c) Stirrups with NSC, and (d) stirrups with HSC

3.6 Comparison of Predictions and Experimental Results

The experimental results were compared with the existing models for GFRP connectors. The first model is provided by the CSA S6-19 (CSA 2019b), while the second is the one proposed by Alkatan. Table 3.5 shows that the models underestimate the strength of composite GFRP RC elements. One reason is due to the assumption of crack along the shear occurrence before applying the test which reduces the overall friction shear capacity required by CSA S6-19 (CSA

2019b). On the other hand, Alkatan model does not account for pre-cracking effect and assume the cold joint interface to be rough. Moreover, the model incorporates the concrete strength contribution. Therefore, it showed a better prediction accuracy.

Table 3.5: Comparison with analytical models.

Specimen	Experimental, (kN)	Predicted, (kN)		Experimental / predicted	
		CSA S6-19 (CSA 2019b)	Alkatan (2016)	CSA S6-19 (CSA 2019b)	Alkatan (2016)
S1-15Z-N	304	86	-	3.53	-
S2-15Z-N	322	139	-	2.32	-
G1-15Z-N	298	56	237	5.32	1.26
G2-15Z-N	308	81	289	3.8	1.07
X0-000-N	293	30	-	9.77	-
S4-10C-N	404	139	-	2.91	-
G4-10C-N	399	64	215	6.23	1.74
G4-10C-N*	387	64	215	6.05	1.69
G6-10C- N	439	81	279	5.42	1.57
G8-10C- N	451	98	300	4.6	1.5
G4-13C-N	419	94	306	4.46	1.37
S4-10C-H	1052	139	-	8.42	-
G4-10C-H	668	64	435	10.44	1.54
G6-10C-H	890	81	471	10.99	1.89
G8-10C-H	897	98	506	9.15	1.77
Mean*				6.60	1.53
Standard Deviation*				2.54	0.24
COV (%) *				39	16

*For the GFRP-RC specimens only

3.7 Conclusions

This research presents the results of a novel experimental investigation on the feasibility of using GFRP reinforcement as friction shear reinforcement at the cold joint interface. The study

included testing 15 large-scale push-off specimens under concentric monotonic load to induce pure shear along the interface. The following conclusions were drawn.

1. GFRP stirrups showed an excellent and competitive performance as shear friction reinforcement compared to the steel counterparts.
2. For NSC specimens, the GFRP-RC specimen (G6-10C-N) with the closest reinforcement ratio to the steel-RC one (S4-10C-N) had a 9% higher ultimate load. This percentage was 18% when HSC was used.
3. The NSC specimens reinforced with 0.24 to 0.48% GFRP stirrups as shear friction reinforcement showed 32-54% increase in the peak load compared to the un-reinforced specimen. For HSC specimens using the same reinforcement ratios, this increase was 22-45%.
4. Friction shear capacity is primarily dependent on concrete contribution provided by the aggregate interlock and the cement matrix. Increasing the concrete strength resulted in 43-160% higher shear capacities with stiffer but more brittle behaviour.
5. Specimens with 0.36% or more GFRP reinforcement ratio (reinforcement stiffness of 176 MPa) exhibited large deformations before failure due to the dowel effect, similar to the steel-RC specimens. For the specimens with less than 0.36%, sudden load drop after the peak load occurred.
6. Specimens with reinforcement ratios of 0.42 and 0.48 %, close to the CSA S6-19 CSA S6-19 (CSA 2019b) specified limit of 0.44%, resulted in residual capacities of 83 and 90% of the peak, respectively.
7. The CSA S6-19 (CSA 2019b) design formula showed overly conservative results especially for HSC specimens.

CAPTER 4. GFRP STIRRUPS AS FRICTION SHEAR REINFORCEMENT FOR DIFFERENT CONCRETE INTERFACES

Authors and Affiliations

- Basel H. Aljada, M.Sc. Student, Department of Civil Engineering, University of Manitoba.
- Amr El-Ragaby, Associate Professor, Department of Civil Engineering, University of Wisconsin-Platteville.
- Ehab F. El-Salakawy, Professor, Department of Civil Engineering, University of Manitoba.

Journal and Status

ASCE Journal of Composites for Construction, under review.

Reference:

Aljada, B.H., El-Ragaby, A., and El-Salakawy, E.F. "GFRP Stirrups as Friction Shear Reinforcement for Different Concrete Interfaces" ASCE, Journal of Composites for Construction, under review

Note:

The manuscript had been slightly edited from the original paper by renumbering the tables and figures to include the chapter number. The abbreviations of the specimen names are explained in Appendix A under Section A.1. In addition, the reference list and list of notations have been moved to the appropriate sections in the thesis as indicated in the Table of Contents.

4.1 Abstract

Shear transfer at the concrete-to-concrete interface is vital in concrete structures. Shear friction connectors are utilized at the interface to maintain their structural integrity. Due to the high tensile strength, the linear elastic behavior, and the non-corrodible nature of glass fiber reinforced polymers (GFRP), it can be used as shear friction reinforcement. However, the overall friction shear at the junction greatly depends on the interface condition. Thus, 18 push-off specimens were constructed and tested until failure under monotonic concentric load to evaluate the performance of using GFRP in this application. The main tested parameters were the shear plane conditions (not roughened, roughened cold joint, or monolithic), type (steel or GFRP), and ratio (0.24 to 0.48 %) of reinforcement crossing the shear plane. The monolithic specimens had the highest peak loads. Nevertheless, resulting in more brittle failure. Also, roughening the interface did not affect the overall behavior. Moreover, the conservative coefficient of friction recommended by the Canadian Highway Bridge Design Code based on steel shear friction reinforcement, does not reflect the actual behavior of GFRP.

Keywords: Shear connectors, Glass Fiber Reinforced Polymers (GFRP), friction shear, cold joint, Monolithic, residual loads.

4.2 Introduction

A pre-cast concrete girder and a cast-in-place slab are typical components of concrete composite members. They are adopted in the Accelerated Bridge Construction (ABC) approach to expedite the construction process and consequently reduce the overall cost. Furthermore, they also produce shallower and lighter structures if the strain compatibility at the interface, composite action, is achieved (Loov and Patnaik 1994). Nevertheless, these merits will be achieved only if the friction shear-induced at the interface is counteracted. Friction shear generally causes slippage of the members and may be accompanied by a complete separation. As a result, each element (girder and slab) will resist the load separately without a composite action, as shown in Figure 4.1-a. Reinforcement crossing the shear plane, friction shear reinforcement, is essential to resist the friction shear and maintain the composite action and the structural integrity of the composite elements, as shown in Figure 4.1-b.

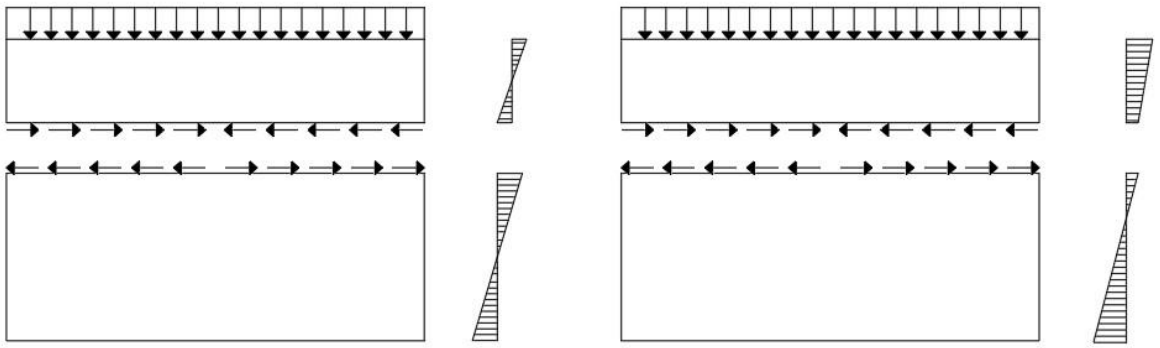

(a) (b)

Figure 4.1: Horizontal shear transfer in composite beams, (a) non composite, and (b) composite.

Birkeland and Birkeland (1966) first introduced the friction shear hypothesis, where the slippage at the interface causes crack widening, and tension stresses in the reinforcement. Accordingly, the reinforcement exerts compression (clamping) stresses on the concrete, which in return, reduces the crack widening and provides frictional resistance along the interface (Santos and Júlio 2012). This phenomenon is known as the clamping stresses. The original

shear friction hypothesis was later developed by several studies and consequently adopted by almost all international building codes (Liu et al. 2019). This hypothesis can be applied to different concrete interfaces, monolithic and cold joints, assuming that shear stresses at the interface are transferred by friction only. Zilch and Reinecke (2000) alleged that three mechanisms resist friction shear at the concrete-to-concrete interface; cohesion or adhesion (τ_a), shear friction (τ_{sf}), and the dowel action provided by the reinforcement crossing the shear plane (τ_{sr}). Figure 4.2 shows the contribution of these three mechanisms. The contribution of each component is dependent on the amount of loading and the corresponding slippage at the interface (*S*).

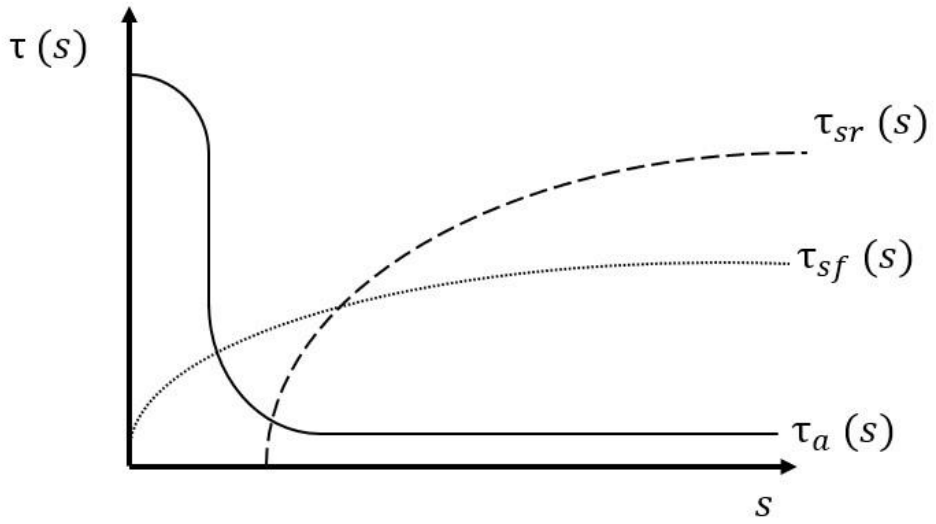

Figure 4.2: Load transfer mechanism (Zilch and Reinecke 2000*)*

Steel reinforcement as friction shear reinforcement has been studied thoroughly and is currently adopted by international design codes (Liu et al. 2019). However, the steel reinforcement is susceptible to corrosion, especially in harsh environments and when de-icing salt is used, resulting in structural deterioration. Thus, utilizing the non-corrodible GFRP with high tensile strength seems to be a viable solution for this application.

GFRP has been extensively studied over the last few decades and has proven efficient in resisting shear and flexural stresses (El-Sayed et al. 2005; Rahman et al. 2017; El-Gendy and

El-Salakawy 2019; Mohamed et al. 2020) and therefore was adopted in several design codes such as ACI-440.11-22 (ACI 2022) and CSA S806-12 (CSA 2021). However, due to a lack of experimental data and analytical models, these design codes did not include design provisions or models for utilizing GFRP as a friction shear reinforcement. Steel-RC codes (ACI 2019; CSA 2019a) and previous studies (Birkeland and Birkeland 1966; Badoux and Hulsbos 1967; Mast 1968; Hofbeck et al. 1969; Loov and Patnaik 1994) are all based on the fact of reinforcement yielding at failure. However, this contradicts the GFRP property of having perfect linear elastic behavior with sudden brittle failure without yielding plateau (Connor and Kim 2016). Accordingly, the available design guidelines of steel-RC members cannot be extended for GFRP applications.

Mattock and Hawkins (1972) studied the effect of steel reinforcement crossing the shear plane. The variable pf_y, where p is the shear reinforcement ratio and f_y is the reinforcement's yielding stress, was used to investigate this effect on shear capacity. Several reinforcement ratios, combinations of different bar diameters and spacings, of constant yielding stress were investigated. This study, along with Saemann and Washa (1964), Birkeland and Birkeland (1966), Badoux and Hulsbos (1967), Hofbeck et al. (1969), Mattock and Hawkins (1972), and Mansur et al. (2008) observed that the increase in reinforcement ratio and/or yielding stress across the joint results in an increase in shear strength.

Furthermore, concrete elements may be placed monolithically or at different times, cold joints. The interface surface condition plays a crucial role in the friction shear capacity. Hanson (1960) investigated this phenomenon through 62 push-off specimens and 10 T-shaped beams. The author concluded that the composite action is assured if the joint integrity between the pre-cast girder and cast-in-situ slab is maintained. The finished surface was intentionally roughened to achieve a 9.5 mm depth. The results have shown the significant effect of rough connection over the smooth connection on shear capacity. Saemann and Washa (1964) tested 42 T-beams with

three levels of roughness: smooth, intermediate, and rough. Intermediate roughness was 3.2 mm, while rough was 9.5mm. Birkeland and Birkeland (1966) and Badoux and Hulsbos (1967) also studied the effect of interface roughness. These studies showed a significant effect of interface roughness on shear capacity, evidenced by higher shear capacity for rough interfaces. Badoux and Hulsbos (1967) reported a 75% increase in shear capacity when using the rough interface. This agrees well with the results of Birkeland and Birkeland (1966), which showed that monolithic casting might provide a shear capacity ranging between 70 and 112% higher than the ordinary construction joint. They also found that intentionally roughened surfaces can provide 40 - 75% more shear capacity than ordinary construction joints. Recent studies by Mattock (2001) and Kahn and Mitchell (2002) reported similar behaviors.

Connor and Kim (2016) investigated crack parameters (slip and width) and orientation angle of reinforcing bars crossing the crack plane. Nine push-off specimens with different reinforcement orientations (45, 90, and 135 degrees) using GFRP and conventional reinforcements were included to evaluate the strength provided by concrete interlock and reinforcement. The authors concluded that shear stress can be expressed as a function of crack width (w), crack slip (Δ), and orientation angle, while the total shear stress is the summation of reinforcement and concrete stresses. In addition, the failure in GFRP bars was related to the dowel mechanism, which is influenced by crack width and slip. It was also found that the shear strength of GFRP-RC specimens increases steadily with the gradual increase of crack and slip. On the other hand, steel gained strength rapidly. The authors did not cover the effect of different parameters, such as reinforcement ratio and shear plane condition.

This paper is a part of ongoing research investigation at the University of Manitoba to evaluate the performance of GFRP bars and stirrups as shear friction reinforcement in concrete elements.

4.3 Experimental Program

4.3.1 Material properties

All specimens were constructed using ready-mixed concrete with a targeted strength of 35 MPa at 28 days, using a maximum aggregate size of 19 mm. However, the actual compressive strength was determined on the test day by testing 100 × 200 mm concrete cylinder samples according to ASTM C39-20. Sand-coated No.10 or No.13 GFRP bent bars were used for the connectors. Also, No.10M steel bars were used for steel shear connectors. No.15 GFRP and No.10 bent bars and stirrups (GFRP or steel) were used away from the shear plane. The properties of the used bars (GFRP and steel), as provided by the manufacturer or obtained from laboratory tests, are listed in Table 4.1.

Table 4.1: Mechanical properties of GFRP bent bars.

Bar type	Nominal diameter (mm)	Bar area (mm^2)	Modulus of elasticity (GPa)	Tensile strength (MPa)	Strain at ultimate, (%)
10M (Steel)	11.3	100	200	460 [a]	0.23 [a]
No.13 (GFRP)	12.7	129 [b] [153] [c]	53 [d]	1,078 [d]	2.03 [d]
No.10 (GFRP)	9.5	72 [b] [82] [c]	49 [d]	1,125 [d]	2.28 [d]

[a] Yield strength for the steel bars determined as per CSA G30.18-09 (CSA 2019b).

[b] Determined as per CSA S807-19 (CSA 2019c).

[c] Measured area by immersion test as per Annex A of CSA S806-12 (CSA 2021).

[d] Measured as per Annex C of CSA S806-12 (CSA 2021).

4.3.2 Test specimens

Eighteen large-scale push-off specimens were constructed and tested under monotonic concentric load until failure. Each specimen comprised two L-shaped concrete blocks in which the block was 725-mm long, 600-mm wide, and 300-mm thick. In addition, a 25 mm gap was provided between the two L-blocks to allow for slippage. As such, the full specimens were 1,050-mm long, 600-mm wide, and 300-mm thick, resulting in a 400 × 300 mm shear plane of

area 12×10^4 mm^2. Each block was reinforced with No.15 longitudinal bars and No.10 stirrups (steel or GFRP) away from the shear plane to prevent premature failures other than those along the shear plane. Specimens were cast either in two stages to simulate the condition of the cold joint interface (concrete-concrete) or monolithically. In the case of cold joint specimens, the first block was placed with the shear connectors projected from the block and the intended surface treatment. For the not roughened concrete interface, the surface was left as is, while for the intentionally roughened one, the concrete surface was chiseled and trowelled to remove the laitance and achieve a minimum of 6-mm amplitude as required by ACI 318-19 (ACI 2019). Seven days after casting the first block, the second block was placed and connected to the first through the shear connectors. Figure 4.3 shows the different interface roughness levels. In contrast, the two L-shaped blocks were poured simultaneously for the monolithic specimens.

(a) (b)

Figure 4.3: (a) Not roughened interface and (b) roughened interface.

Specimens were classified into three series according to the interface condition. Series I included seven specimens with not-roughened cold joints: one specimen without shear connectors, five specimens with different GFRP reinforcement ratios (0.24, 0.36, 0.42, and 0.48%), and one specimen with a 0.33% steel reinforcement ratio for comparison purposes. This series includes a duplicate specimen (with 0.24%) that was totally reinforced with GFRP to investigate the effect of the type for reinforcement away from the shear plane, if any. Series

II had five specimens corresponding to those in Series I but with intentionally roughened cold joints. Series III had six specimens similar to those in Series I (except the specimen without shear connectors) but cast monolithically. Table 4.2 shows the detailed test matrix where the first character represents the connector type (G = GFRP, S = Steel, or X = no connectors). The second character indicates the number of connectors, which is the number of stirrups' branches, double the number of stirrups, (0, 2, 4, 6, or 8). The third character represents the connector diameter (10 or 13). The last character represents the shear plane condition (C = cold joint, CR = cold joint roughened, and M = monolithic). For example, specimen G6-10-M has six GFRP connectors using 3-No.10 closed stirrup, and the two L blocks were placed monolithically. The details of tested specimens with the different reinforcement configurations and casting stages are provided in Figures 4.4 and 4.5, respectively.

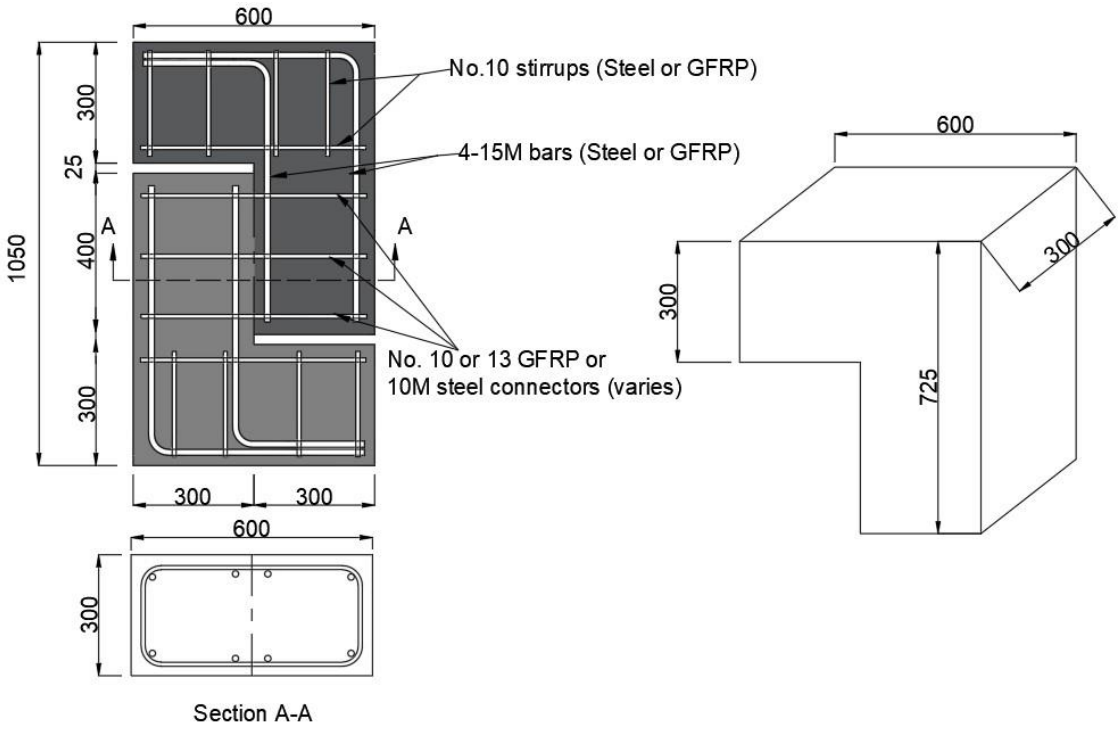

(a) (b)

Figure 4.4: Test specimen, (a) specimen geometry, and (b) typical L-block geometry

(a)

(b)

(c)

Figure 4.5: Casting stages: (a) reinforcement for typical L-block with the intended connectors, (b) casting the first L-block, and (c) reinforcement for the monolithic specimen

Table 4.2: Test matrix

Specimen	Series	Connector type	Number of connectors	Area, mm^2	Reinforcement ratio (%)	shear plane condition
X0-00-C	I	N/A	N/A	N/A	N/A	Cold joint
S4-10-C		10M Steel	4	400	0.33	
G4-10-C		No.10 GFRP	4	288	0.24	
G4-10-C*			4	288	0.24	
G6-10-C			6	432	0.36	
G8-10-C			8	576	0.48	
G4-13-C		No.13 GFRP	4	508	0.42	
S4-10-CR	II	10M Steel	4	400	0.33	Cold joint roughened
G4-10-CR		No.10 GFRP	4	288	0.24	
G4-10-CR*			4	288	0.24	
G8-10-CR			8	576	0.48	
G4-13-CR		No.13 GFRP	4	508	0.42	
S4-10-M	III	10M Steel	4	400	0.33	Monolithic
G4-10-M		No.10 GFRP	4	288	0.24	
G4-10-M*			4	288	0.24	
G6-10-M			6	432	0.36	
G8-10-M			8	576	0.48	
G4-13-M		No.13 GFRP	4	508	0.42	

* Replicate specimens using GFRP bars and stirrups in the L-shaped blocks, away from the shear plane.

4.3.3 Test setup and instrumentation

Figure 4.6 shows the test setup and instrumentation. All specimens were placed vertically on a concrete block under a 5000-kN hydraulic actuator to apply a concentric monotonic load with a displacement-controlled rate of 0.1 mm/minute. This push-off test is adopted to induce pure shear without any associated moment along the shear plane. Two linear variable displacement transducers (LVDTs) were installed on each side of the push-off specimen to measure the slippage of the two L-blocks along the shear plane. One PI-gauge was provided on each side of the specimen at the center of the shear plane to measure the crack width through the test. Strain gauges were attached to the connectors at the interface to measure reinforcement strain during testing up to failure.

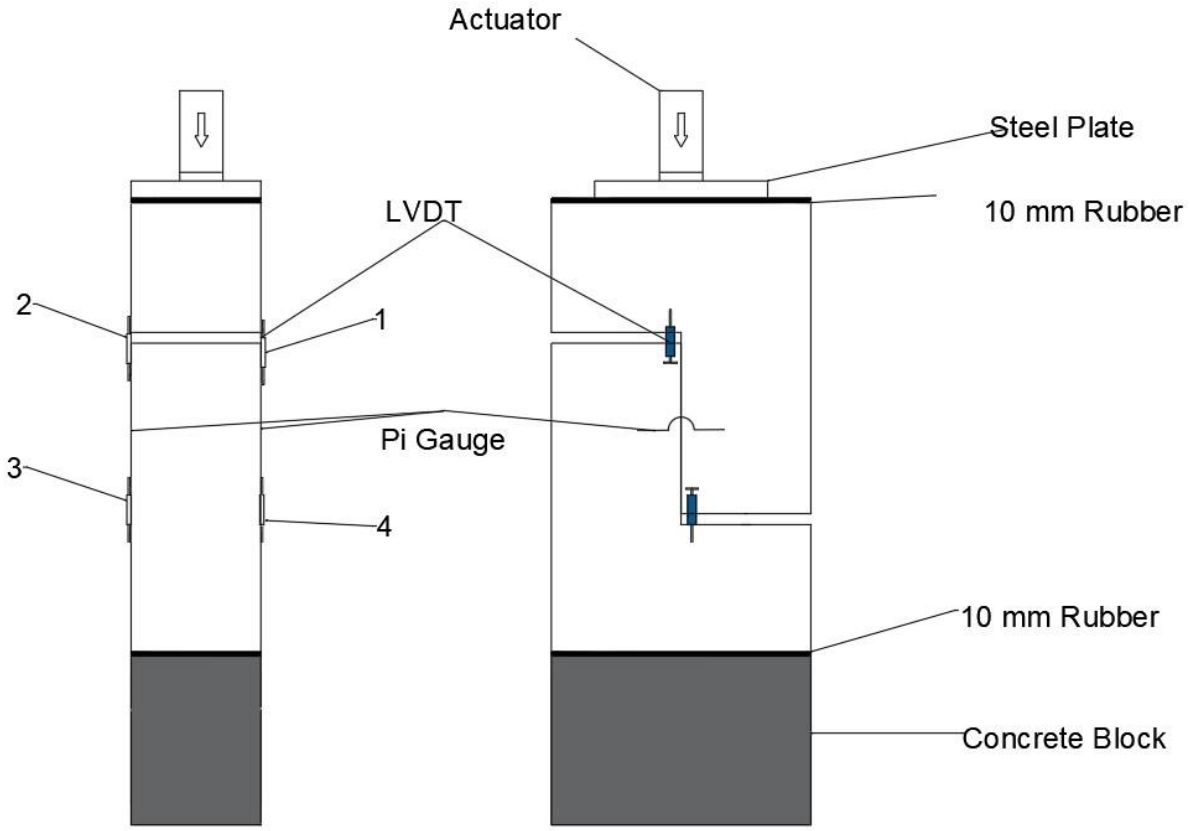

(a)

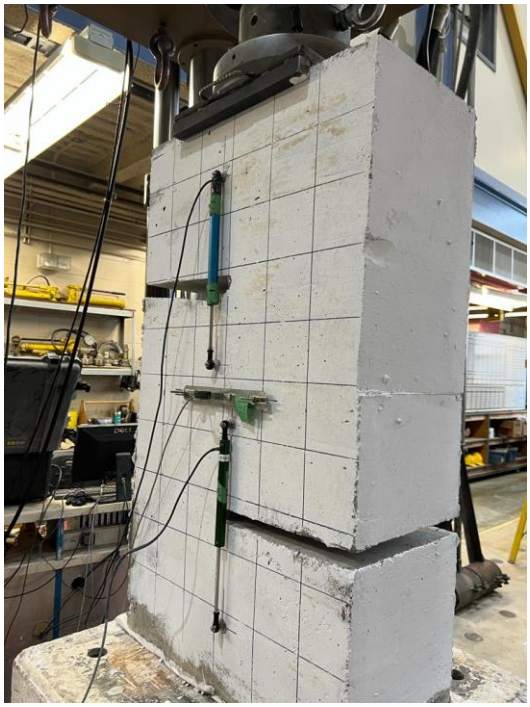

(b)

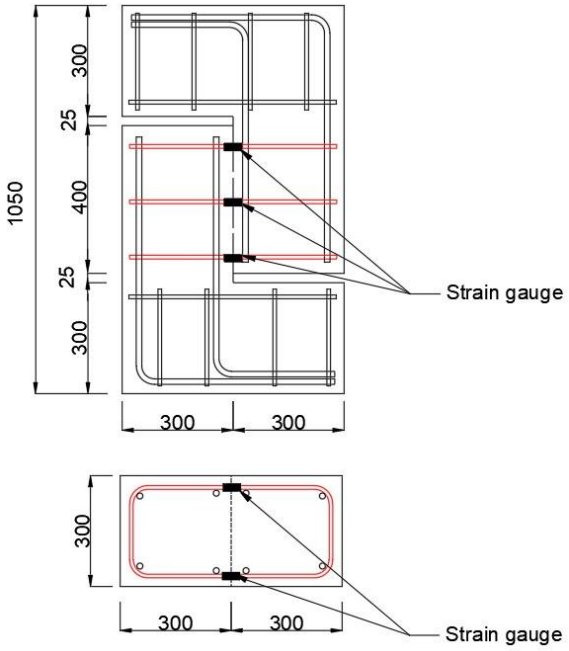

(c)

Figure 4.6: Test Set-up, (a) schematic drawing, (b) photo of a specimen in the set-up, and (c) strain gauge arrangements

4.4 Experimental Results and Discussions

4.4.1 General behaviour, cracking, and mode of failure

Table 4.3 presents various test results including peak load, relative slippage corresponding to the peak load, strains in the reinforcement, and residual load capacities. The general behavior can be divided into three phases, pre-cracking, post-cracking, and post-peak. The pre-cracking phase was affected by the shear plane condition. The other two phases were contingent on the shear plane condition in addition to the reinforcement ratio.

In both Series I and II specimens (cold-joint interface), the initial cracks occurred internally in the blocks, similarly to what was observed by Rahal et al. (2016). The concrete resisted the friction shear stresses before cracking with a negligible reinforcement contribution. A specimen without shear connectors crossing the shear plane (X0-00-C) was tested to predict the contribution of the

concrete surface in resisting the friction shear. After cracking, shear stresses were resisted by a combination of friction due to the aggregate interlock and the clamping stresses, along with the dowel action provided by the connectors crossing the shear plane. The formation of wide visible cracks along the shear interface evidenced the failure of those specimens. Due to the better bond between the two L-blocks, Series III showed a different behavior where transverse cracks were developed away from the shear plane prior to the main crack at the interface. In addition, the specimens in this series attained additional capacity after the crack formation at the interface in contrast to those in series I and II. Figure 4.7 shows the typical cracking patterns for each series. Phases I, II, and III are shown in Figure 4.8.

Table 4.3: Test results

Specimen	Series	Actual concrete strength f_c' (MPa)	Reinforcement ratio (%)	$E\rho_v$, (MPa)	Ultimate load, (kN)	Residual capacity (kN)	Residual capacity/ ultimate load (%)	Ultimate relative slippage, (mm)	Strain at ultimate load ($\mu\varepsilon$)
S0-00-C	I	36	-	-	293	-	-	0.18	-
S4-10-C		33	0.33	666	404	254	63	0.33	220
G4-10-C			0.24	118	399	247	62	0.20	410
G4-10-C*			0.24	118	387	261	67	0.20	280
G6-10-C		36	0.36	176	439	342	78	0.21	440
G8-10-C		33	0.48	235	451	373	83	0.22	500
G4-13-C		36	0.42	223	419	377	90	0.20	310
S4-10-CR	II	40	0.33	666	560	323	58	0.43	2,100
G4-10-CR			0.24	118	452	314	69	0.24	410
G4-10-CR*			0.24	118	417	313	75	0.26	260
G8-10-CR		35	0.48	235	423	355	84	0.32	3,300
G4-13-CR			0.42	223	438	372	85	0.26	230
S4-10-M	III	45	0.33	666	924	481	52	0.93	2,500
G4-10-M		46	0.24	118	642	354	55	0.78	5,000
G4-10-M*		40	0.24	118	611	362	59	0.60	3,300
G6-10-M		37	0.36	176	694	409	59	0.82	3,940
G8-10-M		35	0.48	235	719	455	63	0.84	4,300
G4-13-M		34	0.42	223	671	433	65	0.68	2,950

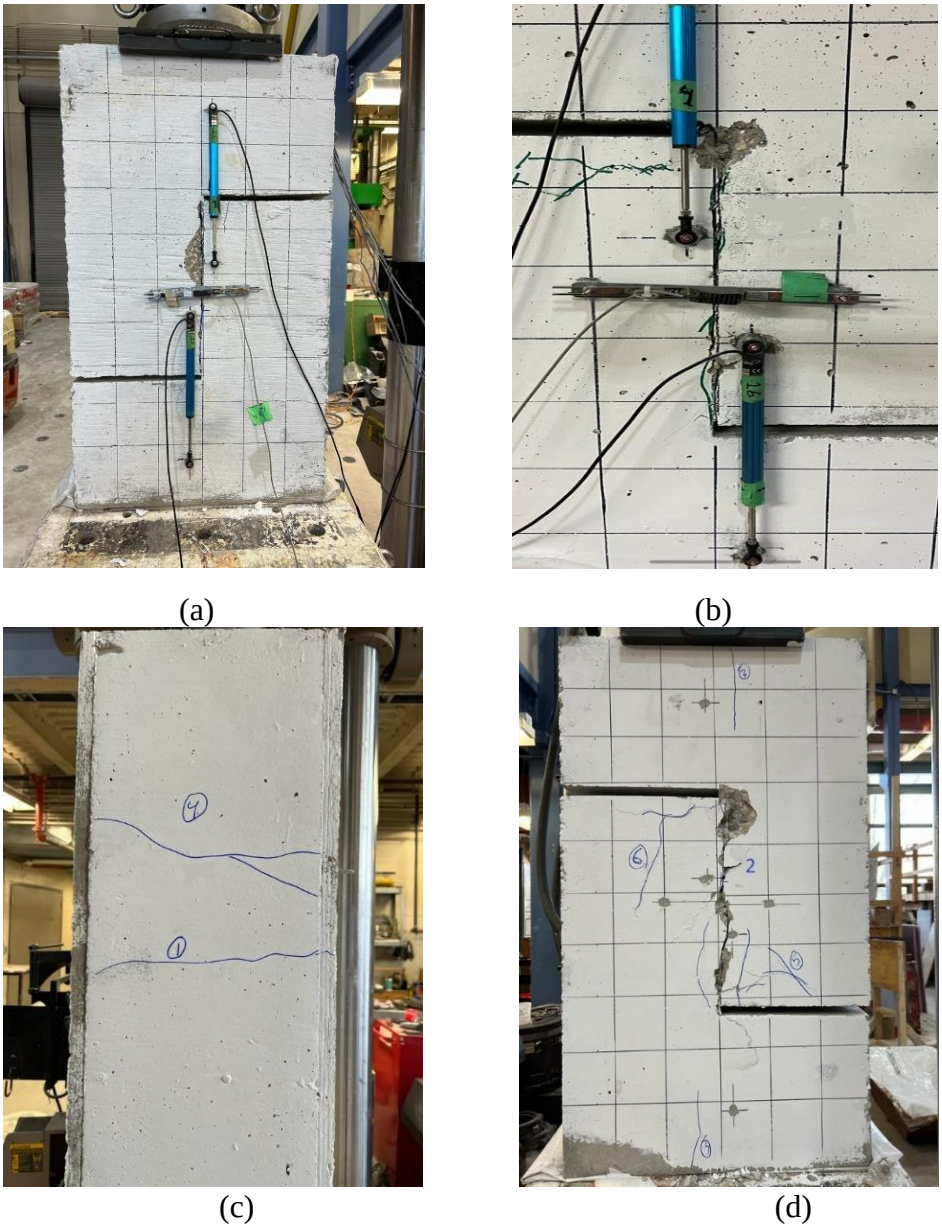

(a) (b)

(c) (d)

Figure 4.7: Typical mode of failure: (a) cold joint, (b) cold joint roughened, (c) monolithic front view, and (d) monolithic side-view

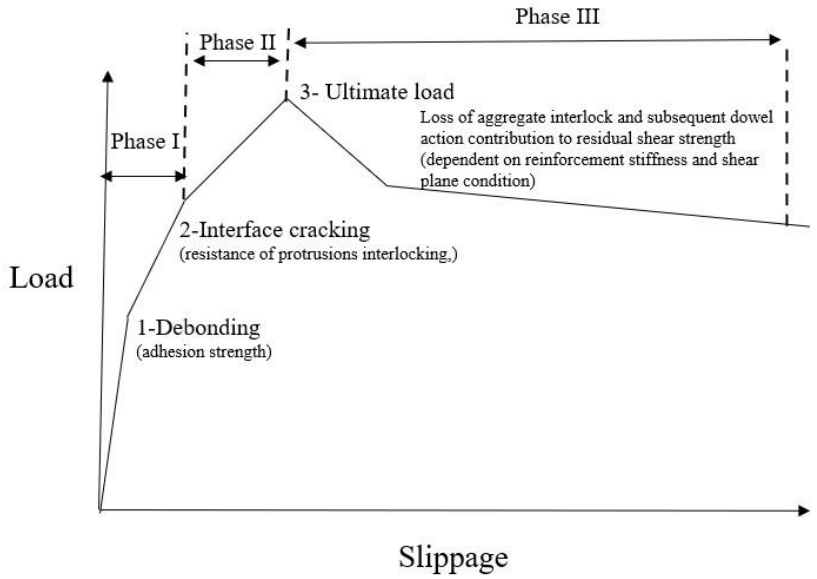

Figure 4.8: Typical load-slip relationship

4.4.2 Phase I: pre-cracking

A softening behaviour was noticed after reaching the cracking load through the peak load (point 3 in Figure 4.8). This phase was characterized by increased slippage, interface crack widening, and higher reinforcement strains compared to the previous phase, similarly to the observations by (Mansur et al. 2008). Accordingly, for all specimens, the crack formation was followed by loss of adhesion. Also, the adhesion continued to decrease with the increase in the slipping and crack dilation after cracking. Nevertheless, the reinforcement started to have a significant contribution, demonstrated by increased strain. Shear connectors exhibited tensile stresses due to the increase in crack dilation, which as a result, provided the intended clamping force. The shear reinforcement ratio mainly controlled this phase for the different interface conditions, the more the reinforcement ratio the more the shear capacity. Moreover, interface roughness had a crucial role in shear resistance. The monolithic specimens had the highest peak loads for the same shear friction reinforcement. Furthermore, the reinforcement type, steel or GFRP, also affected this phase due to the distinct differences in modulus of elasticity and shear strength of the two materials.

4.4.3 Phase II: post-cracking

A softening behaviour was noticed after reaching the cracking load and climbing to the peak load (point 3 in Figure 4.8). This phase was characterized by increased slippage, crack widening, and higher reinforcement strains compared to the previous phase (Mansur et al. 2008). Accordingly, for all specimens, the crack formation was followed by loss of adhesion. Also, the adhesion continued to decrease with the increase in the slipping and crack dilation after cracking. Nevertheless, the reinforcement started to have a significant contribution, demonstrated by increased strain. Shear connectors exhibited tensile stresses due to the increase in crack dilation, which as a result, provided the intended clamping force. The shear reinforcement ratio mainly controlled this phase for the different interface conditions, the more the reinforcement ratio the more the shear capacity. Moreover, interface roughness had a crucial role in shear resistance. In other words, the cold-joint specimens with roughened interface had higher post-cracking loads than the not roughened ones, where the monolithic specimens had the highest values. Lastly, the reinforcement type, steel or GFRP, also affected this phase due to the difference in modulus of elasticity and shear strength between the two materials.

4.4.4 Phase III: Post-peak

Significant deformations characterize this phase depicted in concrete spalling corresponding to the rapture of the GFRP bars. This phase started with a drop in the load after reaching the peak load, followed by substantial relative slippage and crack dilatation. However, due to the linear elastic behavior of GFRP, the load started to increase again after the initial load drop. The load drop after the peak load and the increase in the residual load capacities depended on the reinforcement area crossing the shear plane. Furthermore, the friction shear resistance continued to drop throughout this phase as sliding increased, weakening the aggregate interlock mechanism until the load was

resisted merely by the reinforcement through dowel action (Liu et al., 2019) until rupture or shearing of the GFRP reinforced as previously concluded by

Specimen X0-00-C, without connectors, had 0.18-mm relative slippage corresponding to the peak load. Whereas all other GFRP-RC specimens in Series I had approximately the same relative slippage ranging from 0.20 - 0.22 mm (11 - 22% higher than X0-00-C). On the other hand, the steel-RC specimen had higher slippage valued 0.33 mm. Specimens in Series II had similar values to those in Series I. On the other hand, Series III specimens had relatively higher slippages values due to reasons discussed later in the paper.

4.4.5 Reinforcement strain

At cracking load, strains in the reinforcement were minimal (100- 150 με for the cold-jointed specimens), indicating that the reinforcement's contribution before the cracking is insignificant. Nevertheless, the corresponding strain to the peak load had a wide range for cold-jointed specimens with a maximum value of 500 με. This agrees with the results of previous work (Harries et al. 2012), which concluded that the reinforcement contribution is unpredictable. For Series I, all GFRP connectors exhibited more than 12,000 με prior to the rapture. Specimen S4-10-C showed 220 and 4,000 με at the peak and the residual loads, respectively. This indicates that the steel connectors did not reach the yielding strain at the peak load. Series II specimens had similar behaviours and strain values to those in Series I.

Series III, with monolithic joints, had a different behaviour than those in Series I and II. The GFRP strain values corresponding to the cracking load were higher (330- 410 με). After the cracks became visible, the shear connectors mainly resisted the shear stresses, evidenced by the significant increase in reinforcement strain. The strain corresponding to the peak load of the GFRP-RC specimens in Series III was between 3,000 and 5,000 με. In comparison, the steel-RC specimen

had a smaller change in the strain rate after cracking, which continued to increase until reaching the yielding strain corresponding to the peak load. Figure 4.9 shows the load-strain relationship for all tested specimens.

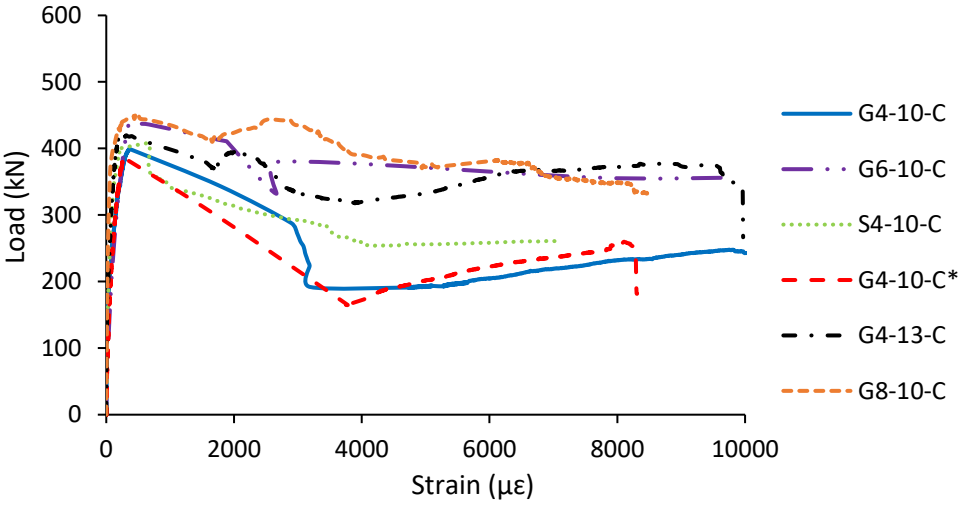

(a)

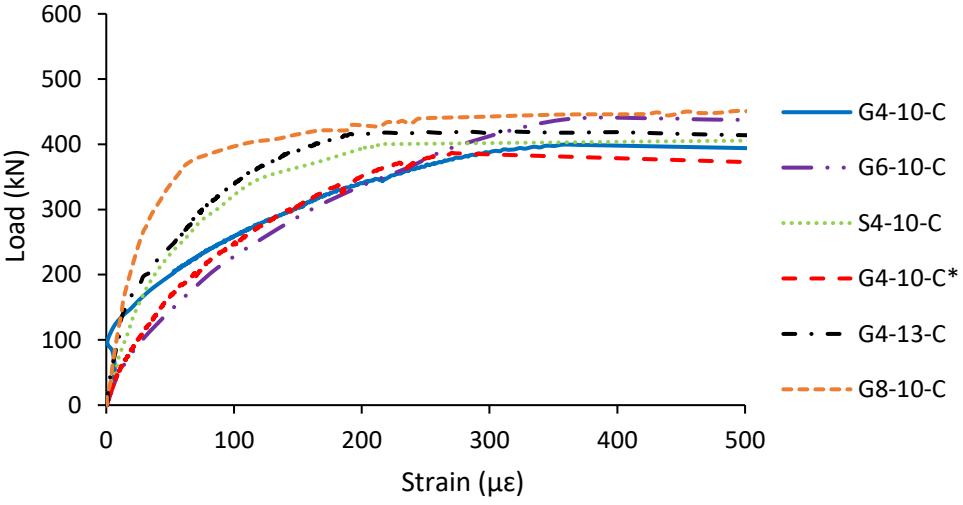

(b)

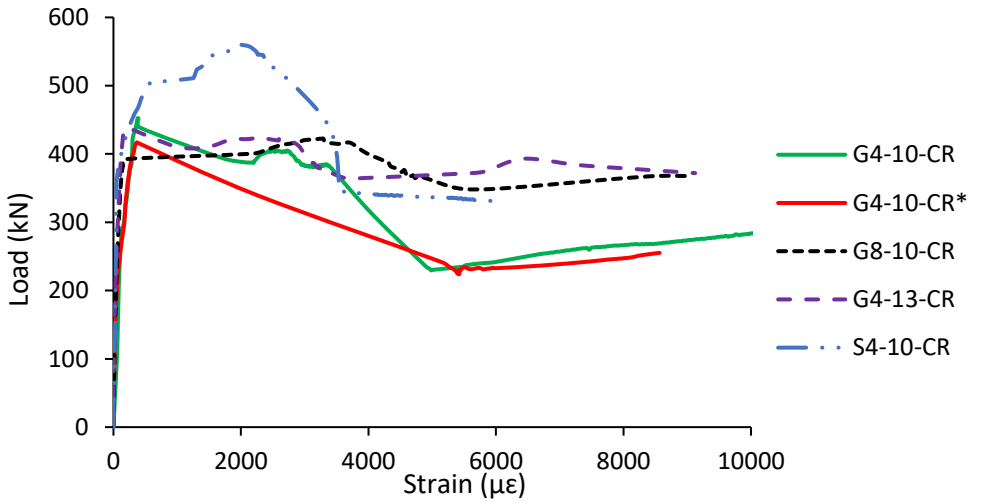
600
500
400
300
200
100
0
Load (kN)
0
2000
4000
6000
8000
10000
Strain (με)
G4-10-CR
G4-10-CR*
G8-10-CR
G4-13-CR
S4-10-CR

(c)

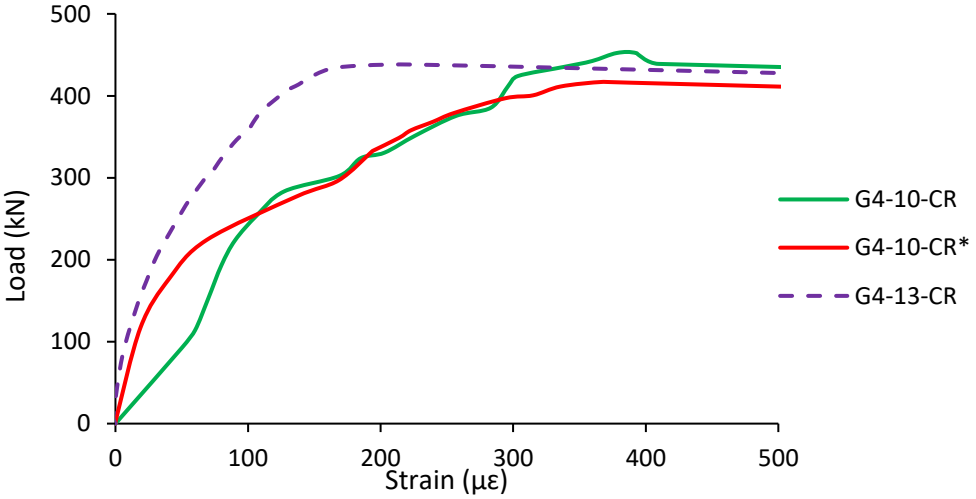
500
400
300
200
100
0
Load (kN)
0
100
200
300
400
500
Strain (με)
G4-10-CR
G4-10-CR*
G4-13-CR

(d)

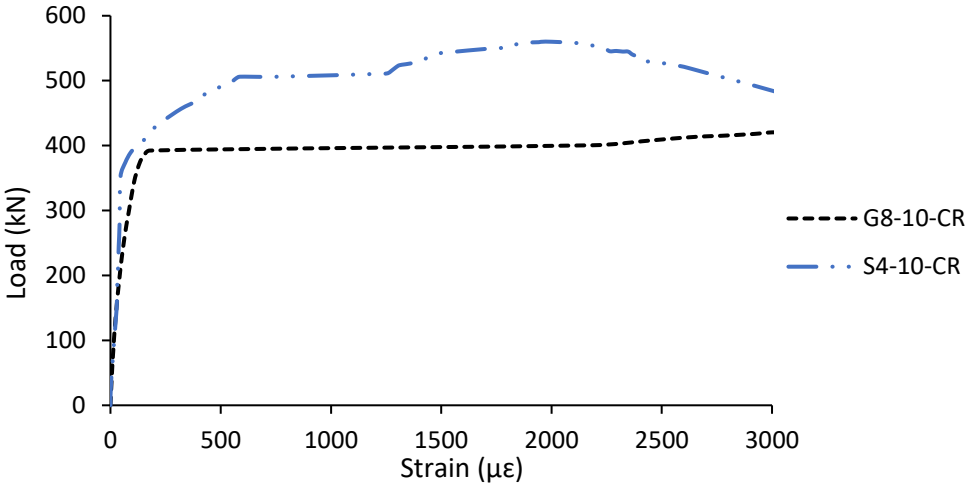
600
500
400
300
200
100
0
Load (kN)
0
500
1000
1500
2000
2500
3000
Strain (με)
G8-10-CR
S4-10-CR

(e)

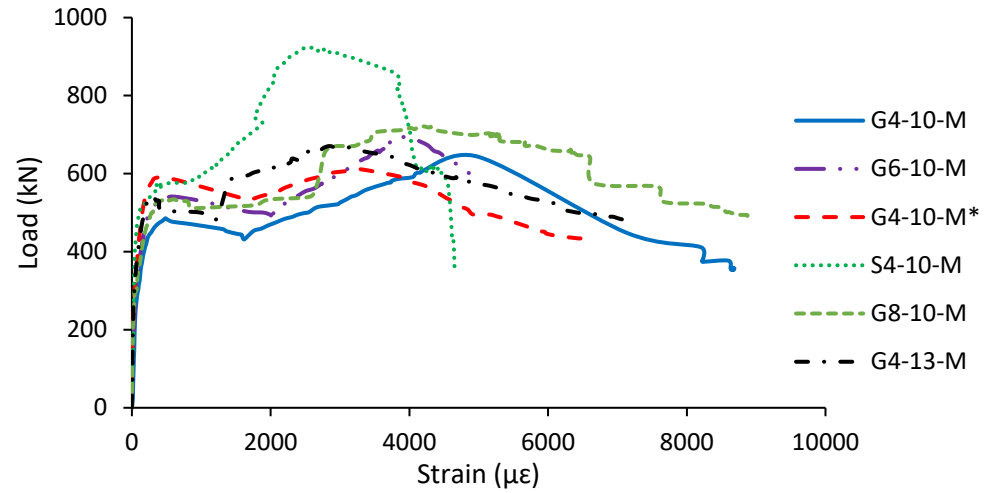

(f)

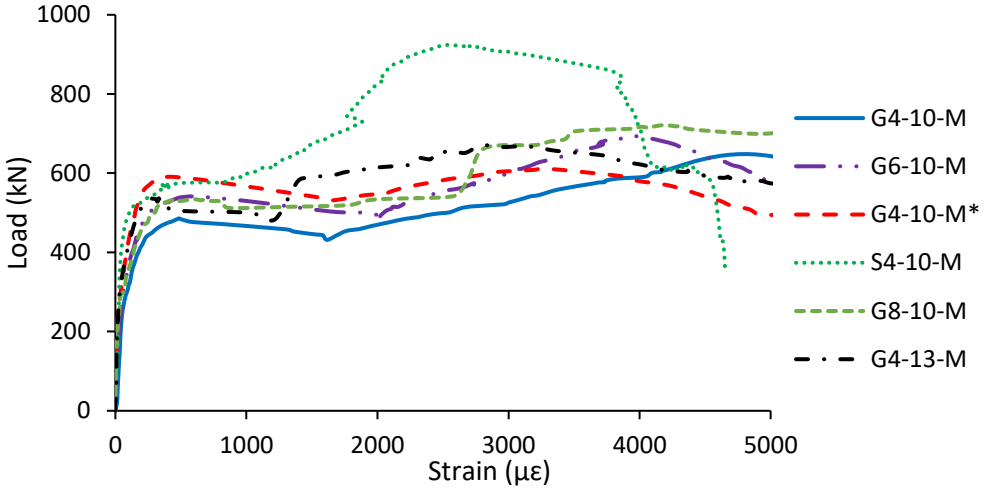

(g)

Figure 4.9: Load-strain relationship, (a) Series I, (b) Series I up to the peak load, (c) Series II, (d) Series II (GFRP less than 0.48% reinforcement ratio) up to the peak load, (e) Series II (GFRP with 0.48% reinforcement ratio and the steel specimen) up to the peak load (f) Series III, and (g) Series III up to the peak load.

4.4.6 Effect of reinforcement stiffness ($E\rho_v$)

The peak load for the steel-RC specimens was reached before the reinforcement yielding. This was also noticed by Harries et al. (2012), especially for specimens with high-strength steel.

Accordingly, the clamping force is represented in terms of the modulus of elasticity (E) rather than the yielding strength. This exploits the GFRP property of having linear-elastic behavior up to rapture.

To investigate the effect of reinforcement stiffness ($E\rho_v$) solely, the results were depicted separately in terms of the load-slip relationship for each Series, as shown in Figure 4.10. The GFRP-RC specimens in Series I had a peak load ranging from 387 to 451 kN (32 - 54% higher than X0-00-C), corresponding to Increasing the reinforcement stiffness from 118 to 235 MPa. Increasing the reinforcement stiffness also increased the residual load significantly from 247 to 342 kN (39%). This shows that the reinforcement stiffness controlled the post-peak behavior. Furthermore, the higher reinforcement ratio reduced the crack width associated with the failure of the first GFRP bar. Moreover, it reduced the load drop after reaching the peak load. For example, the load dropped from 398 to 191 kN (52% of the peak load) for specimen G4-10-C. In comparison, it dropped from 439 to 342 kN (22% of the peak load) in G6-10-C. In this context, increasing the reinforcement stiffness to 223 and 235 MPa resulted in 12 and 5% higher residual loads than G6-10-C, respectively. In addition, these specimens exhibited lower crack widths averaging 0.55 mm and ultimately enhanced the concrete contribution due to the higher clamping stresses. Specimens with reinforcement stiffnesses higher than 176 MPa, showed similar behavior to the steel-RC specimen in terms of deformations, as demonstrated in high strains in the connectors and slippage in the concrete block prior to the GFRP rapture. Specimens in Series II and III had similar behavior to those of Series I due to the reinforcement ratio.

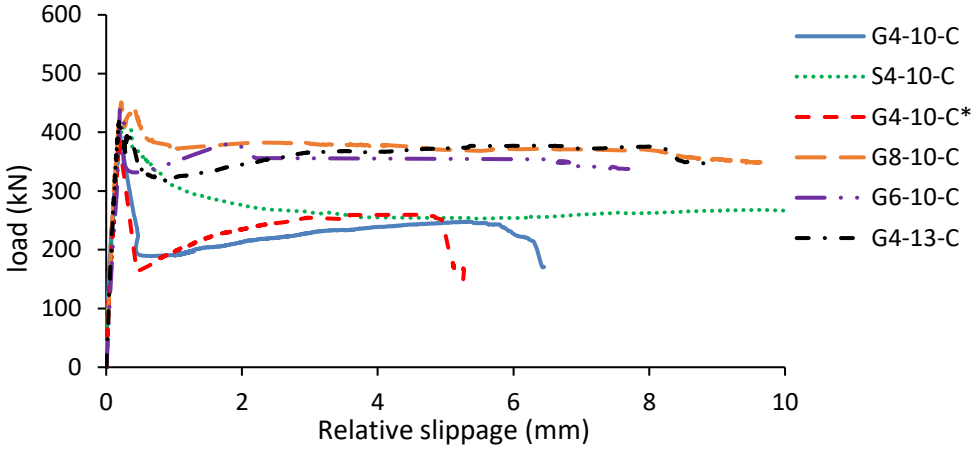
load (kN)
Relative slippage (mm)
G4-10-C
S4-10-C
G4-10-C*
G8-10-C
G6-10-C
G4-13-C

(a)

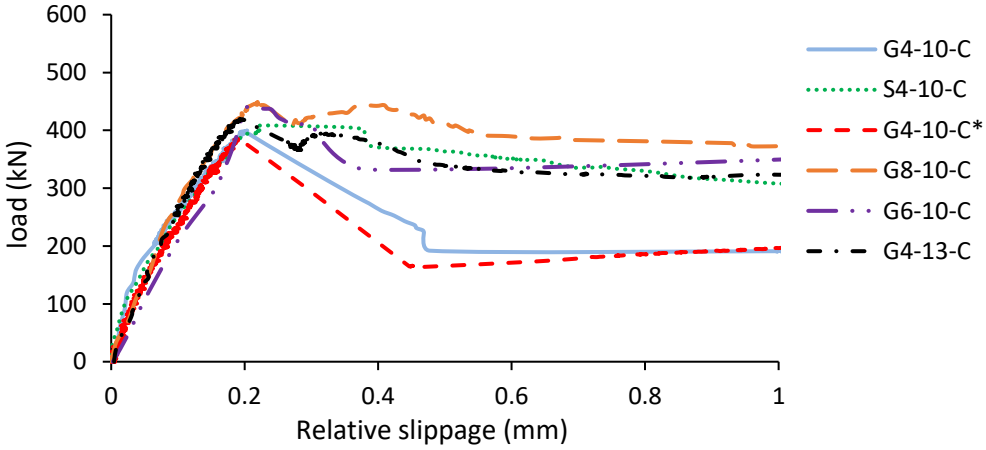
load (kN)
Relative slippage (mm)
G4-10-C
S4-10-C
G4-10-C*
G8-10-C
G6-10-C
G4-13-C

(b)

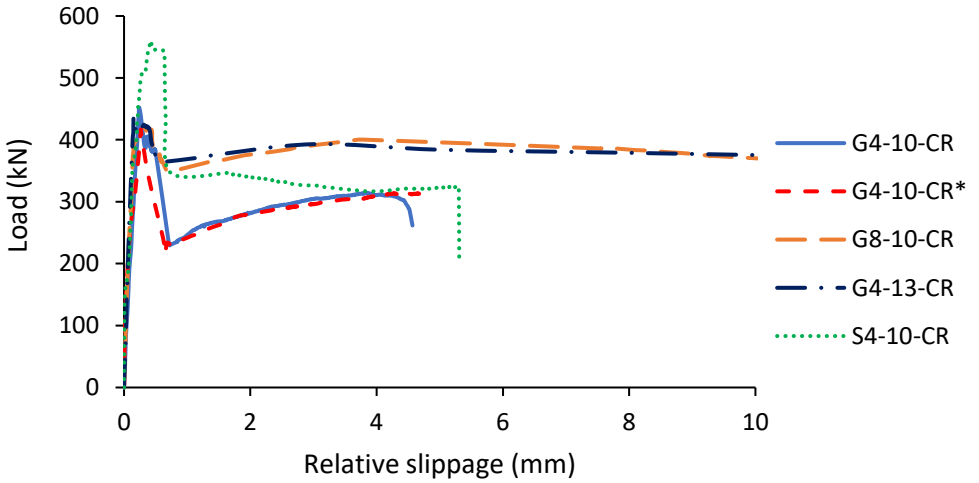
Load (kN)
Relative slippage (mm)
G4-10-CR
G4-10-CR*
G8-10-CR
G4-13-CR
S4-10-CR

(c)

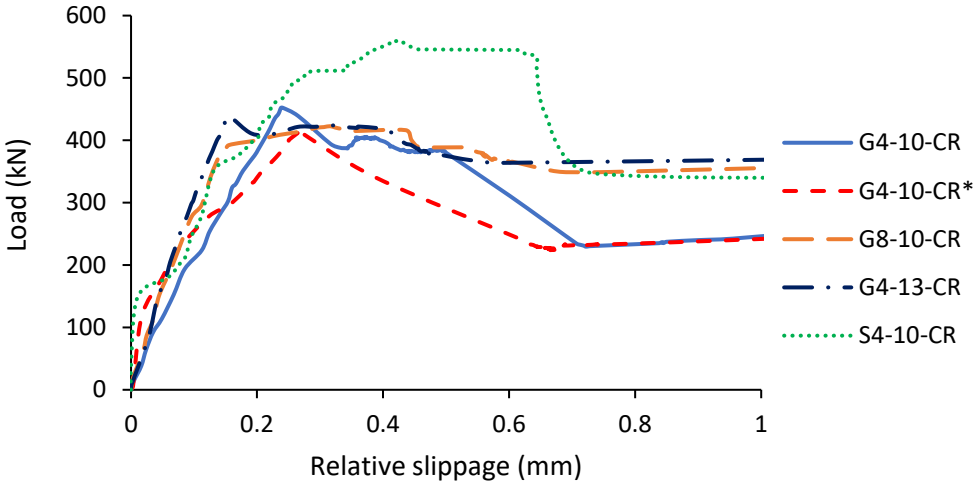
600
500
400
300
200
100
0
Load (kN)
0
0.2
0.4
0.6
0.8
1
Relative slippage (mm)
G4-10-CR
G4-10-CR*
G8-10-CR
G4-13-CR
S4-10-CR

(d)

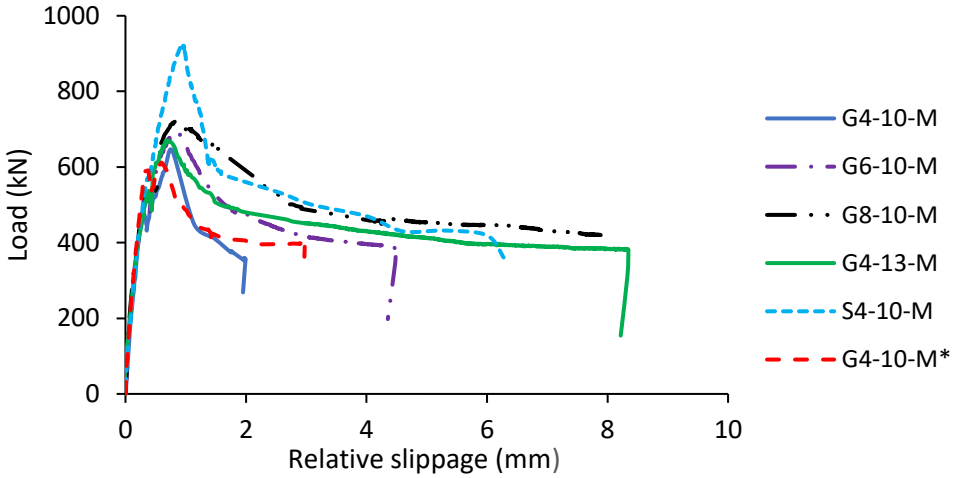
1000
800
600
400
200
0
Load (kN)
0
2
4
6
8
10
Relative slippage (mm)
G4-10-M
G6-10-M
G8-10-M
G4-13-M
S4-10-M
G4-10-M*

(e)

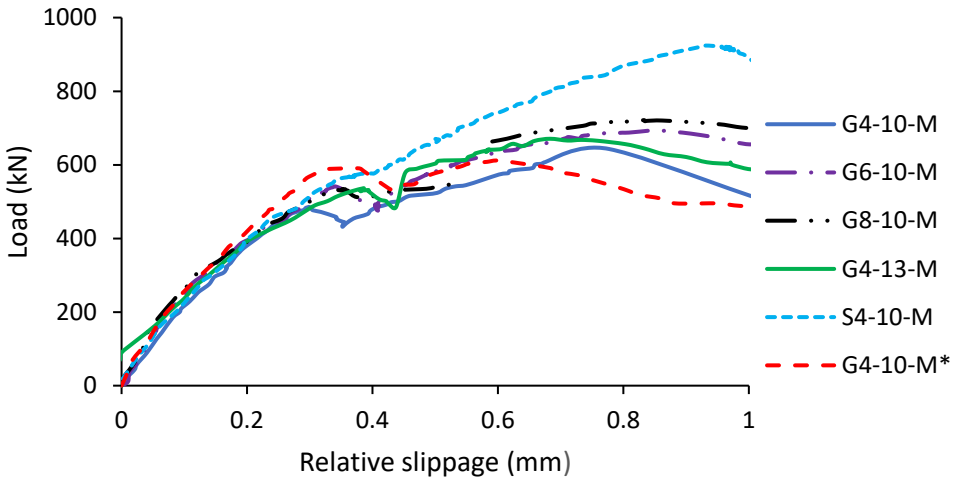

(f)

Figure 4.10: Load-slip relationship**:** (a) Series I, (b) Series I close up to 1.0 mm, (c) Series II, (d) Series II close up to 1.0 mm, (e) Series III, and (f) Series III close up to 1.0 mm.

4.4.7 Effect of interface roughness

The first visible crack for cold-jointed specimens, whether with an intentionally roughened or not roughened interface, coincided with the shear plane corresponding to the peak load. After that, the crack widened until a noticeable concrete spalling occurred. Nevertheless, the cracking was observed before that, demonstrated in the slope change in the strain and slippage values (point 2 in Figure 4.8). In contrast, monolithic specimens had cracks distributed randomly prior to the one at the shear plane. This is attributed to the stronger bond at the interface, which led to higher cracking loads than the specimens in the other series. The load-slip relationship for specimens with the same reinforcement stiffness but with different shear plane condition were plotted in Figure 4.11 to investigate the effect of interface roughness.

Roughening the interface for the specimens in Series II did not significantly affect the peak load, slippage, or strain compared to Series I. This justifies the assumption that Kahn and Mitchell (2002) and Alkatan (2016) made, assuming the left-as-is surface to be a rough interface.

Meanwhile, the steel-RC specimen in Series II had a 39% higher peak load than the one in Series I. Due to the high reinforcement stiffness, the steel-RC specimen, S4-10-CR, and G8-10-CR in Series II continued to carry additional loads after the full development of the interface crack. As a result, the steel connectors reached the yielding strain at the peak load. This shows that the interface roughness effect is more noticeable with high reinforcement stiffnesses. In addition, roughening the surface resulted in having a 27% higher residual load for S4-10-CR than S4-10-C. On the other hand, G4-10-CR and G4-10-CR* had 27 and 20% higher residual loads than G4-10-C and G4-10-C*, respectively. In addition, specimens with higher reinforcement ratios in Series II had the same residual loads as in Series I, and consequently, the residual loads were due to the dowel action of the shear connectors.

Monolithic specimens exhibited a distinct post-cracking behavior regardless of reinforcement stiffness and type. For all specimens in this series, the interface crack was developed and started to be visible at a load of approximately 540 kN prior to the peak load in contrast to the other two Series. The cracking load for the cold-jointed specimens was significantly less, around 300 kN. This shows the superior bond between the concrete blocks poured monolithically. Moreover, monolithic specimens exhibited the highest relative slippages corresponding to the peak load, which induced higher strain in the reinforcement. In other words, higher clamping stress. Furthermore, higher slippages activated the dowel action of the connectors. As a result, the dowel action was activated, witnessed in the high strain values. Accordingly, the peak loads for monolithic GFRP-RC specimens were 58 – 61 % higher than those for the not-roughened interface. The steel-RC specimen, S4-10-M, had 128 and 89 % higher peak and residual loads, respectively, than S4-10-C. The results of the steel-RC monolithic specimen were in good agreement with Birkeland and Birkeland (1966), Mattock (2001), and Kahn and Mitchell (2002).

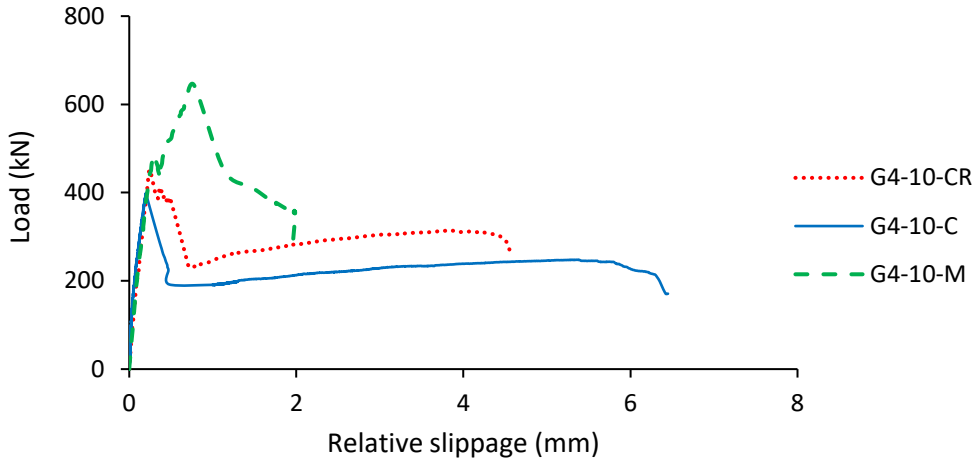
800
600
400
200
0
Load (kN)
0
2
4
6
8
Relative slippage (mm)
G4-10-CR
G4-10-C
G4-10-M

(a)

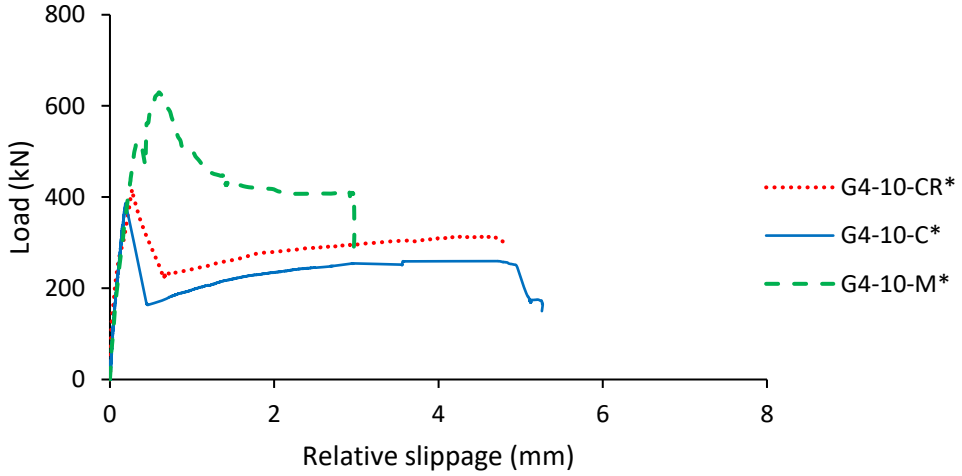
800
600
400
200
0
Load (kN)
0
2
4
6
8
Relative slippage (mm)
G4-10-CR*
G4-10-C*
G4-10-M*

(b)

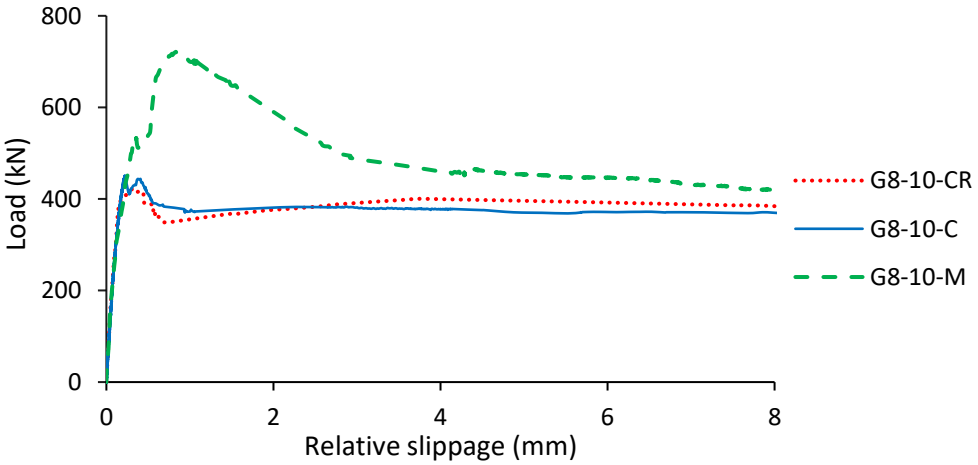
800
600
400
200
0
Load (kN)
0
2
4
6
8
Relative slippage (mm)
G8-10-CR
G8-10-C
G8-10-M

(c)

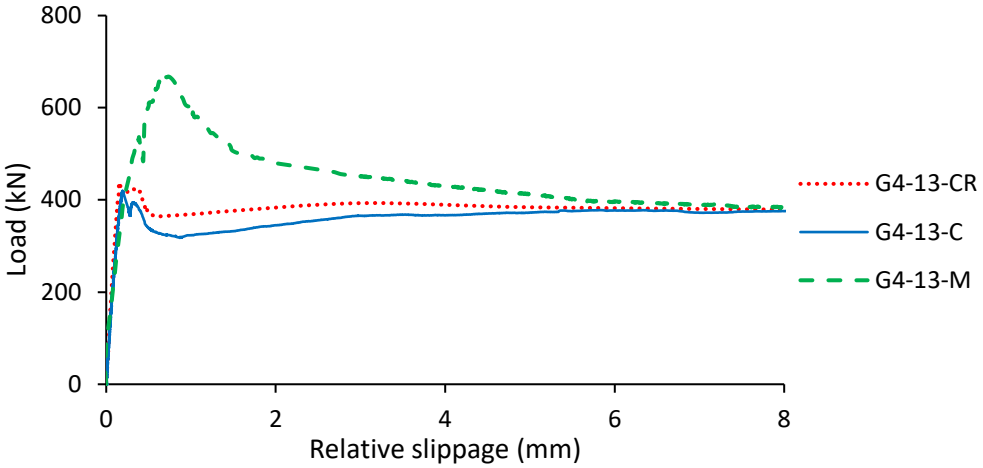

(d)

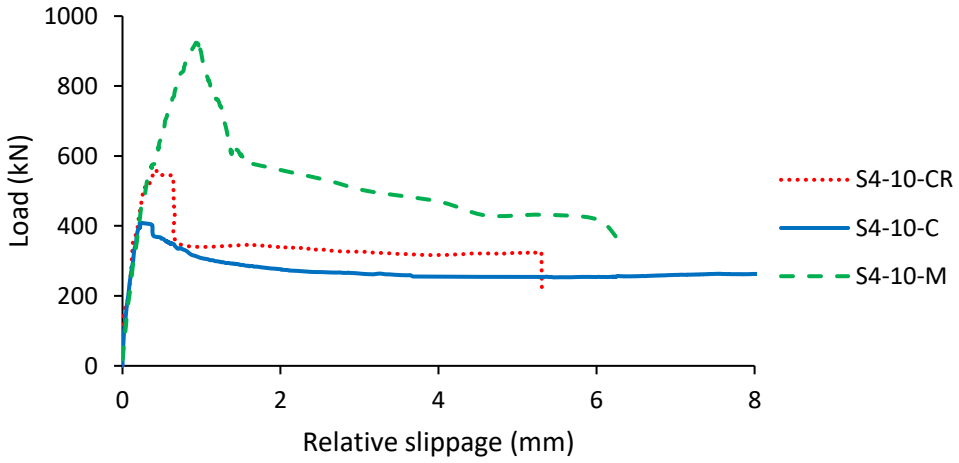

(e)

Figure 4.11: Effect of shear plane conditions: (a) GFRP-RC (118 MPa), (b) GFRP-RC (118 MPa) *, (c) GFRP-RC (235 MPa), (d) GFRP-RC (223 MPa), II, and (e) steel-RC (666 MPa)

4.4.8 Effect of reinforcement type

Series I, II, and III had specimens with the same number of connectors using either steel or GFRP reinforcement. Figure 12 shows the load-slip relationship for those specimens to solely explore the effect of the reinforcement type. Similar pre-cracking and post-cracking behaviour with 398 and 404 kN peak loads for specimens G4-10-C and S4-10-C, respectively. However, the steel-RC specimen gradually dropped after reaching the peak load. Then, the connectors reached the yielding strain with no significant load change. On the other hand, despite the more considerable load drop in the GFRP-RC specimen, the load started to climb up again owing to the linear elastic

behaviour of the GFRP. It continued to increase, reaching a similar residual load to the steel-RC counterpart specimen associated with crack widening and an increase in the slipping.

In Series II, the steel-RC specimen, S4-10-CR, had a 24% higher peak load than the GFRP-RC counterpart specimen, G4-10-CR. This demonstrates that the interface roughness effect is more pronounced in the steel-RC specimens, as discussed earlier. However, the post-peak behaviour was almost the same for the GFRP and steel connectors, similar to Series I. However, Series III had a distinguished behaviour, where the steel-RC specimen (S4-10-M) had a 44% higher peak load than the GFRP-RC counterpart specimen (G4-10-M). The difference in the load remained the same in the post-peak phase.

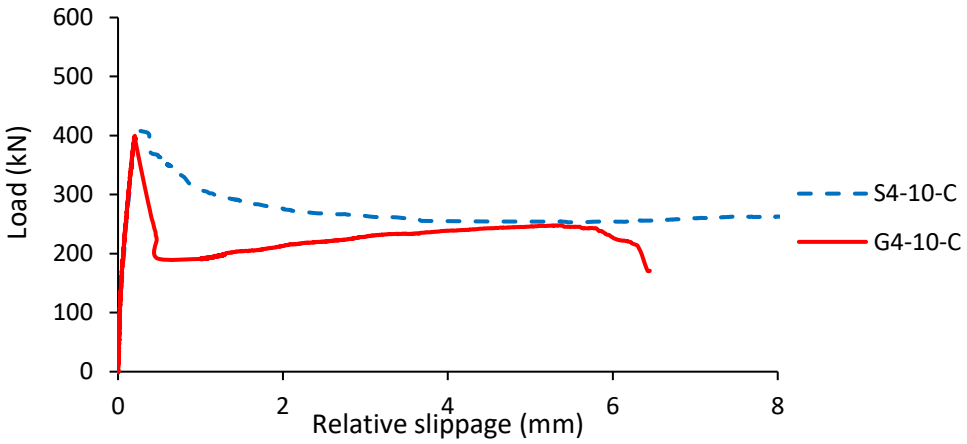

(a)

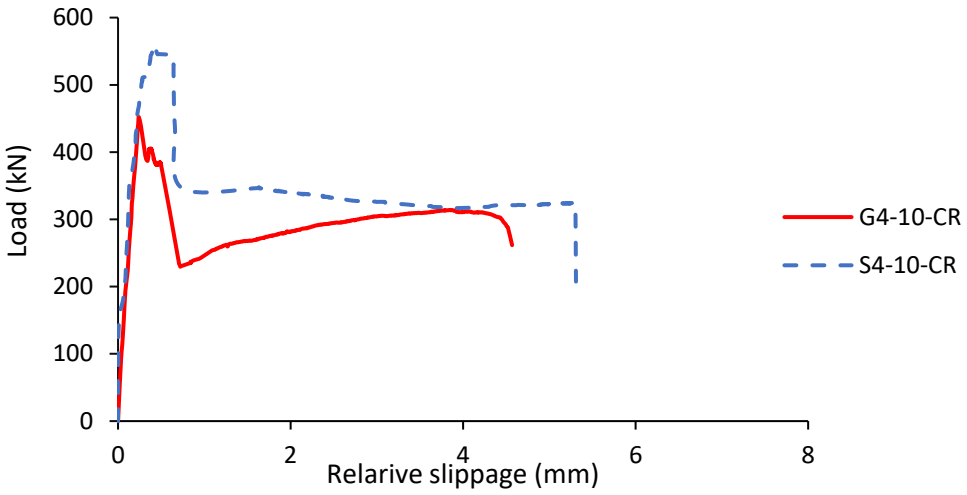

(b)

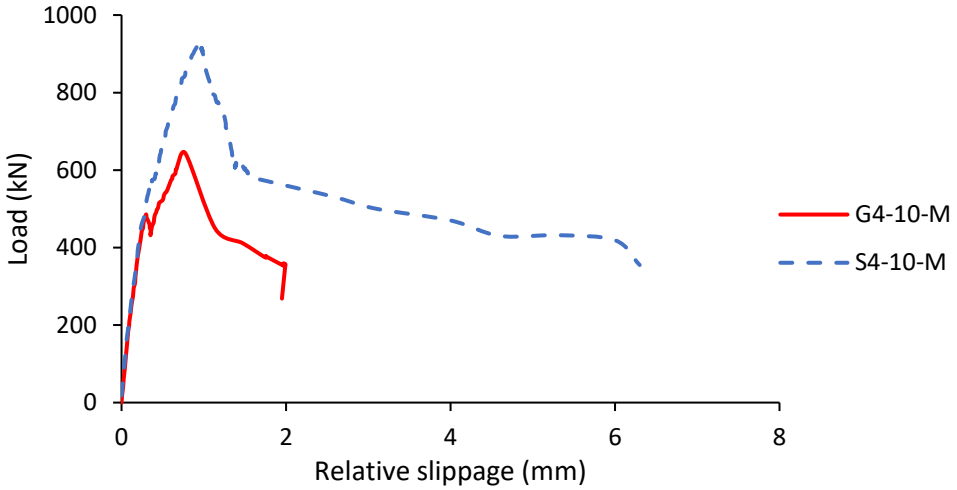

(c)

Figure 4.12: Effect of connector type: (a) cold-joint not-roughened, (b) cold-joint roughened, and (c) monolithic

4.5 Comparison of Predictions and Experimental Results

The experimental results of the GFRP-RC specimens were compared with the model provided by the CSA S6-19 (CSA 2019d). The model adopts the same formula used for steel reinforcement replacing the yielding stress (f_y) with $E_f \times \varepsilon_f$, where E_f is the modulus of elasticity of FRP, and the strain in FRP (ε_f) = 0.004 with a minimum reinforcement ratio of 0.44%. The model requires

that a crack shall be considered along the shear plane and that cohesion and friction, maintained by the reinforcement crossing the shear plane, are responsible for resisting the relative displacement. The standards proposed the following equations to calculate the factored shear resistance:

$$v = \phi_c(c + \mu\,\sigma) \qquad \text{Equation 4-1}$$

$$\sigma = \rho_v E_f \varepsilon_f + \frac{N}{A_{cv}} \qquad \text{Equation 4-2}$$

$$\rho_v = \frac{A_{vf}}{A_{cv}} \qquad \text{Equation 4-3}$$

ϕ_c = resistance factor for concrete (taken = 1), c = cohesion stress at the interface, μ = friction coefficient at the interface, σ = total compressive stress to the shear plane, ρ_v = shear reinforcement ratio, N = unfactored permanent load normal to the shear plane, A_{cv} = area of the concrete section resisting shear transfer, and A_{vf} = area of the reinforcement crossing the shear plane where $\phi_c(c + \mu\,\sigma)$ shall not exceed 0.25 $\phi_c\, f'_c$. Values of c and μ depend on the interface condition, which are given in Table 4.4.

Table 4.4: Values of c and μ as in CSA S6-19 (CSA 2019b)

Surface condition	c (MPa)	μ
Concrete placed against hardened concrete with the surface clean but not intentionally roughened	0.25	0.60
For concrete placed against hardened concrete with the surface clean and intentionally roughened to a full amplitude of at least 5 mm and a spacing of about 15 mm	0.50	1.00
Concrete placed monolithically	1.00	1.40

Table 4.5 shows that the models underestimate the strength of composite GFRP RC elements. One reason is due to the assumption of crack along the shear occurrence before applying the test which reduces the overall friction shear capacity required by the code. However, the adopted interface coefficients in this equation, which are the same coefficients adopted for steel, do not represent the actual behaviour for GFRP.

Table 4.5: Code comparison.

Specimen	Experimental (kN)	Predicted (kN)	Experimental/ predicted
G4-10-C	398	64	6.23
G4-10-C*	387	64	6.05
G6-10-C	439	81	5.42
G8-10-C	451	98	4.6
G4-13-C	419	94	4.46
G4-10-CR	452	116	3.90
G4-10-CR*	417	116	3.59
G8-10-CR	423	173	2.45
G4-13-CR	438	167	2.62
G4-10-M	642	199	3.23
G4-10-M*	629	199	3.16
G6-10-M	694	239	2.90
G8-10-M	719	278	2.59
G4-13-M	671	270	2.49
Mean			3.84
Standard Deviation			1.32
COV (%)			34

4.6 Conclusions

This research investigated the application of GFRP stirrups as shear friction reinforcement for concrete joints. Eighteen large scale push-off specimens were constructed and tested up to failure

under monotonic load. The test variables included (1) the shear plane roughness: cold joints (roughened, not roughened, and monolithic), (2) type of shear reinforcement (steel or GFRP), and (3) shear reinforcement ratio (0.24 to 0.48 %). Based on the analysis of the test results, the main findings can be summarized as follows.

1. GFRP stirrups have shown good performance as friction shear reinforcement due to their linear-elastic behaviour up to failure.
2. Specimens with reinforcement stiffness less than 176 MPa exhibited sudden load drop after reaching the peak load.
3. Roughening the interface had no significant effect on the peak load, slippage, and reinforcement strain for GFRP-RC specimens except the one with the highest reinforcement stiffness of 235 MPa. On the other hand, surface roughness increased the peak load by 39% for the steel-RC specimen.
4. Monolithic specimens had significantly higher cracking and peak loads than the cold-jointed specimens, as expected. These specimens exhibited higher slippages at the peak load resulting in higher strain in the reinforcements, and consequently, higher clamping stresses and dowel action.
5. Reinforcement contribution in monolithic specimens was more significant compared with the cold-jointed specimens.
6. For the specimens with reinforcement ratios of 0.42 and 0.48% that are close to the minimum reinforcement ratio of 0.44%! required by the CSA S6-19 (CSA 2019d), the residual loads were 90 and 83% of the peak loads for cold-jointed not roughened interface, respectively. These percentages were 85 and 84% for the counterpart specimens with roughened interface and 65 and 63% for the monolithic specimens, respectively.

7. The design formula of the CSA S6-19 (CSA 2019d) showed overly conservative results with a 3.84 mean, 1.54 standard deviation and 34% COV compared to the test results.

CHAPTER 5: CONCLUSION AND FUTURE WORK

5.1 Summary

This research study investigated the behaviour of 26 large-scale GFRP push-off specimens. The specimens were tested under monotonic axial load to induce pure direct shear without moment at the shear plane. The study was developed to evaluate the effect of reinforcement shape (Z-bars or closed stirrups), ratio (0.17, 0.24, 0.33, 0.36, 0.42, 0.48%), and type (steel or GFRP), Shear plane condition (cold-joint not roughened interface, cold-joint roughened, and monolithic), and concrete strength (35 and 70 MPa) on the overall friction shear behaviour. All specimens were 1,050 × 600 × 300 mm. Test results were compared with the available design models.

5.2 Conclusions

Based on the results obtained from this study, the following conclusions can be drawn:

1. GFRP stirrups showed an excellent and competitive performance as shear friction reinforcement compared to the steel counterparts.
2. Using high GFRP reinforcement ratio (0.36% or more with a reinforcement stiffness of 176 MPa) ensures large deformations before the reinforcement rupture in a similar manner to the steel-RC counterpart specimens.
3. Specimens with closed stirrups exhibited higher values of slippage than Z-shaped counterpart bars, resulting in additional tensile stresses in the GFRP bars leading to higher peak loads.
4. Specimens with reinforcement ratios of 0.42 and 0.48 % that are close to the minimum reinforcement ratio of 0.44% required by the CSA S6-19 (CSA 2019b) resulted in having

residual loads of 90 and 83%, respectively, for cold-jointed not roughened interface. Whereas the residual loads were 85 and 84% for the same specimens but with roughened interface. Lastly, the residual loads were 65 and 63% for the monolithic specimens.

5. Monolithic specimens exhibited higher slippages corresponding to the peak load resulting in higher strain in the reinforcement, and. consequently, higher clamping stresses.
6. Friction shear capacity is primarily dependent on concrete contribution provided by the aggregate interlock and the cement matrix. Increasing the concrete strength resulted in 43-160% higher shear capacities with stiffer and more brittle behaviour.
7. The CSA S6-19 (CSA 2019b) design formula showed overly conservative results especially for HSC specimens.

5.3 Future Work

The obtained results of this study embrace the fundamentals of developing an analytical model to predict the capacity of GFRP in resisting friction shear. However, future studies are recommended to cover the following:

1. A crack might exist along the shear plane in the cold-joint interfaces. Accordingly, the effect of pre-cracking existence on the friction shear capacity needs to be investigated.
2. Using higher reinforcement ratios than the used ones in this study to specify an upper limit for the analytical model.
3. The behaviour of FRP-RC composite elements of ultra-high-performance concrete (UHPC) requires a detailed investigation.
4. Anchorage requirements and the friction shear capacity of GFRP headed bars.
5. The behaviour of different FRP composites including CFRP and BFRP as friction shear reinforcement.

6. Perform a finite element analysis to validate the experimental results and to encompass wider range of parameters.

REFERENCES

ACI Committee 222. (2019). "Guide to Protection of Metals in Concrete Against Corrosion" ACI 222R-19. American Concrete Institute (ACI): Farmington Hills, Detroit, MI.

ACI Committee 318. (2019). "Building Code Requirements for Structural Concrete and Commentary." ACI 318-19. *American Concrete Institute (ACI)*, Detroit, MI.

ACI Committee 440. (2022). "Building Code Requirements for Structural Concrete Reinforced with Glass Fiber-Reinforced Polymer (GFRP) Bars–Code and Commentary." ACI 440.11-22. *American Concrete Institute (ACI)*, Detroit, MI.

Almomani, M., Mahmoud, K., and El-Salakawy, E. F. (2022). Experimental Investigation of Large-Scale Eccentrically Loaded GFRP-Reinforced High-Strength Concrete Columns. *Journal of Composites for Construction*, *26*(2). https://doi.org/10.1061/(asce)cc.1943-5614.0001186.

Anderson, A.R. (1960). Composite Designs in Precast and Cast-in-Place Concrete. *Progressive Architecture*, *41*(9), 172–179.

Alkatan, J. (2016). "FRP Shear Transfer Reinforcement for Composite Concrete Construction." MSc Thesis, University of Windsor, Windsor, ON.

ASTM (2020)." Standard Test Method for Compressive Strength of Cylindrical Concrete Specimens", ASTM C39-20, American Society for Testing and Materials, West Conshohocken, Pennsylvania.

Badoux, J. C., and Hulsbos, C. L. (1967). "Horizontal shear connection in composite concrete beams under repeated loads". *ACI Journal*, *64*(12), 811–819.

Birkeland, P. W., & Birkeland, H. W. (1966). Connections in Precast Concrete Construction. *ACI Journal*, *63*(3), 345–368.

Connor, A. B., & Kim, Y. H. (2016b). Shear-transfer mechanisms for glass fiber-reinforced polymer reinforcing bars. *ACI Structural Journal*, *113*(6), 1369–1380. https://doi.org/10.14359/51689034.

CSA (2021). "Design and construction of building structures with fibre-reinforced polymer." CSA S806-12 (R2021). *Canadian Standards Association (CSA),* Toronto, ON.

CSA (2019a). "Design of concrete structures." CSA A23.3-19. *Canadian Standards Association (CSA)*, Toronto, ON.

CSA (2019b) "Carbon steel bars for concrete reinforcement." CSA G30.18-09 (R2019), *Canadian Standards Association (CSA),* Toronto, ON.

CSA (2019c). "Specification for fibre-reinforced polymers." CSA S807-19, *Canadian Standards Association (CSA),* Toronto, ON.

CSA (2019d). "Canadian highway bridge design code." CSA S6-19. *Canadian Standards Association (CSA)*, Toronto, ON.

El-Gendy, M., and El-Salakawy, E. (2019). "Effect of flexural reinforcement type and ratio on the punching behavior of RC slab-column edge connections subjected to reversed-cyclic lateral loads." *Engineering Structures, 200*. https://doi.org/10.1016/j.engstruct.2019.109703

El-Sayed, A., El-Salakawy, E., and Benmokrane, B. (2005). "Shear Strength of One-Way Concrete Slabs Reinforced with Fiber-Reinforced Polymer Composite Bars". *Journal of Composites for Construction, 9*(2), 147–157. https://doi.org/10.1061/(ASCE)1090-0268(2005)9:2(147).

Gohnert, M. (2003). "Horizontal shear transfer across a roughened surface", *Cement and Concrete Composites*, *25*(3), 379–385.

Hanson, N. W. (1960). "Precast-prestressed Concrete Bridges: 2. Horizontal Shear Connections". *PCA Journal*, *2*(2), 38–58.

Harries, K. A., Zeno, G., and Shahrooz, B. (2012). "Toward an improved understanding of shear-friction behavior". *ACI Structural Journal*, *109*(6), 835-844.

Hofbeck, J. A., Ibrahim, I. 0, and Mattock, A. H. (1969). "Shear Transfer in Reinforced Concrete". *Journal Proceedings*, *66*(2), 66–79.

Hunter, L. E. (1953). Construction and Expansion Joints for Concrete. *Civil Engineering and Public Works Review*, *48*(560), 157–158.

Kahn, L. F., and Mitchell, A. D. (2002). "Shear friction tests with high-strength concrete". *Structural Journal*, *99*(1), 98-103.

Liu, J., Fang, J.-X., Chen, J.-J., and Xu, G. (2019). "Evaluation of Design Provisions for Interface Shear Transfer between Concretes Cast at Different Times". *Journal of Bridge Engineering*, *24*(6). https://doi.org/10.1061/(asce)be.1943-5592.0001393.

Loov, R. (1978). Design of Precast Connections. *Paper presented at a seminar organized by Compa International Pte, Ltd*, 8 pages.

Loov, D. Phil, R. E., Eng, P., & Patnaik, A. K. (1994). "Horizontal Shear Strength of Composite Concrete Beams with a Rough Interface", *PCI Journal, 39(1), 48-69.*

Mansur, M. A., Vinayagam, T, and Tan, K.-H. (2008). "Shear Transfer across a Crack in Reinforced High-Strength Concrete". *Journal of Materials in Civil Engineering*, *20*(4), 294–302. https://doi.org/10.1061/ASCE0899-1561200820:4294.

Mast, R. F. (1968). "Auxiliary Reinforcement in Concrete Connections". *ASCE, Journal of the Structural Division*, *94*(6), 1485–1504. https://doi.org/10.1061/JSDEAG.0001977.

Mattock, A. H. (1974). "Shear Transfer In Concrete Having Reinforcement At An Angle To The Shear Plane". *Special Publication*, *49*, 17–42.

Mattock, A. H. (2001). "Shear Friction and High-Strength Concrete". *ACI Structural Journal*, *98*(1), 50–59.

Mattock, A. H., and Hawkins, N. M. (1972). "Shear transfer in reinforced concrete—Recent research". *PCI Journal*, *17*(2), 55–75.

Mohamed, A. M., Mahmoud, K., and El-Salakawy, E. F. (2020). "Behavior of simply supported and continuous concrete deep beams reinforced with GFRP bars." *Journal of Composites for Construction*, *24*(4), 04020032.

Mirza, S., & Ali, M. S. (2017). Infrastructure crisis — A proposed national infrastructure policy for Canada. *Canadian Journal of Civil Engineering*, *44*(7), 539–548. https://doi.org/10.1139/CJCE-2016-0468.

Patnaik, A. K. (2001). "Behavior of composite concrete beams with smooth interface". *ASCE, Journal of Structural Engineering*, *127*(4.), 359–366.

Pianca, F., Schell, H., & Cautillo, G. (2005). "The performance of epoxy coated reinforcement": Experience of the Ontario ministry of transportation. *International Journal of Materials and Product Technology*, *23*(3–4), 286–308. https://doi.org/10.1504/IJMPT.2005.007732.

Rahal, K. N., Khaleefi, A. L., and Al-Sanee, A. (2016). "An experimental investigation of shear-transfer strength of normal and high strength self compacting concrete". *Engineering Structures*, *109*, 16–25. https://doi.org/10.1016/j.engstruct.2015.11.015.

Rahman, S. M. H., Mahmoud, K., and El-Salakawy, E. (2017a). Behavior of Glass Fiber–Reinforced Polymer Reinforced Concrete Continuous T-Beams. *Journal of Composites for Construction*, *21*(2). https://doi.org/10.1061/(asce)cc.1943-5614.0000740.

Saemann, J. C., and Washa, G. W. (1964). "Horizontal shear connections between precast beams and cast-in-place". *Journal of ACI*, *61*(11), 1383–1410.

Santos, P. M., & Júlio, E. N. (2012). "A state-of-the-art review on shear-friction". *Engineering Structures*, *45*, 435-448.

Walraven, J. C. (1981). "Fundamental analysis of aggregate interlock". *ASCE, Journal of the Structural Division.*, *107*(11), 2245–2270.

Walraven, J., & Stroband, J. (1994). Shear friction in high-strength concrete. *Special Publication*, *149*, 311-330.

Zilch, K., & Reinecke, R. (2000). "Capacity of shear joints between high-strength precast elements and normal-strength cast-in-place decks". *PCI/FHWA/FIB International Symposium on High Performance Concrete Precast/Prestressed Concrete Institute Federal Highway Administration Federation Internationale du Beton*, 551–560.

APPENDIX A

OVERALL RESEARCH PROGRAM

A.1 Research Program

A total of 26 specimens were tested to evaluate the capacity and performance of GFRP as friction shear reinforcement. Reinforcement ratio and shape (Z-bar and closed stirrups), shear plane condition, and concrete strength were the investigated parameters in this study. The program was divided into five series: Series I contained four specimens connected with Z-shaped bars with cold-joint not roughened interface. Series II, III, and IV were reinforced with closed stirrups and had cold-joint not roughened interface, cold-joint roughened interface, and monolithic shear plane, respectively, to investigate the effect of shear plane condition. The previous four series were poured using normal-strength concrete (NSC) of 35 MPa. Series V had four specimens with high-strength concrete (HSC) of 70 MPa imitating to four of Series II with stirrups to explore the effect of concrete strength on the overall behaviour. Double L-shaped, large-scale specimens, as shown in Figure A.1, were used. Shear plane length and width were 400 and 300 mm, respectively. A gap of 25 mm was provided between the two L-shaped blocks to allow for slipping. For cold-joint specimens, the first L-shaped block was placed horizontally with the intended friction shear reinforcement projection. After seven days, the second part was placed horizontally and connected to the first block through the reinforcement with the intended interface treatment Whereas the two blocks were placed simultaneously for monolithic specimens. Both L-shaped blocks are reinforced with size 15M longitudinal bars and size 10M stirrups to strengthen the specimen away from the shear plane. This is implemented to ensure failure occurrence to coincide with the shear plane. All specimens were subjected to a concentric monotonic axial load across the shear plane to induce shear without any associated moment on the shear connectors. Table A.1 shows the detailed test

matrix for this research program. The first character represents the type of connectors utilized in the specimen (G= GFRP, S = Steel and X = no reinforcement). The second character represents the number of connectors crossing the shear plane. The third character composed of two parts represents connector diameter and shape (C = closed stirrups and Z = Z shape bar). The fourth character represents the shear plane condition (M = monolithic, CR = cold joint roughened, and CN = cold joint not roughened). Last character represents the concrete strength (N = NSC and H = HSC). For example, specimen G4-10C-CR-N has four GFRP connectors using size 10M closed stirrups with cold joint roughened interface utilizing NSC. In each journal article, the names of the specimens have been modified slightly to better fit the investigated parameters and discussions presented in that paper, as shown in Table A.2.

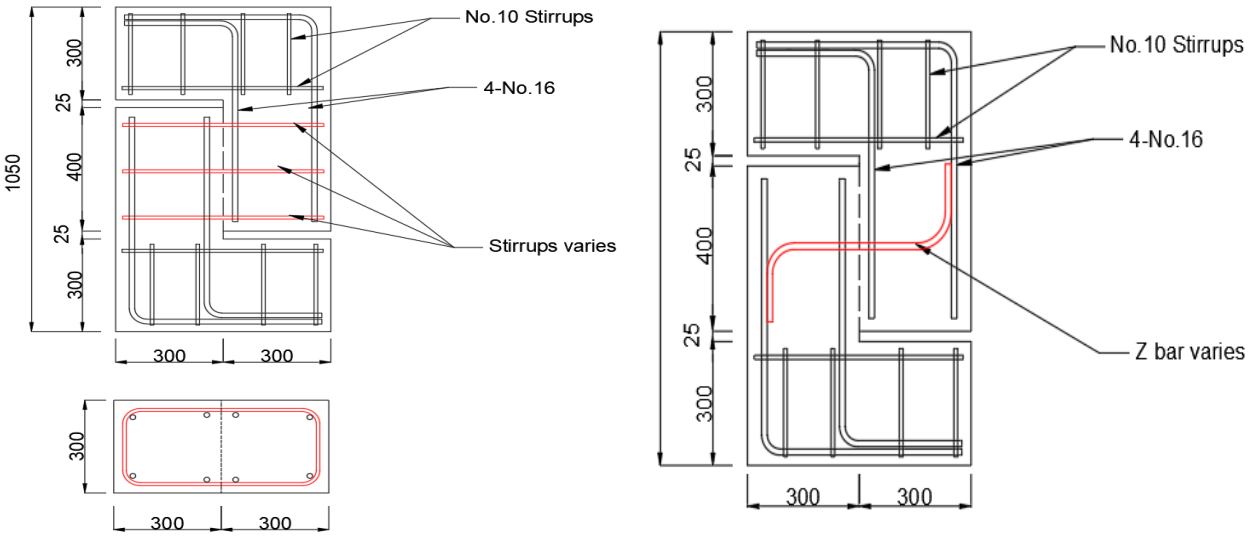

(a) (b)

Figure A.1: Specimens design, (a) closed stirrups, and (b) Z-shaped bars

Table A.1: Detailed test specimens

Specimen	Series NO.	Concrete strength (MPa)	Connector Type	Connector Shape	Number of connectors	Area (mm^2)	Reinforcement ratio (%)	Shear plane condition
S1-15Z-C-N	I	35	15M Steel	Z-bars	1	200	0.17	Cold joint, not roughened.
S2-15Z-C-N					2	400	0.33	
G1-15Z-C-N			No.15 GFRP		1	200	0.17	
G2-15Z-C-N					2	400	0.33	
X0-000-C-N	II		-	-	-	-	-	
S4-10C-C-N			10M Steel	Closed Stirrups	4	400	0.33	
G4-10C-C-N			No.10 GFRP		4	288	0.24	
G4-10C-C-N*					4	288	0.24	
G6-10C-C-N					6	432	0.36	
G8-10C-C-N					8	576	0.48	
G4-13C-C-N			No.13 GFRP		4	508	0.42	
S4-10C-CR-N	III		10M Steel		4	400	0.33	Cold joint, roughened.
G4-10C-CR-N			No.10 GFRP		4	288	0.24	
G4-10C-CR-N*					4	288	0.24	
G8-10C-CR-N					8	576	0.48	
G4-13C-CR-N			No.13 GFRP		4	508	0.42	

S4-10C-M-N	IV		10M Steel		4	400	0.33	Monolithic
G4-10C-M-N			No.10 GFRP		4	288	0.24	
G4-10C-M-N*					4	288	0.24	
G6-10C-M-N					6	432	0.36	
G8-10C-M-N					8	576	0.48	
G4-13C-M-N			No.13 GFRP		4	508	0.42	
S4-10C-C-H	V	70	10M Steel		4	400	0.33	Cold joint, not roughened
G4-10C-C-H			No.10 GFRP		4	288	0.24	
G6-10C-C-H					6	432	0.36	
G8-10C-C-H					8	576	0.48	

* Replicate specimens using GFRP bars and stirrups in the L-shaped blocks, away from the shear plane.

Table A.2: Specimens' ID for the research program and the journal articles

Specimens	Series	Chapter 3: Article I	Chapter 4: Article II
S1-15Z-C-N	I	S1-15Z-N	N/A
S2-15Z-C-N		S2-15Z-N	N/A
G1-15Z-C-N		G1-15Z-N	N/A
G2-15Z-C-N		G2-15Z-N	N/A
X0-000-C-N	II	X0-000-N	X0-00-C
S4-10C-C-N		S4-10C-N	S4-10-C
G4-10C-C-N		G4-10C-N	G4-10-C
G4-10C-C-N*		G4-10C-N*	G4-10-C*
G6-10C-C-N		G6-10C-N	G6-10-C
G8-10C-C-N		G8-10C-N	G8-10-C
G4-13C-C-N		G4-13C-N	G4-13-C
S4-10C-CR-N	III	N/A	S4-10-CR
G4-10C-CR-N		N/A	G4-10-CR
G4-10C-CR-N*		N/A	G4-10-CR*
G8-10C-CR-N		N/A	G8-10-CR
G4-13C-CR-N		N/A	G4-13-CR
S4-10C-M-N	IV	N/A	S4-10-M
G4-10C-M-N		N/A	G4-10-M
G4-10C-M-N*		N/A	G4-10-M*
G6-10C-M-N		N/A	G6-10-M
G8-10C-M-N		N/A	G8-10-M
G4-13C-M-N		N/A	G4-13-M
S4-10C-C-H	V	S4-10C-H	N/A
G4-10C-C-H		G4-10C-H	N/A
G6-10C-C-H		G6-10C-H	N/A
G8-10C-C-H		G8-10C-H	N/A